FABRICATION OF MULTIFUNCTIONAL POLYMER INTERFACES: POSTPOLYMERIZATION MODIFICATION ON TWO-DIMENSIONAL SURFACES AND SPHERICAL POLYMER SUPPORTS

by

LI CHEN

(Under the Direction of Jason Locklin)

ABSTRACT

Reactive polymer containing substrates have been extensively studied as a fundamental platform to generate precisely defined and tailorable surfaces with various functionalities for a broad range of applications in biology, material science, and coating industry. Postpolymerization modification (PPM) provides arrays of simplified and facile approaches to alter physicochemical properties of the reactive polymer interface, to which diverse polymer structures are rapidly introduced without individual synthesis. Herein, two types of polymer substrates, planar surfaces and spherical microbeads, were explored using PPM for the fabrication of biocompatible glycosurface and ion exchange resin respectively. First, a versatile and convenient strategy for preparation of surface-grafted glycopolymer constructs, using poly(pentafluorophenyl acrylate) (poly(PFPA)) polymer brushes as a platform, was investigated on the coating process optimization, aminolysis condition, ligation efficiency, and bioactivity of immobilized delicate biomolecules. Subsequently, this proposed glycosurface model was used to analyze the adherence and gliding motility of *Mycoplasma pneumoniae*, a common cause of human respiratory tract infections. Studies on the nature and density of ligated receptors as well

as the resulting gliding frequency of *M. pneumoniae* provided guidance for cell behavior and infection outcome in different receptor environments. In addition to the functionalization of two-dimensional polymer surfaces, spherical polymeric beads were also studied to generate a new type of strong acid cation exchange resins using PPM and sulfur(VI) fluoride exchange (SuFEx)-based strategy. Polystyrene based resin in various degree of fluorosulfonation was illustrated as a great precursor to generate sulfate cation exchange resins and other functional particles. The controllable charge density and ion exchange capacity, as well as morphology, were fully investigated in order to demonstrate the effectivity and superiority of this mild hydrolysis approach. Finally, three types of ion exchange resins were prepared using that precursor, including monofunctional sulfuric, phosphonic acid and bifunctional phosphonic/sulfuric acid ion exchange resins. The metal ions sorption capacity, efficiency and selectivity of each resin were also discussed.

INDEX WORDS: CLICK CHEMISTRY, MULTIFUNCTIONAL INTERFACES, GLYCOSURFACES, POSTPOLYMERIZATION MODIFICATION, POLYMERIC MICROBEADS, ION EXCHANGE RESINS

FBARICATION OF MULTIFUNCTIONAL POLYMER INTERFACES: POSTPOLYMERIZATION MODIFICATION ON TWO-DIMENSIONAL SURFACES AND SPHERICAL POLYMER SUPPORTS

by

LI CHEN

B.S., Shandong University, China, 2014

A Dissertation Submitted to the Graduate Faculty of The University of Georgia in Partial Fulfillment of the Requirements for the Degree

DOCTOR OF PHILOSOPHY

ATHENS, GEORGIA

2019

FABRICATION OF MULTIFUNCTIONAL POLYMER INTERFACES:

POSTPOLYMERIZATION MODIFICATION ON TWO-DIMENSIONAL SURFACES AND SPHERICAL POLYMER SUPPORTS

by

LI CHEN

Major Professor:	Jason Locklin
Committee:	Geert-Jan Boons
	Sergiy Minko

Electronic Version Approved:

Suzanne Barbour
Dean of the Graduate School
The University of Georgia
August 2019

DEDICATION

This dissertation is dedicated to my parents for their tremendous support, understanding, and unconditional love throughout my life.

And for without whom none of this would be possible.

ACKNOWLEDGEMENTS

First and foremost, I would like to thank my family. Mom and Dad, thank you for always believing in me and supporting each decision I made. I am the luckiest child in the world to have parents like you who give me enough space and freedom to do whatever interests me, and teach me fail is as important as success. I am here today because of you. My sisters, thank you for taking care of everything for me when I was thousand miles away from home. To all of my other family, thank you from the bottom of my heart for all your encouragement and support. It means so much to me that you all have been with me, celebrating each small accomplishment I made in my life. I am so grateful for everything you have done for me.

Next, I want to thank my PI, Jason Locklin, the greatest and most supportive mentor in the world. It's been an incredible journey that I gradually become mature, confident, and professional under your extremely patient mentorship and guidance. Thank you for all the amazing opportunities you have offered. Your great passion and dedication in your work will always inspire and encourage me in my near future career life. I truly appreciate all you have done. To my committees, Dr. Geert-Jan Boons and Dr. Serigy Minko, thank you for your time, advice, and knowledge to help me better conduct my projects.

To all my labmates I have worked with in the past five years: Joe, Evan, Jing, Anandi, Jeremy, Josh, Deb, Karson, Qiaohong, Yutian, Jessica, Grant, Jess, Scott, Apisata, DeMichael, Tim, Cato, Madi, and Kristian, thank you for being so nice and friendly. All of those memories, jokes and science discussion would definitely make me miss you all when I leave the States. Karson, the best desk buddy, and Deb, the best Chemistry teacher, thank you for teaching and

showing me how to be a professional and productive graduate student when I started graduate school. Those memories that we worked together and danced “awkwardly” on Friday will remain in my heart. Qiaohong and Yutian, thank you for cheering me up when I was frustrated or depressed. Apisata, my last desk buddy in Locklin lab, you are an incredible CHEF and friend. I will miss all the authentic Thai food you made for me and your hilarious face when you came to Kungfu Tea shop first time. Jing, who was the first one I met from Locklin lab, thank you for sharing all the valuable experience in research and job-hunting with me. To Cato and Kristian, my trustful coworkers and friends, I really enjoy chit-chat and sometimes science discussion with you. Special thanks to DeMichael for polishing this dissertation’s title. In addition, I want to thank all my collaborators: Caitlin, Dr. Krause, Ed, Pradeep, and Dr. Averick. I am so honored to have opportunities to collaborate with these great minds.

Finally, a big “thank you” to thank all my other friends who always have my back, your friendship means a lot to me. A special thanks to Chengcheng and Yi, your encouraging and inspirational words have helped me get through every challenges and rough patches in the past five years, and those wonderful adventures we shared together will remain forever in my memory. There are way too many of you to name, but you know who you are. I am so grateful to meet each of you and share a great time with you.

TABLE OF CONTENTS

Page

LIST OF TABLES

Page

LIST OF FIGURES

Page

CHAPTER 1

INTRODUCTION AND LITERATURE REVIEW

Polymer Coatings

The deposition of bulk material surface with polymer, forming polymeric thin films, is widely applied in different fields to manipulate surface properties, such as wettability, friction, biocompatibility and icing or fogging resistance.[1-5] The existing toolbox for polymer coating includes simple casting, spin coating, spray coating and doctor blading, etc.[6] Most of these techniques rely on weak intermolecular interactions between polymer materials and anchors on solid surface, such as hydrogen bonding, van der Waals forces and electrostatic forces, resulting in delamination, robustness and durability issues. Alternatively, polymers with reactive pendant or end groups can be grafted onto surface through covalent bond, forming so-called polymer brushes,[7] to fabricate coated scaffolds with more chemical and mechanical robustness.

Commonly, polymer brushes are made using “grafting-to” or “grafting-from” techniques (Figure1.1). The “grafting-to” method is experimentally simple. It simply involves synthesizing polymers in solution, followed by surface immobilization through the reactive moieties on polymer chains and functional groups on modified surface. Since the coating materials are prepared beforehand, one can run full characterization of the polymer including molecular weight and polydispersity, allowing the grafting density to be directly calculated from coating thickness and density.[8] However, one limitation of this method is the relative low thickness, and films in 100 nm range are inaccessible. This is due to the steric crowding of reactive handles on

surface occupied by already immobilized polymer chains, making it difficult to achieve high grafting densities.[7]

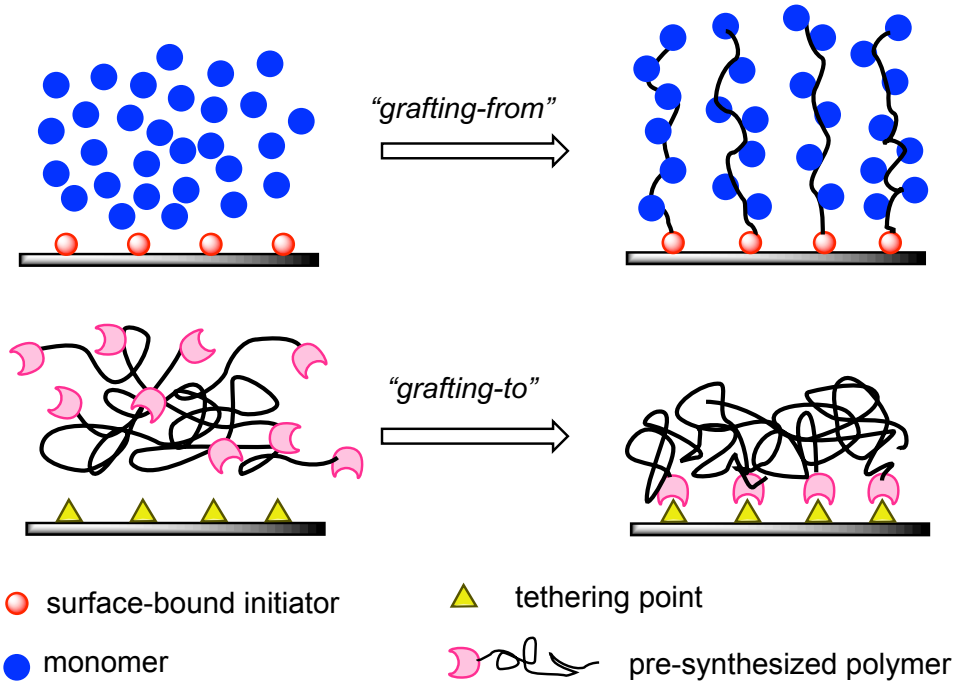

Figure 1.1. Polymer brushes fabrication by "grafting-to" and "grafting-from" approaches

Various strategies have been used to immobilize pre-synthesized polymer onto solid surfaces by introducing reactive groups to either polymer chains or solid surfaces. For example, thiol end-functionalized polystyrene can be successfully tethered to gold or gold-coated surfaces via sulfur.[9, 10] In the case of silica surfaces, a self-assembled monolayer is first modified, followed by the conjugation of polymers. Minko *et al*[11] modified substrates with 3-glycidoxypropyl trimethoxysilane to generate epoxy-monolayer on the surface and then hydroxyl or amine-functionalized polymers reacted with epoxy groups to generate grafted polymer layers.

On the other hand, surface-initiated polymerization from initiators bound on surface, "grafting-from" method, provides a better control over grafting density and thickness of brushes.

In this technique, initiators are first anchored to the surface and then monomers are polymerized in a solution from the tethered initiators. Over the last decades, many polymerization strategies have been used to grow brushes form surfaces, such as atom transfer radical polymerization (ATRP),[12, 13] cationic or anionic polymerization,[14, 15] ring-opening polymerization (ROP),[16, 17] reversible addition fragmentation chain transfer polymerization (RAFT),[18] and nitroxide-mediated radical polymerization (NMP).[7, 19] One of the main limitation is the difficulty of analyzing "grafting-from" polymers, due to the extremely low amount of polymer generated on the surface, and it is still under debate whether the solution polymerization can accurately mimic that of surface.[7, 20]

Chemical Modification of Polymer Surface

Polymer thin-film formation on solid surface provides versatile avenues to control surface properties by introducing complex functionalities on two- or three-dimensional platforms. The most straightforward approach to fabricate complex surface for specific application involves the polymerization of monomers with desired functional groups with demanded properties.[21] Despite tremendous approaches and techniques of monomer synthesis and polymerization developed previously, several significant limitations may arise in different perspectives. For example, the modification of monomer may experience low yield or incompatible reaction conditions required to conjugate desired functional groups, making it too laborious and costly to produce appreciable amounts of polymer materials. Besides, some materials cannot tolerate polymerization conditions required to reach desired molecular weight and polydispersity. Most biomolecules or highly reactive functionalities will denature or degrade when the polymerization is carried out in organic solvents, high temperature, or UV light. With these in mind, an alternative approach is needed for chemical modification of substrates.

Postpolymerization modification (PPM) is utilized to incorporate complex functionalities onto polymer surfaces that would otherwise be difficult to fabricate with direct polymerization of modified monomers. In PPM, a base polymer containing reactive pendant groups is first synthesized, followed by a second conjugation reaction to covalently link any desired functionalities. Click chemistry, first introduced by K. B. Sharpless in 2001,[22] is often used in PPM because of its high reaction rate, chemical orthogonality, high yield, and mild reaction condition which are of critical significance especially with biomacromolecules or nanostructures.[23, 24] "Click-like" reactions include thiol-based addition (thiol-ene, thiol-yen, thiol-isocyanate, thiol-Michael addition),[25] Cu^{I}-catalyzed and strain-promoted azide-alkyne cycloaddition,[26, 27] some Diels-Alder reactions,[28] activated ester conjugation, and non-aldol carbonyl chemistry.[29, 30] Of these examples, activated esters are probably the most commonly employed polymer repeating unites in PPM especially for biological applications. This is because of plenty of free amine groups present in proteins which can react with activated esters through aminolysis. Commonly used activated esters in PPM include azlactone, *N*-hydroxysuccinimide (NHS) esters, and pentafluorophenyl (PFP) esters (Scheme 1.1).

Azlactones are lactone-based active esters that can undergo ring-opening reaction with nucleophiles such as alcohol, thiol or amine groups. However, it generally has a slower reaction rate than NHS or PFP esters.[31] Despite NHS is currently widely applied in biomacromolecules immobilization on polymer surfaces through covalent attachment of active esters to lysine or *N*-terminus of peptide backbones,[32, 33] its poor solubility, reduced reactivity, hydrolysis, and other side reactions prevent NHS being an ideal clickable polymer unit used in PPM.[34-36] On the other hand, it has been reported that PFP groups are less prone to hydrolysis, soluble in a broad range of organic solvents, and more reactive towards poor nucleophiles, even with secondary and

aromatic amines.[37] Furthermore, poly(pentafluorophenyl acrylate) (poly(PFPA)) bearing PFP units, particularly, has very high reaction rates toward aminolysis, showing extremely fast kinetics with a pseudo-first-order rate constant of 2.46×10^{-1} s^{-1} observed between poly(PFPA) and primary alkyl amines.[38] Unlike polymer bearing NHS esters, poly(PFPA) can react not only with primary alkyl amines but also aromatic amines under the same reaction condition.

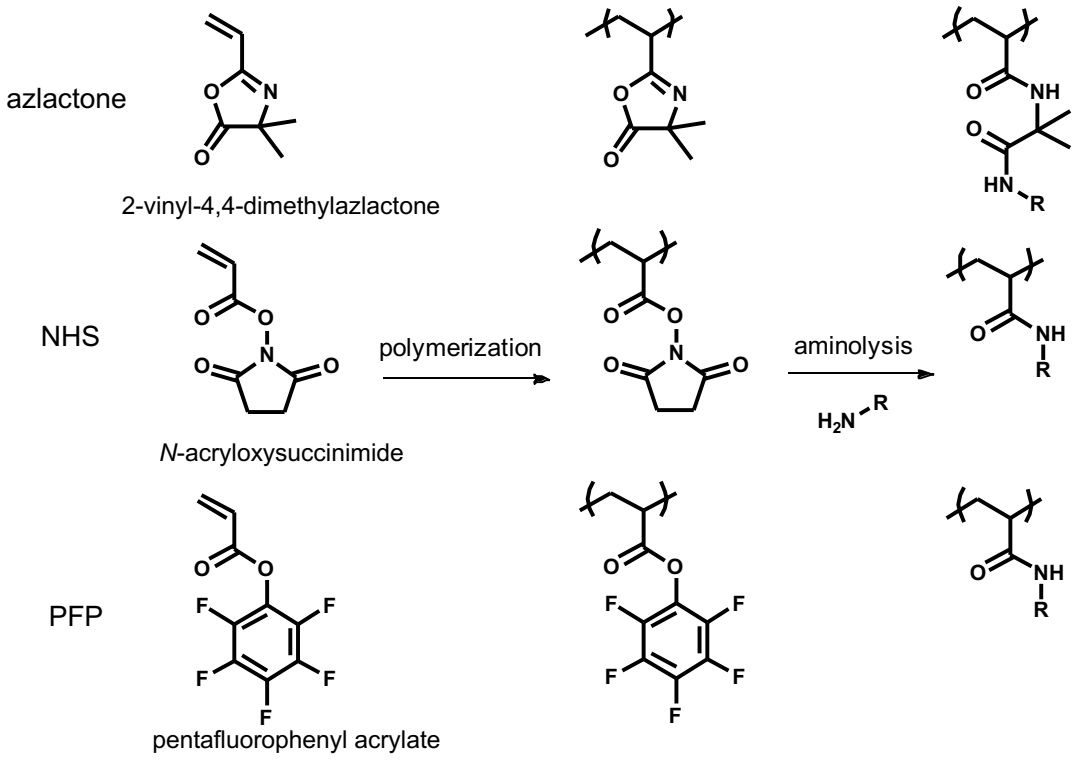

Scheme 1.1. Examples of aminolysis of commonly used activated esters in PPM

Sulfur(VI) Fluoride Exchange (SuFEx) Click Chemistry

In 2014, a new type of click reaction was introduced by K. B. Sharpless and his coworkers — the sulfur(VI) fluoride exchange (SuFEx) reaction, exploiting the exchange of S-F bonds for S-O bonds to make small coupling molecules, polymers and biomolecules.[39] Shown in

Scheme 1.2, SuFEx is the reaction between sulfonyl fluoride (-SO_2F) or fluorosulfate (-OSO_2F) and a silyl ether, forming a stable sulfonate or sulfate linkage in the presence of a powerful, non-nucleophilic base or fluoride anion.[40] The universal stability and reactivity of S-F bond make this reaction applicable in many conditions and fields. Unlike common homolytic scission of sulfonyl chloride, the cleavage of sulfonyl fluoride is solely heterolytic, resulting in its stability against oxidation/reduction.[41, 42] In addition, it is much more stable towards hydrolysis or thermolysis under harsh reaction conditions, compared to other sulfonyl halides.[43, 44] Sulfonyl fluorides have even been reported to be stable under vacuum UV irradiation at λ=157 nm.[45] Therefore, SuFEx has drawn major interest in recent years due to its stability under ambient oxygen and water, and its precursor materials, especially sulfonyl fluorides' universal stability mentioned above.

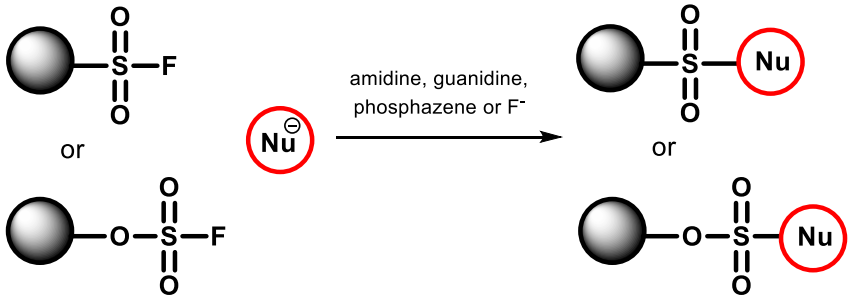

Scheme 1.2. General SuFEx click reaction between a nucleophile, silyl ether, and sulfonyl fluoride or fluorosulfate

More recently, the versatility of SuFEx has been widely established for small molecule synthesis,[39, 46, 47] bulk polymerization,[48, 49] bioconjugation,[50, 51] postpolymerization modification,[52, 53] and surface coating.[54] Sharpless *et al*[48] first reported a straightforward synthetic route for high molecular weight polysulfates based on SuFEx click chemistry. Two bisphenol A (BPA)-like fluorosulfate and silyl ether monomers were first synthesized by treating

BPA with gas SO_2F_2 or R_3SiCl, followed by SuFEx click in the presence of 20 mol% 1,8-Diazabicyclo[5.4.0]undec-7-ene (DBU) to form BPA-polysulfate with 95% yield (Mn = 30,900 Da). SuFEx also provides a simple platform to functionalize chain-end of polymers, and make multifunctional and multimorphological surfaces by PPM. Averick research group first applied SuFEx in the end-functionalization of polymers. Polymers with SuFEx handle (aryl *tert*-butyldimethylsilyl ether (aryl-TBDMS)) were synthesized using activators created by electron transfer atom transfer radical polymerization. Then PPM was conducted on aryl-TBDMS terminated polymers with phenyl fluorosulfate in the presence of DBU to afford corresponding end-modified polymers. Yatvin *et al*[55] presented a flexible platform with polymer brushes bearing sulfonyl fluoride for PPM on surface. Poly(fluorosulfonylpropyl methacrylate) brushes were grown from an azo-based silane initiator monolayer using radical polymerization with UV light. A variety of other chemical functional groups were also grafted to the brushes, including alkyne, thiol and diene, to demonstrate the facile utility and orthogonal reactivity of SuFEx click reaction. The combination of SuFEx and other click reactions will open doors in new material design.

Glycopolymers

Carbohydrates are a significant class of biomacromolecules, and present on the cell surface as free polysaccharides or as bioconjugates with proteins or lipids. They contribute to plenty of critical biological events in a biological body, such as cell differentiation, inflammation, immune defense, fertilization, and cellular recognition, all of which are mainly regulated by carbohydrate-carbohydrate (CCIs) and carbohydrate-protein interactions (CPIs).[56, 57] To increase binding strength of CCIs and CPIs, most of naturally occurring glycoconjugates have complicated structures, displaying multiple carbohydrates units that engage in multivalent

interactions ("multivalency effect" or "glycocluster effect"). Glycopolymers are synthetic polymers bearing multiple identical carbohydrates along their backbones. It was reported that these man-made glycopolymers can amplify carbohydrates signals similar to natural sacchardes.[58-60]

Since the first synthetic glycopolymer was reported in 1998,[61] a variety of other glycopolymers have been introduced, using various polymer materials and synthetic or polymerization techniques. Generally, glycopolymers are fabricated either by direct polymerization of saccharide-containing monomers or by PPM glycosylation of pre-synthesized polymers. A range of polymerization techniques have been used to polymerize carbohydrate-containing monomers, including free radical polymerization,[62-64] ATRP,[65, 66] ROP, RAFT,[67, 68] and NMP[69, 70] etc. These synthetic approaches offer great routes to control the ratio, density, orientation and composition of pendant saccharides along the polymer chain, better mimicking carbohydrates natural presentation and complicated structures.

PPM provides an alternative and simpler approach to produce a library of glycopolymers as some glycomonomers are laborious to obtain and tending to self-polymerize during fabrication process. There have been several reports of synthetic routes to obtain aminosaccharides containing polymers via PPM. Due to amine as a good nucleophile compared to hydroxyl groups on carbohydrates, polymers bearing active carbonyl groups such as carboxylic acid, NHS ester and anhydride have been used to conjugate aminosaccharides. Auzely-Velty *et al*[71] synthesized a series of water-soluble poly(*N*-vinylpyrrolidone-*co*-maleic acid) copolymers with galactose pedant groups via amide linkages between amine and anhydride. The resulting glycopolymers showed good inhibitory properties against model RCA_{120} lectin. Other approaches used in nonaminated saccharides often combine click

chemistry, highly efficient and versatile for glycoconjugation. For example, a block copolymer containing di(ethylene glycol) methyl ether methacrylate and 2-hydroxyethyl methacrylate was fabricated by RAFT polymerization, which was then modified with glucothiose via a thiol-ene click reaction. Chen *et al*[72] found this glycosylated copolymers can form thermo-responsive micelles, a potential carrier for drug delivery. Besides, Haddleton research group investigated the construction of glycopolymers from alkyne containing polymers via Cu^{I}-catalyzed azide-alkyne cycloaddition (CuAAC) chemistry in detail.[66, 73-75]

Grafting carbohydrate moieties or glycopolymer materials onto solid surface is a widely studied field, which can combine the properties of underlying material and the bioactivity of saccharides layer on surface. A variety of substrates have been used for carbohydrates display, such as flat surface, nanoparticles, polymeric scaffold, dendrimers, proteins and peptides etc.[59, 73, 76, 77] Different coupling techniques have been employed for the attachment of saccharides, most of which are discussed above, including "grafting-to" and "grafting-from" techniques, PPM, click chemistry. The anchoring of carbohydrates layers on templates forming glycosurfaces, offers a new avenue for multivalent binding, unraveling its biological functions and obtaining novel applications.

Ion Exchange Resins

Ion exchange resins are polymeric beads that are composed of crosslinked polymer networks with modified ligands capable of selective metal ions complexation. These materials have been used commercially for almost a century worldwide in different fields such as ion chromatography, catalysis, water softening and deionization, sensor technology, environment remediation, and hydrometallurgy.[78-85] Ion exchange resins are insoluble phase to which counterions are bound by electrostatic interaction. When they contact solution phase containing

ions of the same charge with its counterions on surface, an exchange of the two types of counterions can happen, depending on the concertation of ions in solution and the binding affinity of ions in the solution phase relative to the insoluble resin phase (Figure 1.2).[81] The great utility of ion exchange resin is because of its insolubility. The resin can be easily removed or separated simply by filtration. The insolubility also makes them environmentally compatible as the cycle of loading, regeneration and reloading allow them to recycle.

Heavy metals are elements with atomic weight between 63.5 and 200.6, and a specific gravity greater than 5.0.[86] With the fast development in mining, metal plating, battery, paper and pesticides industry, heavy metal wastewater has been an increasingly serious issue, especially in developing countries. Heavy metals are not degradable and tend to accumulate in living entities. Due to the toxicity and resistance to degrade, different methods have been used to remove heavy metals from the wastewater to protect human and environment. These effective techniques include membrane filtration,[87] chemical precipitation,[88, 89] adsorption, ion exchange,[90, 91] and electrochemical treatment.[92] Among these removal methods, ion-exchange resins have been considered as a superior approach and widely used in industry because of its high treatment capacity, high efficiency and fast kinetics.[93]

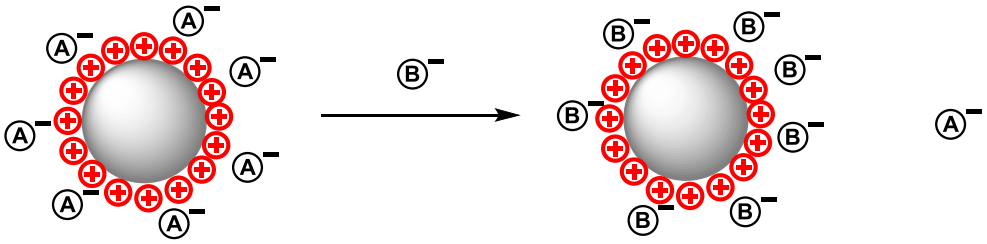

Figure 1.2. Exchange of ions between an insoluble phase (anion exchange resin) and a solution phase

Commonly used cation exchange resins are strongly acidic resins with sulfonic acid groups and weakly acidic resins with carboxylic acid groups. The protons in either sulfonic acid or carboxylic acid serve as exchangeable sites with heavy metal ions, such as Cu^{2+}, Zn^{2+}, Cr^{3+}, Pb^{2+}, Hg^{2+}, etc. As the metal cations containing solution passes through cation exchange resins column, cations attach to the resin surface through exchanges with hydrogen ions. The sulfonic acid resins are used when various ions need to be removed nonselectively from water, while the carboxylic acid resins are good at separating the alkaline earth from the alkali ions. Neither of them can be applied to remove a particular metal ion with presence of other metal ions in water. A specific ion exchange resin is characteristic of one particular ionic species under proper condition, which is called chelating ion exchange resin. This type of resins often has bifunctional or multifunctional groups present on the beads. For example, the bifunctional diphosphonic/sulfonic acid ion exchange resins were reported to complex 98.3% Eu(III), compared to 32.8% with diphosphonic acid resins and 44.9% with sulfonic acid resins.[94] The introduction of diphosphonic acid greatly increased the selectivity towards Eu(III) complexation. Chelating functional groups commonly used in chelating ion exchange resins include iminodiacetate, bipyridine, ketophosphonic acid, phosphonic acid, phosphonoactetic acid, and aminothiophosphonate, etc.[95] These resins find diverse applications in toxic transition and alkaline metal selective removal in water purification.

Objectives and Dissertation Outline

The objectives of this dissertation are as follows: 1) to design and study a versatile and convenient strategy to fabricate surface-grafted glycopolymer constructs using poly(PFPA) polymer brushes as a scaffold, 2) to apply this methodology in *Mycoplasma pneumoniae* to explore the cell's adherence and gliding motility on different cell-membrane mimic polymer coatings in order to better understand the pathogenesis and persistence of *M. pneumoniae*, 3) to exploit and evaluate SuFEx-based strategy to prepare strong acid cation exchange resins with a predictable and reproducible number of sulfuric acid sites on the beads, and 4) to develop different cation exchange resins using SuFEx click chemistry and fluorosulfonated polymer supports and evaluate each resin's capacity, efficiency, selectivity of heavy metal adsorption. The rest of this dissertation is organized into five chapters.

Chapter 2 describes a methodology to conjugate various reducing sugars to poly(PFPA) polymer brushes coated substrates via hydrazine chemistry. Several different carbohydrates, ranging from simple monosaccharides to relatively complex trisaccharides, were used to study coating thickness, hydrophilicity and ligation efficiency using this proposed glycosurface strategy. Among these selected carbohydrates, the interaction between 3'-sialyllactose and wheat germ agglutinin, and *M. pneuomoniae* was studied to demonstrate the presence of conjugated 3'-sialyllactose and the retaining of its bioactivity. Also, a quantification method by backfilling with *p*-nitrobenzaldehyde chromophore was reported to figure out the density of ligated carbohydrates. This chapter was published in *Langmuir*, **2017**, *33*(35), 8821-8828.[96]

Chapter 3 uses the glycosurface fabrication method described in Chapter 2 to generate different sialylated substrates, exploring the impact of sialic acid presentation on *M. pneumoniae* adherence and gliding. 6'- and 3'-sialyllactose were ligated individually or in combination to

poly(PFPA) scaffold in precisely controlled densities. Then, each sialylated coverslip was treated with *M. pneumoniae* suspensions and examined under microscopy. It was shown that the adherence and gliding were dependent on sialic acid and gliding on 3'-sialyllactose surface was hindered by the presence of 6'-sialyllactose. Part of this chapter was published in *Molecular Microbiology*, **2018**, *109*, 735-744.[97]

Chapter 4 describes a new approach for strong acid cation exchange resins fabrication with a predictable and reproducible number of sulfuric acid sites under a mild SuFEx-based condition, eliminating the use of concentrated sulfuric acid. Fluorosulfonated polymer beads were treated with strong base or SuFEx-based reagent system to hydrolyze $–SO_3F$, forming $–SO_4H$. Various characterization methods were employed to confirm the formation of sulfuric acid group, conversion and beads morphology. Besides, the resulting sulfuric acid cation exchange resin effectively demonstrated its utility as an ion exchange resin by cationic dye capture experiment. This fluorosulfonated polymeric support was also a suitable platform for small molecules or biomacromolecules conjugation via SuFEx click. This chapter was published in *Chemical Communications*, **2019**, *55*, 3891-3894.[98]

Chapter 5 further expands the usage of fluorosulfonated polymeric supports. Three different types of ion exchange resins, including monofunctional sulfuric, phosphonic acid and bifunctional phosphonic/sulfuric acid ion exchange resins (S-, P-, and PS-IERs), were prepared on this support by SuFEx chemistry. Basic characterizations on resins were conducted, such as its chemical composition, beads morphology, and acid capacity. Several divalent and trivalent metal ions were first tested with newly reported S-IERs, revealing its preference to metal having high valance in acidic solution. Then, the total Fe(III) sorption capacity was investigated on all

resins. P-IERs were found to be the best materials in Fe(III) adsorption in all the fabricated resins used in this study.

Finally, Chapter 6 summarizes different projects completed for this dissertation and discusses the future directions for these researches.

References

1. Liu, Q. H.; Locklin, J., *ACS Omega* **2018,** *3* (12), 17743-17750.

2. Gao, J.; Martin, A.; Yatvin, J.; White, E.; Locklin, J., *J. Mater. Chem. A* **2016,** *4* (30), 11719-11728.

3. Kang, T.; Banquy, X.; Heo, J. H.; Lim, C. N.; Lynd, N. A.; Lundberg, P.; Oh, D. X.; Lee, H. K.; Hong, Y. K.; Hwang, D. S.; Waite, J. H.; Israelachvili, J. N.; Hawker, C. J., *ACS Nano* **2016,** *10* (1), 930-937.

4. Zhai, L.; Cebeci, F. C.; Cohen, R. E.; Rubner, M. F., *Nano Lett.* **2004,** *4* (7), 1349-1353.

5. Gulati, K.; Ramakrishnan, S.; Aw, M. S.; Atkins, G. J.; Findlay, D. M.; Losic, D., *Acta biomaterialia* **2012,** *8* (1), 449-456.

6. Krebs, F. C., *Sol. Energ. Mat. Sol. C* **2009,** *93* (4), 394-412.

7. Barbey, R.; Lavanant, L.; Paripovic, D.; Schuwer, N.; Sugnaux, C.; Tugulu, S.; Klok, H. A., *Chem. Rev.* **2009,** *109* (11), 5437-5527.

8. Arnold, R. M.; McNitt, C. D.; Popik, V. V.; Locklin, J., *Chem. Commun.* **2014,** *50* (40), 5307-5309.

9. Yockell-Lelièvre, H.; Desbiens, J.; Ritcey, A. M., *Langmuir* **2007,** *23* (5), 2843-2850.

10. Shan, J.; Nuopponen, M.; Jiang, H.; Viitala, T.; Kauppinen, E.; Kontturi, K.; Tenhu, H., *Macromolecules* **2005,** *38* (7), 2918-2926.

11. Minko, S.; Patil, S.; Datsyuk, V.; Simon, F.; Eichhorn, K.-J.; Motornov, M.; Usov, D.; Tokarev, I.; Stamm, M., *Langmuir* **2002,** *18* (1), 289-296.

12. Matyjaszewski, K.; Xia, J., *Chem. Rev.* **2001,** *101* (9), 2921-2990.

13. Pyun, J.; Kowalewski, T.; Matyjaszewski, K., *Macromol. Rapid Commun.* **2003,** *24* (18), 1043-1059.

14. Baskaran, D., Strategic developments in living anionic polymerization of alkyl (meth) acrylates. *Prog. polym. Sci.* **2003,** *28* (4), 521-581.

15. Zirbs, R.; Binder, W.; Gahleitner, M.; Machl, D., in *Macromol. Symp.*, Wiley Online Library: 2007; pp 93-96.

16. Penczek, S.; Cypryk, M.; Duda, A.; Kubisa, P.; Słomkowski, S., *Prog. Polym. Sci.* **2007,** *32* (2), 247-282.

17. Choi, J.; Cho, S. B.; Lee, B. S.; Joung, Y. K.; Park, K.; Han, D. K., *Langmuir* **2011,** *27* (23), 14232-14239.

18. Boyes, S. G.; Granville, A. M.; Baum, M.; Akgun, B.; Mirous, B. K.; Brittain, W. J., *Surf. Sci.* **2004,** *570* (1-2), 1-12.

19. Brinks, M. K.; Studer, A., *Macromol. Rapid Commun.* **2009,** *30* (13), 1043-1057.

20. Turgman-Cohen, S.; Genzer, J., *J. Am. Chem. Soc.* **2011,** *133* (44), 17567-17569.

21. Galvin, C. J.; Genzer, J., *Prog. Polym. Sci.* **2012,** *37* (7), 871-906.

22. Kolb, H. C.; Finn, M. G.; Sharpless, K. B., *Angew. Chem. Int. Ed.* **2001,** *40* (11), 2004-+.

23. Iha, R. K.; Wooley, K. L.; Nystrom, A. M.; Burke, D. J.; Kade, M. J.; Hawker, C. J., *Chem. Rev.* **2009,** *109* (11), 5620-5686.

24. Sumerlin, B. S.; Vogt, A. P., *Macromolecules* **2010,** *43* (1), 1-13.

25. Hoyle, C. E.; Lowe, A. B.; Bowman, C. N., *Chem. Soc. Rev.* **2010,** *39* (4), 1355-1387.

26. Orski, S. V.; Poloukhtine, A. A.; Arumugam, S.; Mao, L. D.; Popik, V. V.; Locklin, J., *J. Am. Chem. Soc.* **2010,** *132* (32), 11024-11026.

27. Rostovtsev, V. V.; Green, L. G.; Fokin, V. V.; Sharpless, K. B., *Angew. Chem. Int. Ed.* **2002,** *41* (14), 2596-+.

28. Arumugam, S.; Orski, S. V.; Locklin, J.; Popik, V. V., *J. Am. Chem. Soc.* **2011,** *134* (1), 179-182.

29. Zou, Y. Q.; Yeh, P. Y. J.; Rossi, N. A. A.; Brooks, D. E.; Kizhakkedathu, J. N., *Biomacromolecules* **2010,** *11* (1), 284-293.

30. Byeon, J. Y.; Limpoco, F. T.; Bailey, R. C., *Langmuir* **2010,** *26* (19), 15430-15435.

31. Arnold, R. M.; Patton, D. L.; Popik, V. V.; Locklin, J., *Acc. Chem. Res.* **2014,** *47* (10), 2999-3008.

32. Jain, P.; Dai, J. H.; Baker, G. L.; Bruening, M. L., *Macromolecules* **2008,** *41* (22), 8413-8417.

33. Tsujii, Y.; Ohno, K.; Yamamoto, S.; Goto, A.; Fukuda, T., *Adv. Polym. Sci.* **2006,** *197*, 1-45.

34. Buck, M. E.; Breitbach, A. S.; Belgrade, S. K.; Blackwell, H. E.; Lynn, D. M., *Biomacromolecules* **2009,** *10* (6), 1564-1574.

35. Chen, G. H.; Huynh, D.; Felgner, P. L.; Guan, Z. B., *J. Am. Chem. Soc.* **2006,** *128* (13), 4298-4302.

36. Pasut, G.; Mero, A.; Caboi, F.; Scaramuzza, S.; Sollai, L.; Veronese, F. M., *Bioconjugate Chem.* **2008,** *19* (12), 2427-2431.

37. Theato, P., *J. Polym. Sci. Pol. Chem.* **2008,** *46* (20), 6677-6687.

38. Arnold, R. M.; Sheppard, G. R.; Locklin, J., *Macromolecules* **2012,** *45* (13), 5444-5450.

39. Dong, J. J.; Krasnova, L.; Finn, M. G.; Sharpless, K. B., *Angew. Chem. Int. Ed.* **2014,** *53* (36), 9430-9448.

40. Yatvin, J.; Brooks, K.; Locklin, J., *Chem. Eur. J.* **2016,** *22* (46), 16348-16354.

41. Bellale, E. V.; Chaudhari, M. K.; Akamanchi, K. G., *Synthesis-Stuttgart* **2009,** (19), 3211-3213.

42. Wiberg, E.; Wiberg, N.; Holleman, A., *Inorganic Chemistry* p. 1655. Academic Press: 2001.

43. Falardeau, E. R.; DesMarteau, D. D., *J. Chem. Eng. Data* **1976,** *21* (3), 386-387.

44. Wray, K. L.; Feldman, E. V., *J. Chem. Phys.* **1971,** *54* (8), 3445-&.

45. Fujigaya, T.; Sibasaki, Y.; Ando, S.; Kishimura, S.; Endo, M.; Sasago, M.; Ueda, M., *Chem. Mater.* **2003,** *15* (7), 1512-1517.

46. Wang, H.; Zhou, F.; Ren, G.; Zheng, Q.; Chen, H.; Gao, B.; Klivansky, L.; Liu, Y.; Wu, B.; Xu, Q., *Angew. Chem. Int. Ed.* **2017,** *129* (37), 11355-11360.

47. Zhang, E.; Tang, J.; Li, S.; Wu, P.; Moses, J. E.; Sharpless, K. B., *Chem. Eur. J.* **2016,** *22* (16), 5692-5697.

48. Dong, J.; Sharpless, K. B.; Kwisnek, L.; Oakdale, J. S.; Fokin, V. V., *Angew. Chem. Int. Ed.* **2014,** *53* (36), 9466-9470.

49. Xiao, X.; Zhou, F.; Jiang, J.; Chen, H.; Wang, L.; Chen, D.; Xu, Q.; Lu, J., *Polym. Chem.* **2018,** *9* (8), 1040-1044.

50. Li, S.; Cohen-Karni, D.; Beringer, L. T.; Wu, C.; Kallick, E.; Edington, H.; Passineau, M. J.; Averick, S., *Polym. J.* **2016,** *99*, 7-12.

51. Liu, Z.; Li, J.; Li, S.; Li, G.; Sharpless, K. B.; Wu, P., *J. Am. Chem. Soc.* **2018,** *140* (8), 2919-2925.

52. Oakdale, J. S.; Kwisnek, L.; Fokin, V. V., *Macromolecules* **2016,** *49* (12), 4473-4479.

53. Li, S.; Beringer, L. T.; Chen, S.; Averick, S., *Polym. J.* **2015,** *78*, 37-41.

54. Zhu, H.; Chen, D.; Li, N.; Xu, Q.; Li, H.; He, J.; Wang, H.; Wu, P.; Lu, J., *Chem. Eur. J.* **2017,** *23* (59), 14712-14717.

55. Yatvin, J.; Brooks, K.; Locklin, J., *Angew. Chem. Int. Ed.* **2015,** *54* (45), 13370-13373.

56. Varki, A.; Cummings, R. D.; Esko, J. D.; Freeze, H. H.; Stanley, P.; Bertozzi, C. R.; Hart, G. W.; Etzler, M. E., *Nematoda--Essentials of Glycobiology*. Cold Spring Harbor Laboratory Press: 2009.

57. Dwek, R. A., *Chem. Rev.* **1996,** *96* (2), 683-720.

58. Otsuka, H.; Akiyama, Y.; Nagasaki, Y.; Kataoka, K., *J. Am. Chem. Soc.* **2001,** *123* (34), 8226-8230.

59. Woller, E. K.; Cloninger, M. J., *Org. Lett.* **2002,** *4* (1), 7-10.

60. Benito, J. M.; Gomez-Garcia, M.; Mellet, C. O.; Baussanne, I.; Defaye, J.; Fernandez, J. M. G., *J. Am. Chem. Soc.* **2004,** *126* (33), 10355-10363.

61. Ohno, K.; Tsujii, Y.; Miyamoto, T.; Fukuda, T.; Goto, M.; Kobayashi, K.; Akaike, T., *Macromolecules* **1998,** *31* (4), 1064-1069.

62. Yang, Q.; Wu, J.; Li, J. J.; Hu, M. X.; Xu, Z. K., *Macromol. Rapid Commun.* **2006,** *27* (22), 1942-1948.

63. Sato, H.; Miura, Y.; Saito, N.; Kobayashi, K.; Takai, O., *Biomacromolecules* **2007,** *8* (2), 753-756.

64. Yang, Q.; Hu, M.-X.; Dai, Z.-W.; Tian, J.; Xu, Z.-K., *Langmuir* **2006,** *22* (22), 9345-9349.

65. Dai, X. H.; Dong, C. M., *J. Polym. Sci., Part A: Polym. Chem.* **2008,** *46* (3), 817-829.

66. Ladmiral, V.; Mantovani, G.; Clarkson, G. J.; Cauet, S.; Irwin, J. L.; Haddleton, D. M., *J. Am. Chem. Soc.* **2006,** *128* (14), 4823-4830.

67. Granville, A. M.; Quémener, D.; Davis, T. P.; Barner-Kowollik, C.; Stenzel, M. H., in *Macromol. Symp.*, Wiley Online Library: 2007; pp 81-89.

68. Spain, S. G.; Albertin, L.; Cameron, N. R., *Chem. Commun.* **2006,** (40), 4198-4200.

69. Sun, X.-L.; Faucher, K. M.; Houston, M.; Grande, D.; Chaikof, E. L., *J. Am. Chem. Soc.* **2002,** *124* (25), 7258-7259.

70. Narumi, A.; Satoh, T.; Kaga, H.; Kakuchi, T., *Macromolecules* **2002,** *35* (3), 699-705.

71. Auzély-Velty, R.; Cristea, M.; Rinaudo, M., *Biomacromolecules* **2002,** *3* (5), 998-1005.

72. Chen, G.; Amajjahe, S.; Stenzel, M. H., *Chem. Commun.* **2009,** (10), 1198-1200.

73. Geng, J.; Mantovani, G.; Tao, L.; Nicolas, J.; Chen, G.; Wallis, R.; Mitchell, D. A.; Johnson, B. R.; Evans, S. D.; Haddleton, D. M., *J. Am. Chem. Soci.* **2007,** *129* (49), 15156-15163.

74. Nurmi, L.; Lindqvist, J.; Randev, R.; Syrett, J.; Haddleton, D. M., *Chem. Commun.* **2009,** (19), 2727-2729.

75. Chen, G.; Tao, L.; Mantovani, G.; Geng, J.; Nyström, D.; Haddleton, D. M., *Macromolecules* **2007,** *40* (21), 7513-7520.

76. Yang, Q.; Xu, Z. K.; Hu, M. X.; Li, J. J.; Wu, J., *Langmuir* **2005,** *21* (23), 10717-10723.

77. Guo, T. Y.; Liu, P.; Zhu, J. W.; Song, M. D.; Zhang, B. H., *Biomacromolecules* **2006,** *7* (4), 1196-1202.

78. Singh, A.; Saraf, S. K., *Int. J. Polym. Mater.* **2009,** *58* (10), 499-508.

79. Li, X.-G.; Huang, M.-R.; Yang, Y., *Polym. J.* **2001,** *42* (9), 4099-4107.

80. Karunakaran, M.; Burkanudeen, A., *Orient. J. Chem.* **2002,** *18* (1), 65-68.

81. Alexandratos, S. D., *Ind. Eng. Chem. Res.* **2008,** *48* (1), 388-398.

82. Gelbard, G., *Ind. Eng. Chem. Res.* **2005,** *44* (23), 8468-8498.

83. Elder, D. P., *J. Chem. Educ.* **2005,** *82* (4), 575-587.

84. Wheaton, R.; Anderson, R., *J. Chem. Educ.* **1958,** *35* (2), 59.

85. Srikanth, M. V.; Babu, G. V. M. M.; Sunil, S. A.; Rao, N. S.; Murthy, K. V. R., *J. Sci. Ind. Res.* **2010,** *69* (8), 629-634.

86. Srivastava, N. K.; Majumder, C. B., *J. Hazard Mater.* **2008,** *151* (1), 1-8.

87. Landaburu-Aguirre, J.; Garcia, V.; Pongracz, E.; Keiski, R. L., *Desalination* **2009,** *240* (1-3), 262-269.

88. Ku, Y.; Jung, I. L., *Water Res.* **2001,** *35* (1), 135-142.

89. Mirbagheri, S. A.; Hosseini, S. N., *Desalination* **2005,** *171* (1), 85-93.

90. Abo-Farha, S.; Abdel-Aal, A.; Ashour, I.; Garamon, S., *J. Hazard Mater.* **2009,** *169* (1-3), 190-194.

91. Doula, M.; Dimirkou, A., *J. Hazard Mater.* **2008,** *151* (2-3), 738-745.

92. Chen, G., *Sep. Purif. Technol.* **2004,** *38* (1), 11-41.

93. Kang, S.-Y.; Lee, J.-U.; Moon, S.-H.; Kim, K.-W., *Chemosphere* **2004,** *56* (2), 141-147.

94. Alexandratos, S. D.; Trochimczuk, A. W.; Crick, D. W.; Horwitz, E. P.; Gatrone, R. C.; Chiarizia, R., *Macromolecules* **1996,** *29* (3), 1021-1026.

95. Popa, A.; Davidescu, C. M.; Negrea, P.; Ilia, G.; Katsaros, A.; Demadis, K. D., *Ind. Eng. Chem. Res.* **2008,** *47* (6), 2010-2017.

96. Chen, L.; Leman, D.; Williams, C. R.; Brooks, K.; Krause, D. C.; Locklin, J., *Langmuir* **2017,** *33* (35), 8821-8828.

97. Williams, C. R.; Chen, L.; Driver, A. D.; Arnold, E. A.; Sheppard, E. S.; Locklin, J.; Krause, D. C., *Mol. Microbiol.* **2018,** *109* (6), 735-744.

98. Kassick, A. J.; Chen, L.; Kovaliov, M.; Mathers, R. T.; Locklin, J.; Averick, S., *Chem. Commun.* **2019**.

CHAPTER 2

A VERSATILE METHODOLOGY FOR GLYCOSURFACES: DIRECT LIGATION OF NONDERIVATIZED REDUCING SACCHARIDES TO POLY(PENTAFLUOROPHENYL ACRYLATE) GRAFTED SURFACES VIA HYDRAZIDE CONJUGATION

Chen, Li; Leman, Deborah; Williams, Caitlin; Krause, Duncan; Locklin, Jason. Accepted by *Langmuir*. Reprinted here with permission of publisher.

Abstract

In this work, we report a convenient and versatile strategy for surface-grafted glycopolymer constructs with the goal of surface modification that controls the chemical presentation and grafting density of carbohydrate sidechains. This approach employs a difunctional hydrazine linker, chemically modified to an active ester containing poly(pentafluorophenyl acrylate) grafted scaffold, to conjugate a variety of saccharides through the reducing end. The successive conjugation steps are carried out under mild conditions and yield high surface densities of sugars, as high as 4.8 nmol·cm^{-2}, capable of multivalency, with an intact structure and retained bioactivity. We also demonstrate this glycosylated surface can bind specific lectins according to the structure of its pendant carbohydrate. To demonstrate bioactivity, this surface platform is used to study the binding events of a human respiratory tract pathogen, *Mycoplasma pneumoniae*, on surfaces conjugated with sialylated sugars.

Introduction

In nature, a complex array of interactions between glycans and proteins are used to mediate and initiate physiological, cellular, and chemical events, such as those found in joint lubrication,[1] cell signaling,[2] pathogen recognition, and development of genetic disorders.[3] In attempts to understand these individual interactions, many strategies have been developed for the attachment and modification of biomolecules to various substrates. Naturally occurring glycans are structurally complex, making them difficult to purify or synthesize. Also, modification of these glycans with reactive functional moieties for site-specific conjugation is further challenging, as modifying these molecules may either require multiple orthogonal protecting groups, or use conditions that lead to significant structural changes which may alter biological function. Specific examples of covalent ligation chemistries for sugars include modification of the carbohydrate structure with amines,[4] that then can be used to conjugate through amidation with activated ester substrates,[5] oxidation to create aldehyde sites for linkage to amines via reductive amination,[6,7] and reducing terminal aldehyde conjugation to amine, followed by reductive amination.[8,9] Each of these techniques, however, involves several steps which can lead to difficult purification or changes in the shape and structure of the sugar, possibly affecting the biological activity due to alterations of recognition and binding affinities.[10,11]

It has been argued that the 3D presentation, concentration and multivalency of natural ligands are of great importance for binding events,[12-14] and that polymer supports can effectively mimic glycans found on a cell surface or protein. Precise spatial control of these synthetic platforms allows the attachment of glycans with specific chemical presentation and functional densities for improved biological recognition and activity.[2,15,16] This class of polymers, called glycopolymers, are of interest in development of biocompatible materials and can be generated

through many different synthetic approaches. Some of these techniques include polymerization of glycomonomers,[2,14,17] such as Kizhakkedathu *et al.* who polymerized monosaccharide based monomers using surface-initiated atom transfer radical polymerization. Another approach uses post-polymerization modification,[18,19] an example being Haddleton *et al.* who used copper click to conjugate azide-modified sugars to an alkyne containing acrylate polymer.[14,20]

Poly(acryloyl hydrazide) (PAH) has been demonstrated to be of great utility in material science due to its ability to undergo rapid and pH reversible reactions with a variety of functional groups. PAH has been utilized to create stimuli-responsive hydrogels,[21] drug delivery systems,[22,23] ion exchange resins,[21] and glycopolymers.[24] The hydrazide moiety located along the backbone of the polymer is an effective conjugation site for many types of aldehyde-containing molecules, including sugars with a reducing end. Hydrazone formation is reversible, stable, and an efficient reaction used to form imines.[25] Because of these excellent properties, hydrazine is commonly used as a bi-functional linker for reversible crosslinking and conjugation. The synthetic routes to synthesizing PAH are often multistep and performed using solution polymerization of protected monomers. Kumar *et al.* synthesized PAH through modification of poly(methyl acrylate) with hydrazine, which required stirring for 12 hours at 60°C.[21] Bertozzi *et al.* polymerized acetoxime acrylate through reversible addition-fragmentation chain transfer using a biotinylated chain transfer agent and then reacted the polymer with hydrazine to obtain PAH.[24]

Several techniques have been used to covalently attach carbohydrates to surfaces. Commonly, surfaces are functionalized with a reactive small molecule that can react with the complementary functional group on the carbohydrate.[24,26,27] The most common example is the use of n-hydroxysuccinimide (NHS) modified surfaces that can react with amine containing

small molecules.[5] Pentafluorophenyl acrylate (PFPA) is an activated ester that has been demonstrated to have greater hydrolytic stability and faster reaction kinetics towards primary amines than NHS. PFPA is easily synthesized through a one-step procedure and can be polymerized to form poly(PFPA) through radical polymerization. High-density polymer brushes (as high as 2.6 chains·nm^{-2}) of poly(PFPA) have been reported using surface initiated polymerization,[28] and lower density brushes (ranging from 0.005-0.05 chains·nm^{-2}) can be formed using a combination of spin-coating and annealing.[29,30] Poly(PFPA) can be easily grafted-to many types of surfaces as well, allowing for use in a wide variety of applications.[31] Once immobilized to a solid support, a one-step post-polymerization modification of poly(PFPA) with hydrazine allows the fabrication of PAH. This then allows for a simple platform to conjugate aldehydes to polymers, nanoparticles, surfaces, and scaffolds for use in patterning, microarrays, and forming gradients of desired functionalities.

Herein, we present the fabrication of stable, grafted-to polymeric surfaces that can be modified in two steps for the immobilization of carbohydrates with a high degree of control over functional density and carbohydrate ratios. This direct conjugation does not require any synthetic preparation or purification of the carbohydrate, and only simple modification including substrate rinsing. With the expense of purified carbohydrates, this method employs small volumes and low concentrations, and offers a more cost effective approach to carbohydrate conjugation. *Mycoplasma pneumoniae* is a human respiratory pathogen and a major cause of community acquired respiratory disease.[32] *M. pneumoniae* recognizes sialyated glycoproteins as receptors for attachment to host cells.[33,34] The proposed carbohydrate conjugation strategy is employed to decorate surfaces with specific sialyated sugars in order to study the interaction of *M. pneumoniae* as well as illustrate possible applications for this proposed methodology.

Experimental

Materials

Wheat Germ Agglutinin Alexa Fluor® 555 conjugate was purchased from Life Technologies. Silicon wafers (orientation <101>, native oxide) were purchased from University Wafer. Quartz microscope slides were purchased from AdValue Technology. 3'-Sialyllactose sodium salt was purchased from Carbosynth and used as received. Lactose was purchased from Aqua Solutions. All other chemicals were purchased from TCI, Alfa Aesar, Oakwood Chemical, or Aldrich and used without further purification.

Amine Monolayer Formation

All substrates (glass, silicon, and quartz) were solvent cleaned using hexane, isopropyl alcohol, acetone, and water by sonication for 5 minutes in each. After drying, the substrates were plasma cleaned for 5 minutes (Harrick Plasma PDC-32G at 0.80 mbar). Monolayers were formed by placing substrates into a solution of 3 mM 3-aminopropyltrimethoxysilane in absolute ethanol overnight, followed by 10 minutes of sonication in fresh ethanol.

PFPA Free Radical Polymerization

Pentafluorophenyl acrylate monomer, synthesized using previously reported methods,[29] was dissolved in anhydrous dioxane (3 M) and then subjected to three cycles of freeze, pump, thaw to degas the solution. Azodiisobutyronitrile (AIBN) (0.1 mol%) was added under positive nitrogen pressure, and the flask was placed in a preheated oil bath (70°C) overnight. The flask was then removed from heat, and the residual dioxane was removed by rotary evaporation. The remaining glassy polymer was dissolved in minimal tetrahydrofuran then precipitated in cold methanol and filtered. The precipitation was then repeated to further purify polymer. Analysis by gel permeation chromatography showed a M_n of 97,600 $g \cdot mol^{-1}$ with a PDI of 2.33.

Surface Fabrication

Substrates (glass, silicon, and quartz) were cleaned using hexane, isopropyl alcohol, acetone, and water through sonication for 5 minutes. After drying, the substrates were plasma cleaned for 5 minutes (Harrick Plasma PDC-32G). Plasma cleaned substrates were placed into a solution of 3 mM 3-aminopropyltrimethoxysilane in absolute ethanol overnight, followed by 10 minutes of sonication in fresh ethanol to form amine-bearing monolayers. A solution of 20 $mg \cdot mL^{-1}$ poly(PFPA) in dry chloroform was prepared and filtered to remove any large particulates. Substrates with freshly prepared amine monolayers were spin coated with PFPA at 2000 rpm for 15 seconds. The films were then annealed at 150°C in a glovebox for one hour. The resulting films were rinsed and sonicated in tetrahydrofuran for 15 minutes to remove any physisorbed polymer, dried under a stream of nitrogen, and cut to the desired size.

Hydrazine Post-Polymerization Modification

Substrates containing grafted-to poly(PFPA) brushes were placed into a flask and purged with nitrogen 3 times. Hydrazine monohydrate (0.3 mmol) was dissolved in 3 mL dry dimethylformamide (DMF) along with triethylamine (2 equiv, 0.6 mmol). The solution was injected into the flask containing the substrates and allowed to stir for 1 hour. The substrates were rinsed with DMF, water, and DMF again and then dried under a stream of nitrogen.

p-Nitrobenzaldehyde Conjugation

p-nitrobenzaldehyde (0.03 mmol) was dissolved in 3 ml DMF/water (1:1) and then aniline (0.30 mmol) and drops of 2 M HCl were subsequently added to obtain a solution with a pH 4.5. Hydrazine modified substrates were placed in the solution and allowed to react for 2 hours with stirring. After 2 hours, the substrates were removed and then rinsed with DMF, water, DMF again, and then dried under stream of nitrogen.

Carbohydrate Conjugation

Carbohydrate conjugations were performed using 10 mM carbohydrate and 100 mM aniline in 100 mM acetate buffer (pH 4.5). Solution was placed onto hydrazine modified substrates and allowed to react in a moisture chamber for 24 hours. The substrates were then thoroughly rinsed with water then dried under a stream of nitrogen.

Micro-Capillary Printing

PDMS stamps with channels of 250 μm made using conventional lithographic methods were used to pattern substrates. The stamps were first plasma cleaned for one minute to allow wicking of aqueous solution. The stamps were then placed on substrates and 3 μL of 3'-sialyllatcose solution wicked into channels through capillary action. The setup was placed into a moisture chamber and allowed to react for 24 hours before removing the stamp and rinsing with water. 100 μL of lactose solution was then placed on the substrate previously patterned with 3'-sialyllactose. The setup was also placed into a moisture chamber and allowed to react for 24 hours before rinsing with water.

Wheat Germ Agglutinin Staining

Sialic acid residues were stained using wheat germ agglutinin Alexa Fluor® 555 conjugate (WGA). The lectin was dissolved in phosphate-buffered saline (PBS, pH 7.4) at a concentration of 1 $mg \cdot mL^{-1}$. Small aliquots were placed onto substrate surfaces to cover patterned regions and allowed to incubate in the dark at room temperature for 15 minutes. The substrates were then rinsed with PBS and dried.

Mycoplasma pneumoniae Culture Preparation

Wild-type *M. pneumoniae* (strain M129) was cultured in 30ml of SP4 growth medium[35] for 72 hours at 37°C in tissue culture flasks. Growth medium was decanted, flasks washed with

30ml PBS, and cells scrapped into PBS. Cells were collected by centrifugation (20,000 × g for 25 minutes at 4°C), suspended in PBS, collected by centrifugation (20,000 × g for 20 minutes at 4°C), and suspended in modified SP4 growth medium[35] (without fetal bovine serum or phenol red and supplemented with 1% ovalbumin and 3% gelatin). Cells were dispersed by passage through a 22.5 gauge needle ten times and filtered twice (0.44μm) to remove clumps of cells.

Live M. pneumoniae Imaging and DAPI Staining

Cell suspensions were incubated on each substrate using a PDMS mold for one hour at 37°C. Unbound cells were then removed, surfaces were washed three times with modified SP4 medium, and fresh modified SP4 medium was added to the substrates. Substrates were imaged with live *M. pneumoniae* using a Leica DM IL inverted microscope (Leica Micro-systems, Buffalo Grove, IL) with a digital charge-coupled-device (CCD) camera (Hamamastsu Photonics K.K., Hamamatsu City, Japan) and analyzed using Openlab version 5.5.0 (PerkinElmer, MA). After imaging live *M. pneumoniae*, cells were fixed with 2% formaldehyde, 0.5% glutaraldehyde in modified SP4 growth medium for 15 minutes at room temperature, permeabilized with Triton-X100 and labeled with the fluorescent stain DAPI for 15 minutes at room temperature in the dark, surfaces are washed with PBS and dried. Cells were then imaged at 100X to visualize DAPI labeling.

Surface Characterization

The thickness of silicon substrate grafted functionalities were measured after each step using spectroscopic ellipsometry (J.A. Woollam, M-2000V) then the data were fit using a Cauchy model within the CompleteEASE® software. Static water contact angle measurements were taken using drop shape analysis (DSA100, Krüss USA, Matthews, NC, DSA3 software) by placing drops of water onto three different spots of each substrate and taking the average angle.

Reaction completion was confirmed by utilizing grazing-angle attenuated total reflectance Fourier transform infrared spectroscopy (GATR-FTIR) (Thermo Scientific, Nicolet 6700/Harrick VariGATR). Each of the quartz substrates was analyzed by UV-visible spectrophotometry (Varian, Cary 50Bio UV-visible spectrophotometer). Surface morphologies were examined by atomic force microscopy via the Scanasyst program on Bruker Multimode AFM (Scanasyst-AIR, $k = 0.4\ N \cdot m^{-1}$, resonant frequency (f_0) = 50-90 kHz).

Results and Discussion

Surface Functionalization

The strategy used for carbohydrate conjugation is shown in Scheme 2.1. Clean substrates were first functionalized with (3-aminopropyl)trimethoxysilane (APTMS), and then poly(PFPA) was spin-cast onto substrates, where some of the ester residues on the backbone react with the amine-bearing monolayer, forming a stable amide bond that prevents delamination. The grafting density of poly(PFPA) was estimated at 0.1 chains·nm^{-2} (Table 2.1). Hydrazine was then reacted with the remaining activated esters on the surface. Hydrazine was chosen as the bifunctional linker because primary amines have a fast reaction rate with poly(PFPA),[29] and the formed PAH can conjugate a variety of reducing glycans ranging from simple monosaccharides and disaccharides to relatively complex oligosaccharides.

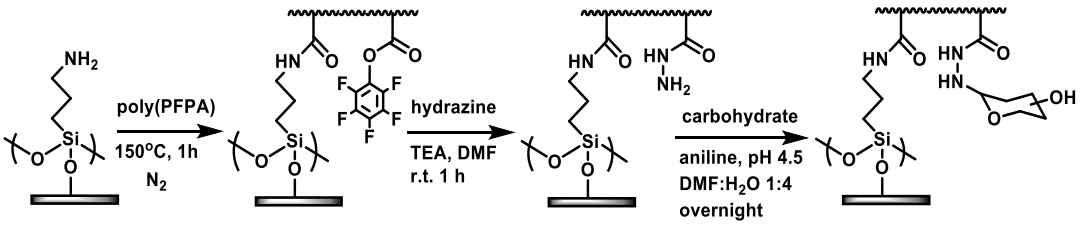

Scheme 2.1. A general carbohydrate functionalization strategy using post-polymerization modification.

Table 2.1. Thickness, density of bulk polymer, molecular weight, grafting density (σ), radius of gyration (R_g) and reduced tethering density (Σ) of poly(PFPA) coated substrates[a]

Thickness	Density	M_n	σ	R_g	Σ
11.3 nm	1.459 g·cm^{-3}	97,600 g·mol^{-1}	0.1017 chain·nm^{-2}	12.7 nm	51

[a] $\sigma = h \cdot \rho \cdot N_A / M_n$, $\Sigma = \sigma \cdot \pi \cdot R_g^2$,[36] where h is the brushes thickness, ρ is the bulk density of the brush, N_A is Avogadro's number; and R_g was measured by Dynamic Light Scattering (DLS) using a 2 mg·mL^{-1} poly(PFPA) solution in tetrahydrofuran (Malvern Instruments Zetasizer Nano ZS (Model ZEN3600) equipped with a 4 mV HeNe laser operating at λ = 633 nm with a measurement angle of 173°).

A reducing sugar, such as lactose, has a dynamic equilibrium (Scheme 2.2) between an open-chain form bearing an aldehyde group, which typically exists less than 0.1% in the equilibrium, and a cyclic pyranose (and furanose) form with a free hemiacetal group.[37] Using the open-chain form of the reducing sugar, the carbohydrate can be conjugated to the hydrazine moiety though the formation of hydrazone and hydrazide, with high chemoselectivity and high yields. Even though such conjugated compounds are thermally and hydrolytically stable under biological conditions, the formation of these conjugates usually has slow kinetics.[38] One methodology to realize a higher reaction rate is to employ an organocatalyst such as aniline, which can increase the overall reaction rate up to 20-fold.[39] The aniline attacks the carbonyl group of the reducing sugar to form an imine intermediate (Scheme 2.2) which is thought to be more rapidly protonated than the carbonyl species, facilitating the subsequent attack by hydrazine, along with regeneration of the aniline catalyst.

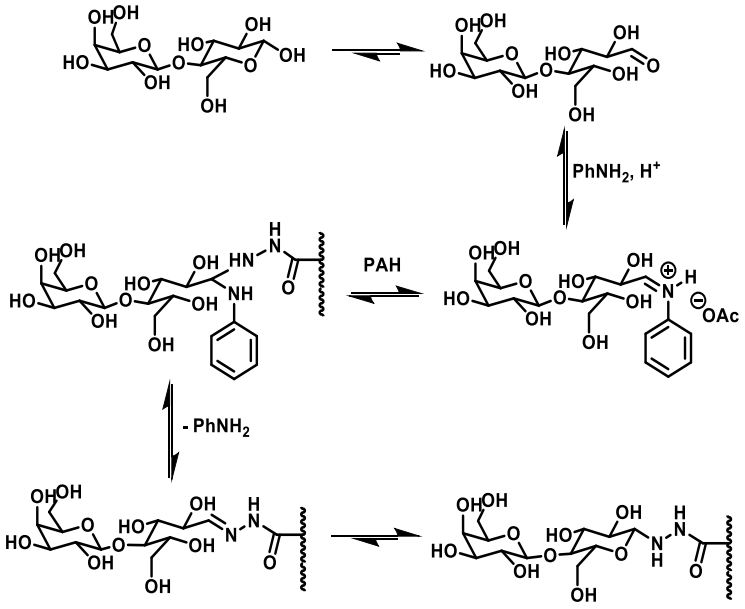

Scheme 2.2. Pathway for carbohydrate hydrozone/hydrazide formation.

Surface Characterization

In order to monitor and confirm substrate functionalization, spectroscopic ellipsometry and drop shape analysis were used to characterize thickness and contact angle changes. These results are shown in Table 2.2. On average, the amine monolayer formed with APTMS was 1.2 nm in thickness with a contact angle of 43°. After spin-coating poly(PFPA), the thickness and contact angle increased to 11 nm and 100°, respectively. Upon reacting the substrate with hydrazine, the thickness of the film decreased to 6.6 nm, and the hydrophilicity of the surface changed drastically from hydrophobic (100°) to nearly wetting (14°). The decrease in film thickness correlates well to the decrease in molecular weight of the polymer sidechain, as we have observed in previous studies.[29,40] After hydrazide formation, we examined carbohydrate conjugation using a variety of substrates, ranging from simple monosaccharides to more complex polysaccharides. Table 2.2 demonstrates that upon carbohydrate conjugation, the thickness of the films increased by ~3-4 nm and the surface remained hydrophilic with low contact angles, all

below 20°. The morphologies of each surface after each transformation were also measured by AFM (Figure 2.1), all of which show a smooth, nearly featureless topology with an RMS roughness less than 1.5 nm.

Table 2.2. Thickness and contact angle data for each functionalization step

	thickness (nm)	contact angle (°)
APTMS	1.2±0.1	43±0.3
poly(PFPA)	11.3±0.4	100±0.6
PAH	6.6±0.1	14±0.7
xylose	9.4±0.2	15±0.3
glucose	9.1±0.5	9±0.6
galactose	9.4±0.5	8±0.9
lactose	10.0±0.3	12±0.7
maltose	9.1±0.2	13±0.3
3'-sialyllactose	9.2±0.3	19±0.6

We also monitored the surface reactions using GATR-FTIR for each reaction step (Figure 2.2). The disappearance of ester carbonyl stretch at 1785 cm^{-1} and the fluorinated aromatic ring C=C stretch at 1525 cm^{-1} upon post-polymerization modification with hydrazine indicates the formation of a hydrazide linkage with clear amide peaks observed at 1658 cm^{-1} and 1540 cm^{-1}. After conjugation with the carbohydrates listed in Table 2.2, however, there were no obvious changes in the FTIR spectrum because of overlapping peaks. In order to further confirm carbohydrate conjugation, we used wheat germ agglutinin staining and *M. pnuemoniae* binding to test the biological activity of conjugated carbohydrates as discussed below.

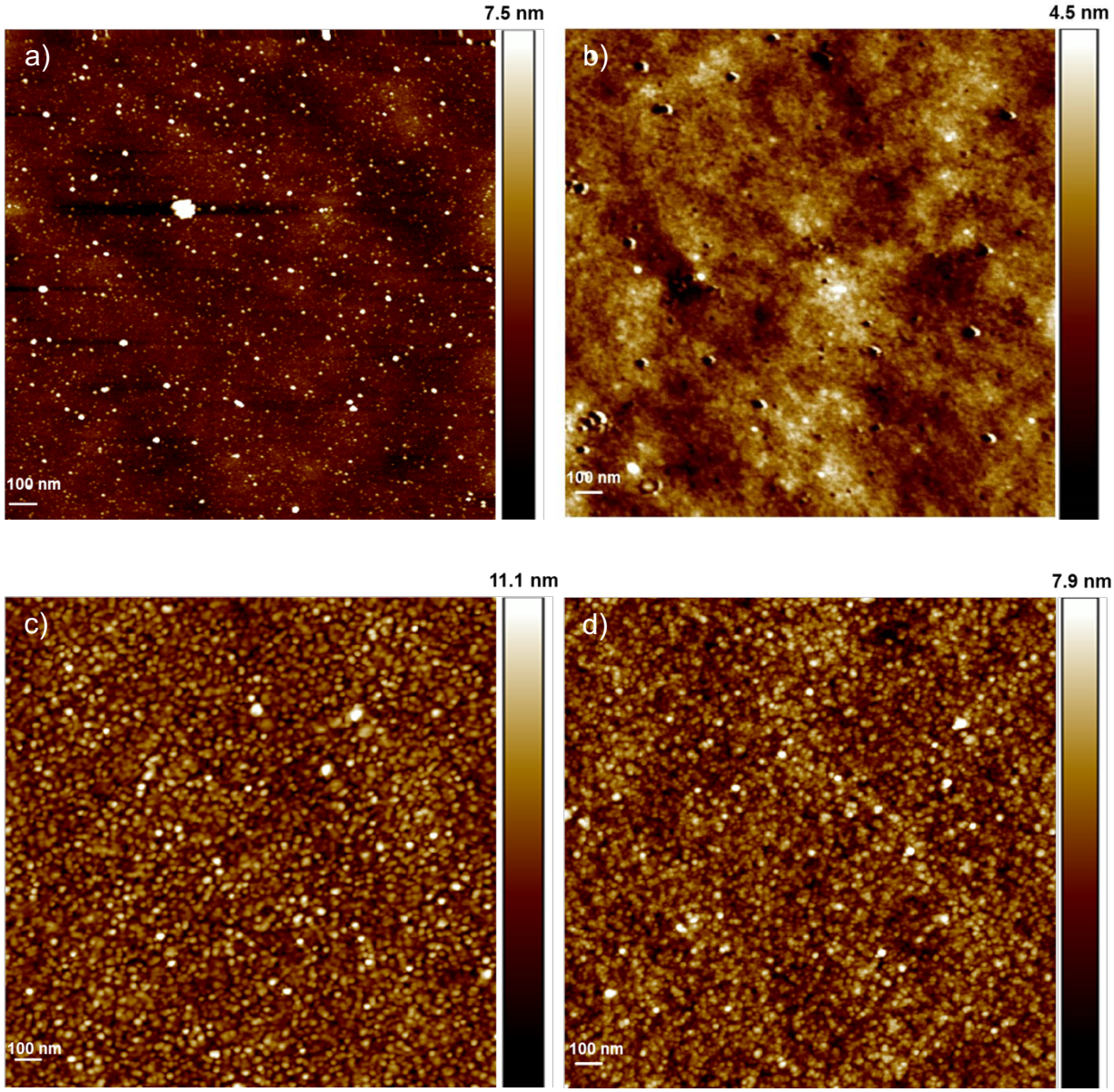

Figure 2.1. AFM images of individual steps in the carbohydrate conjugations, including (a) amine monolayer, (b) poly(PFPA) brush, (c) poly(acryloyl hydrazide) and (d) 3'-sialyllactose conjugated surface as a representative AFM image of a conjugated carbohydrate substrate. The root mean squared (RMS) roughness is (a) 0.969 nm, (b) 0.583 nm, (c) 1.55 nm, and (d) 1.11 nm respectively.

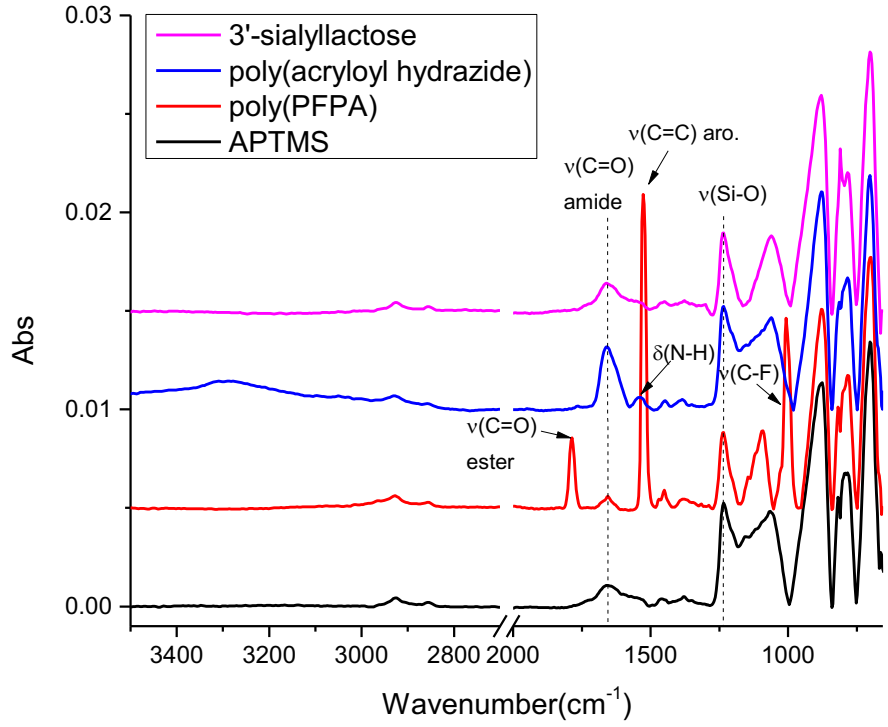

Figure 2.2. FTIR spectra of the individual steps in the carbohydrate conjugation, including amine monolayer, poly(PFPA) brush, poly(acryloyl hydrazide), and sialyllactose conjugated to the surface as a representative spectrum of a conjugated carbohydrate.

Surface Conjugated Carbohydrates Quantification

The aminolysis of grafted poly(PFPA) with 1-pyrenemethylamine (AMP), a UV-active dye, was used to determine the total surface functional group density of the poly(PFPA) brushes. The functional group density was calculated using the absorbance value of conjugated AMP at λ_{max}. The extinction coefficient for AMP was 35133 ± 252 $M^{-1} \cdot cm^{-1}$ at 345 nm, measured by a calibration curve in acetonitrile (Figure 2.3). Using Equation 1, where d is the functional density in $mol \cdot cm^{-2}$, A is absorbance, and ε is extinction coefficient of the chromophore at λ_{max}, the functional group density of the brushes can be calculated. This calculation method is used under

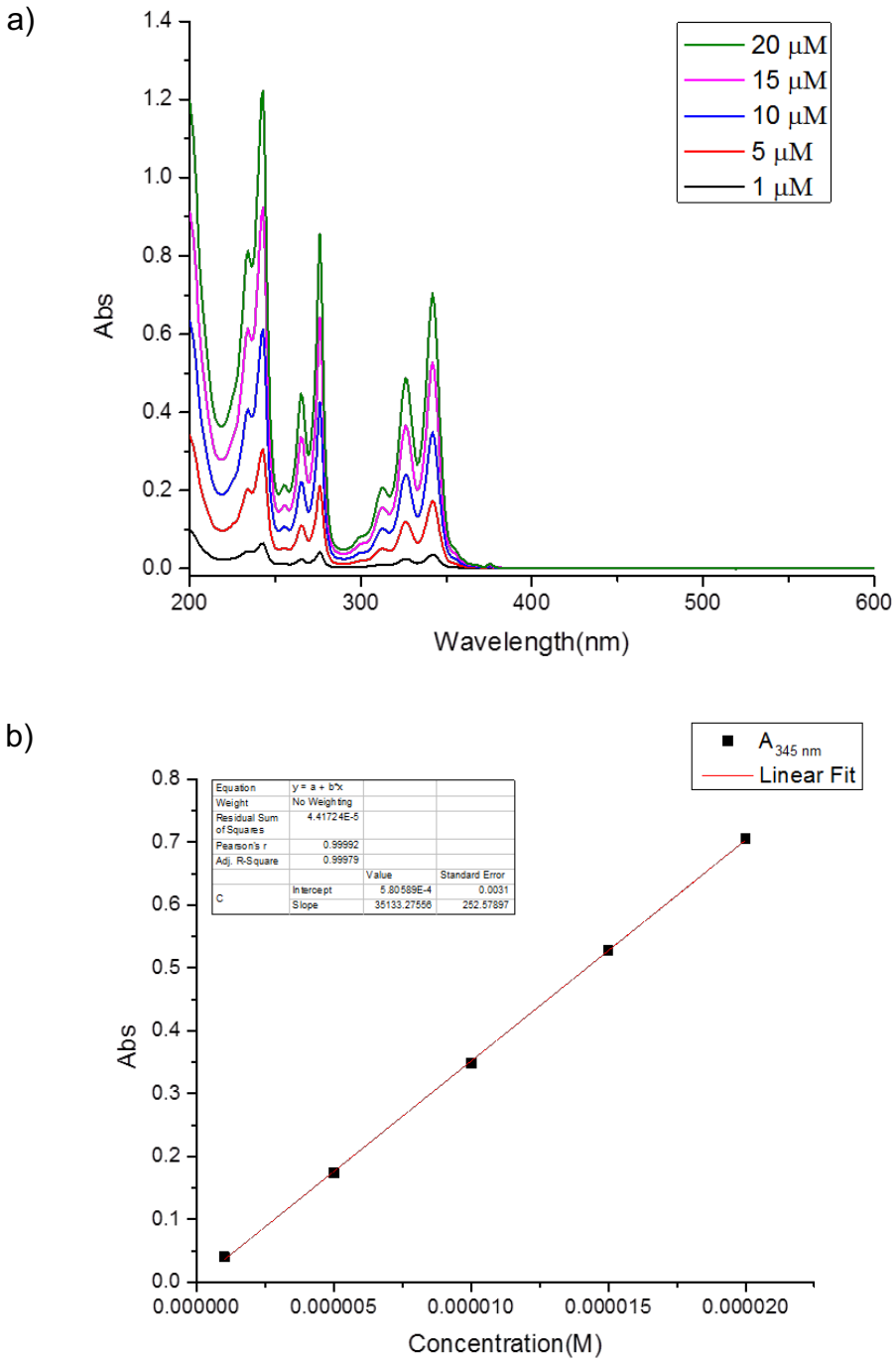

Figure 2.3. (a). UV vis spectrum of 1-pyrenemethylamine and (b). Calibration curve obtained with a series of solutions (absorbance at 345 nm).

the assumption that the difference in extinction coefficient between AMP in solution and AMP conjugated to the polymer film.

$$d = \frac{A}{\varepsilon \cdot 1000} \quad (1)$$

Figure 2.4a shows FTIR spectrum differences on the grafted surface before and after AMP modification, where amide bond formation is evident with the appearance of the amide I stretch at 1660 cm^{-1} and amide II stretch at 1520 cm^{-1}. The UV-vis absorbance of conjugated AMP shown in Figure 2.4b was 0.186±0.0012 at 350nm, which was used to calculate a total functional group density of 5.29±0.034 $nmol \cdot cm^{-2}$.

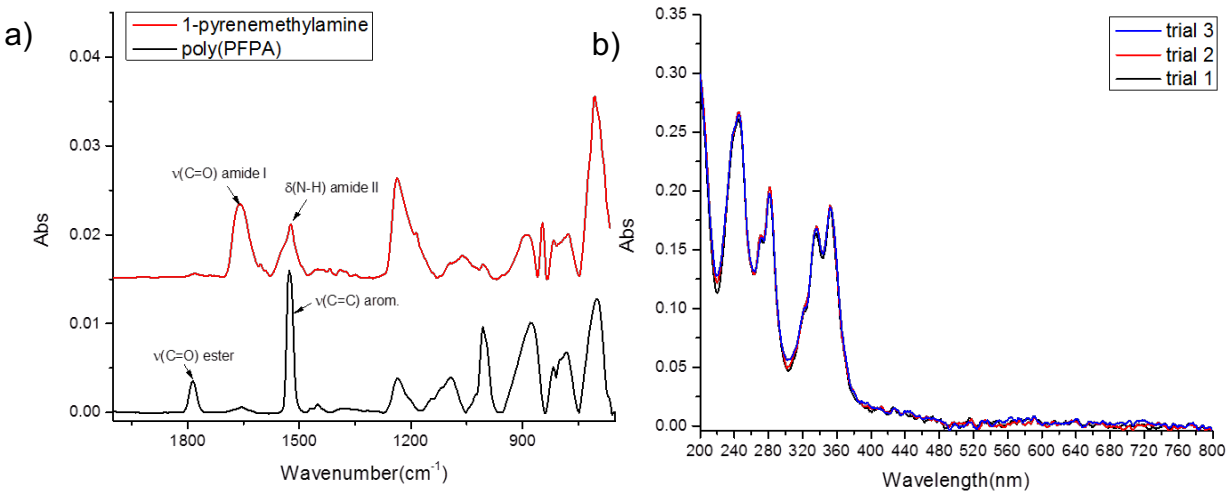

Figure 2.4. FTIR spectra (a) and UV vis spectrum (b) of conjugated 1-pyrenemethylamine on poly(PFPA) coated substrate.

After hydrazine conjugation with PFPA, *p*-nitrobenzaldehyde (NBA) was used to quantify the total number of hydrazide groups available for reaction with the carbohydrates used in this study. The extinction coefficient ε used in the calculation was estimated using the experimentally verified extinction coefficient of *p*-nitrobenzaldehyde hydrazone (NBAH), 23283±59 $M^{-1} \cdot cm^{-1}$ at 330 nm in DMF (Figure 2.5). Through imine formation, UV-vis

spectroscopy can then be used to estimate NBA functional density using the same equation as above. The PAH surface was first immersed into a solution of NBA for 15 minutes. The observed UV vis spectrum revealed the functional group density of hydrazide, which is the total number of reactive sites available for carbohydrate conjugation. The absorbance value of conjugated NBA shown in Figure 2.6b was 0.125±0.0135 at 330 nm, indicating the total hydrazide functional group density of 5.37±0.579 nmol·cm^{-2}, which was close to the total PFPA functional group density after aminolysis, and implies little to no cross-linking between adjacent hydrazide and pentafluorphenol ester moieties. The FTIR spectra in Figure 3a shows the disappearance of two amide peaks for PAH as well as the appearance of nitro group stretches at 1518 cm^{-1} and 1345 cm^{-1}, further confirming the presence of the nitro containing chromophore on the surface. Next, this NBA conjugation was repeated on substrates that had previously reacted with carbohydrates to reveal the density of hydrazide groups remaining after carbohydrate conjugation, which is the yield of the carbohydrate surface reaction. Different carbohydrates substrates were tested and compared to fully functionalized PAH in order to obtain carbohydrate coverages. By comparing the absorbance of NBA between PAH and carbohydrate substrates shown in Figure 2.6b-c and Figure 2.7, the surface coverage can be estimated. For example, the absorbance of conjugated NBA on substrate functionalized with 3'-sialyllactose (Figure 2.6c) was 0.0165±0.0012 measured by three trials, indicating that 13% of the hydrazide groups remain after carbohydrate conjugation. Therefore, the 3'-sialyllactose surface coverage is estimated at 87%, which gives a carbohydrate surface density of 4.67±0.048 nmol·cm^{-2}. Table 2.3 shows the thickness, contact angle, and carbohydrate coverage of different carbohydrate substrates, indicating nearly 80% surface coverage for all of the sugars studied.

Using this method, a carbohydrate coverage of 4.0 nmol·cm^{-2} was achieved in a ~10 nm film, which was enough to facilitate multivalent effects observed in nature.

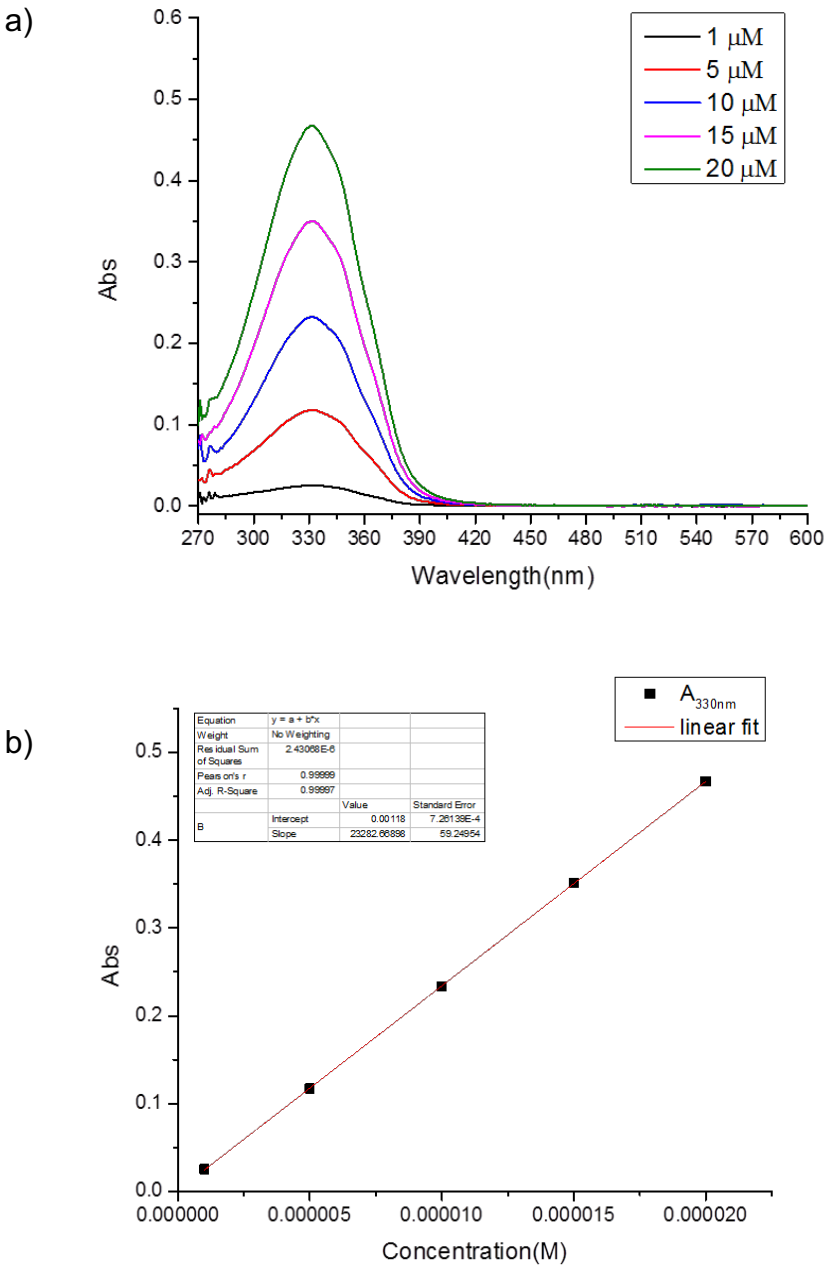

Figure 2.5. (a). UV vis spectrum of *p*-nitrobenzaldehyde hydrazine and (b). Calibration curve obtained with a series of solutions (absorbance at 345 nm).

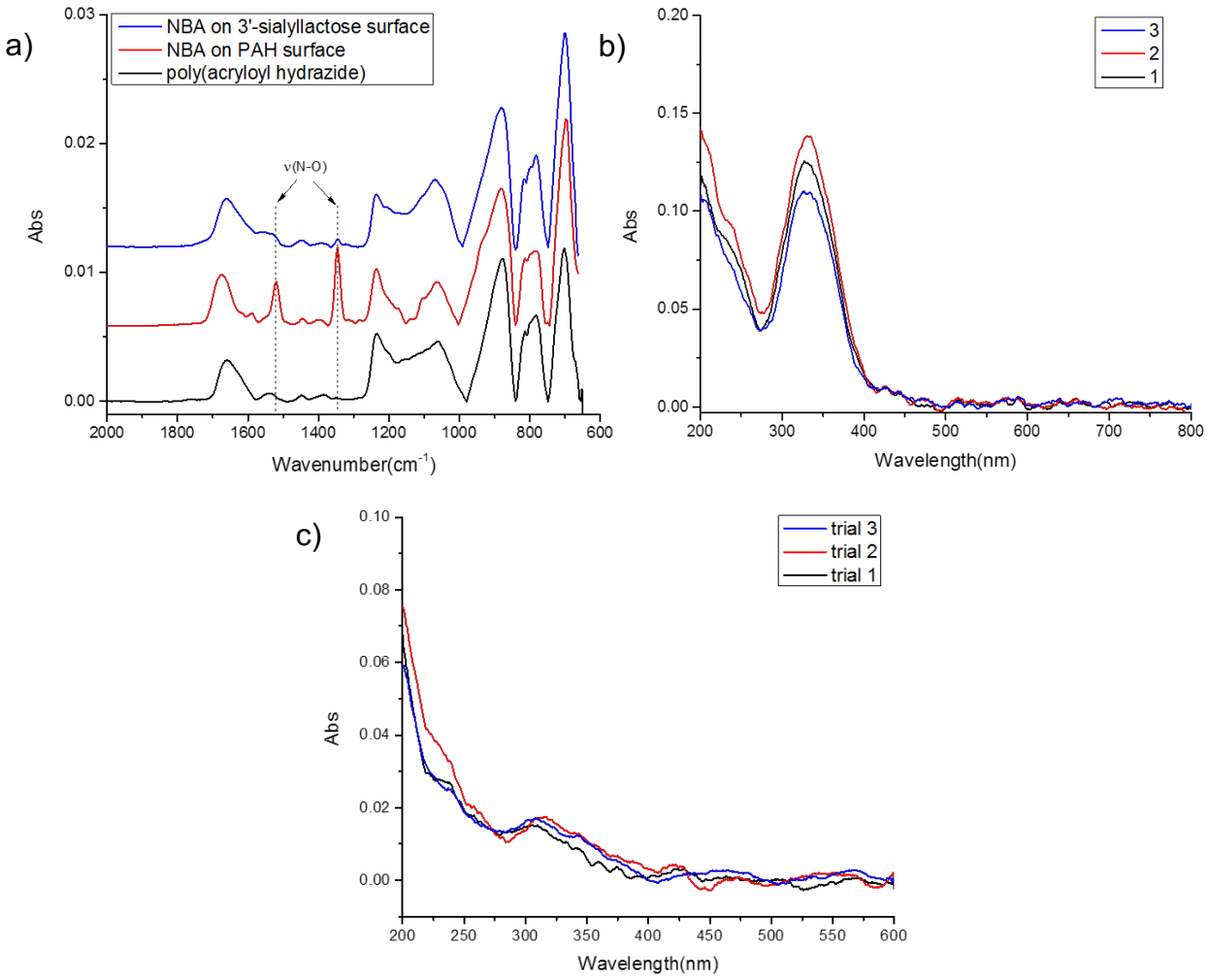

Figure 2.6. (a) FTIR spectra of conjugated NBA on a poly(acryloyl hydrazide) and 3'-sialyllactose surface, (b) UV vis spectrum of the fully functionalized PAH substrate reacted with NBA (in triplicate), (c) UV vis spectrum of NBA conjugated to 3'-sialyllactose substrate (in triplicate).

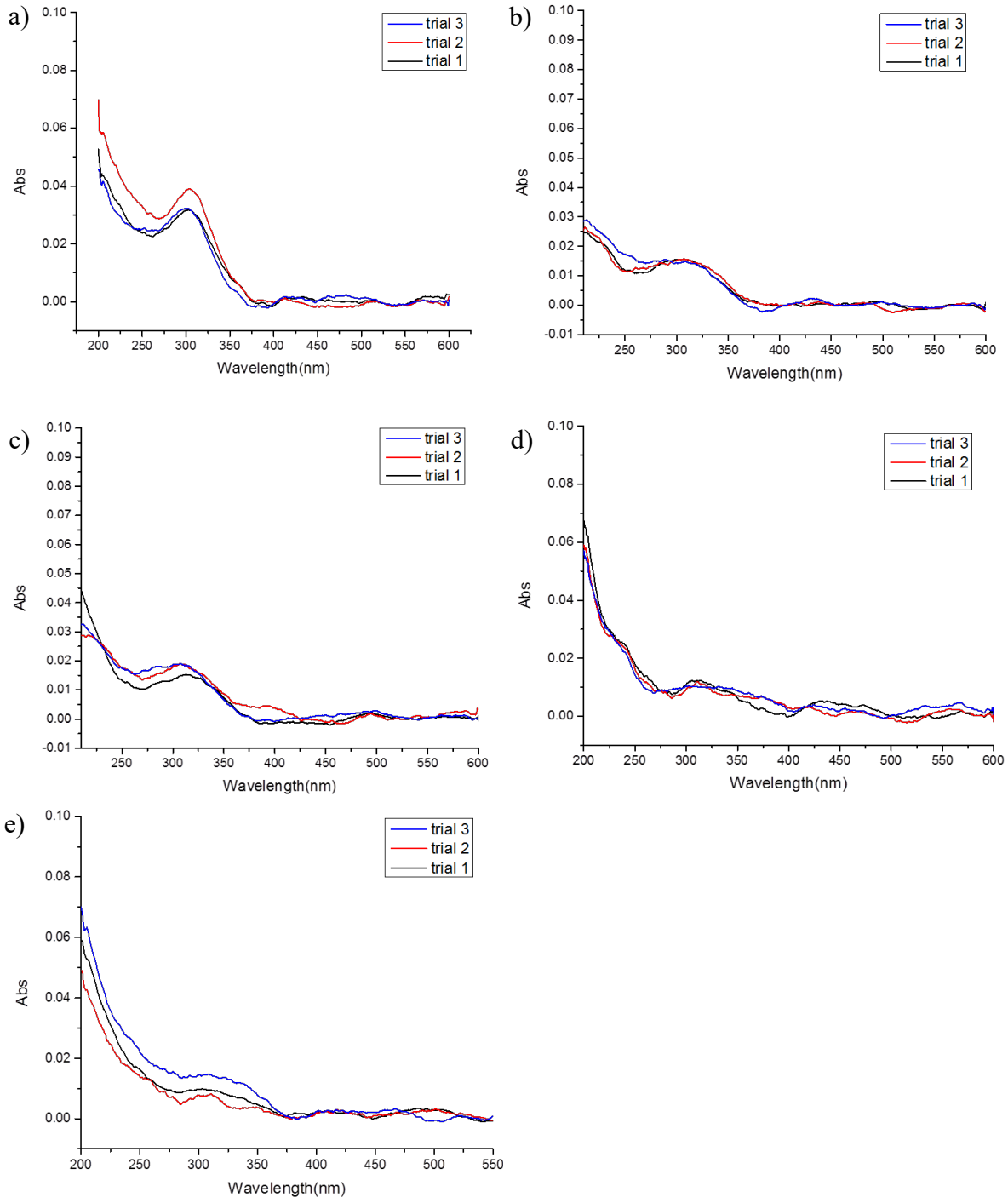

Figure 2.7. UV vis spectrum of nitrobenzaldehyde conjugated to different carbohydrates substrates, each of which was measured in three trials. The absorbance of conjugated

nitrobenzaldehyde was 0.034±0.0040 on xylose (a), 0.015±0.0004 on glucose (b), 0.018±0.0020 on galactose (c), 0.012±0.0009 on lactose (d) and 0.011±0.0033 on maltose (e), respectively.

Table 2.3. Surface Characterization after NBA Functionalization and Calculated Amount of Carbohydrate on Surface

	carbohydrate coverage	# carbohydrate molecule ($nmol \cdot cm^{-2}$)
xylose	73±3.2%	3.92±0.172
glucose	88±0.3%	4.73±0.016
galactose	86±1.6%	4.62±0.086
lactose	90±0.7%	4.83±0.038
maltose	91±2.6%	4.89±0.140
3'-sialyllactose	87±0.9%	4.67±0.048

Wheat Germ Agglutinin Staining

As mentioned above, FTIR, DSA, and SE did not yield direct evidence of the successful conjugation of carbohydrates onto the PAH platform, even though the thicknesses increased and contact angle decreased. Glycopolymers can strongly interact with saccharide recognition proteins (lectins) by multivalent effects.[41] Sialyllactose contains a 3-acetylneuraminic acid moiety which firmly binds to the lectin, wheat germ agglutinin (WGA). Here, WGA Alexa Fluor® 555 was utilized as a fluorescent probe to visualize the presence of sialyllactose conjugated to PAH films. We used reactive microcapillary printing to create 250 μm wide channels of 3'-sialyllactose on a grafted PAH substrate, which was subsequently reacted with lactose after the stamp was removed. After subsequent staining with WGA, Figure 2.8 shows the

3-sialyllactose patterns that mimicked the channel dimensions, where distinct contrast between the patterned lines of lactose and 3'-sialyllatcose are easily observed. The 3'-sialyllactose conjugated channel fluoresced bright green, while the lactose channel was dark, which demonstrates WGA binding selectively to the 3'-sialyllactose-functionalized regions. This staining technique provides indirect evidence for conjugation and confirms the carbohydrate functionalization.

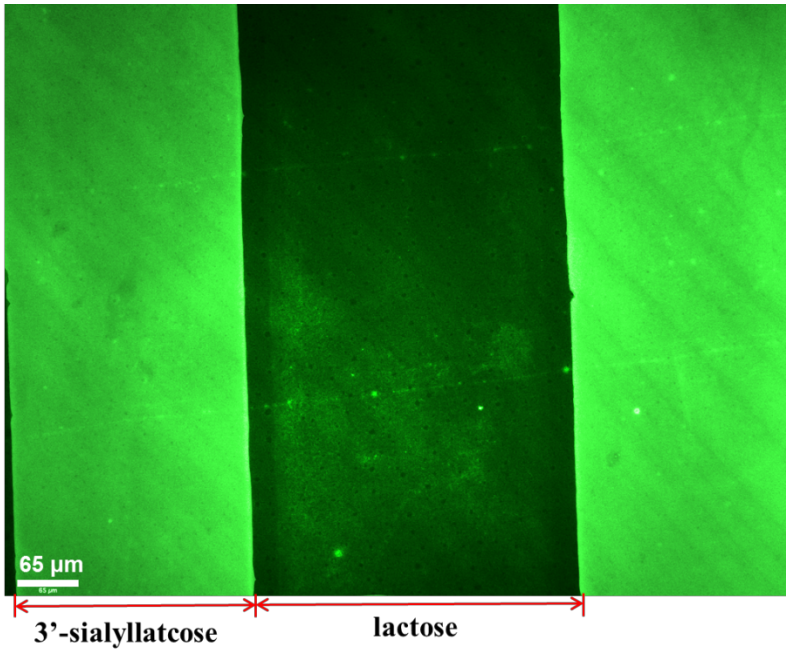

Figure 2.8. 3'-sialyllactose and lactose patterned on a PAH surface stained with fluorescent WGA to indicate successful immobilization of carbohydrates.

Live M. pneumoniae Imaging and DAPI Staining

The retention of biological activity is of great importance for glycoconjugated substrates. To test the preservation of bioactivities of conjugated carbohydrates using this method, glass coverslips were used to fabricate sialyllactose surfaces, where the interaction of incubated *M. pneumoniae* with the surface was observed by phase contrast microscopy. Glycans containing terminal 2,3-sialyl residues have been previously shown to be receptors for *M. pneumoniae*

binding to host cell surfaces.[33] Figure 2.9a shows many mycoplasma cells with a characteristic, extended cell morphology bound to the sialylated surface. DAPI staining confirms these as attached cells on the functionalized surface. As a control for specificity we also examined mycoplasma binding to PAH substrates. Figure 2.9b shows much less mycoplasma binding to PAH than that observed with the sialylated surface, confirming that binding specificity was retained with this surface modification technique.

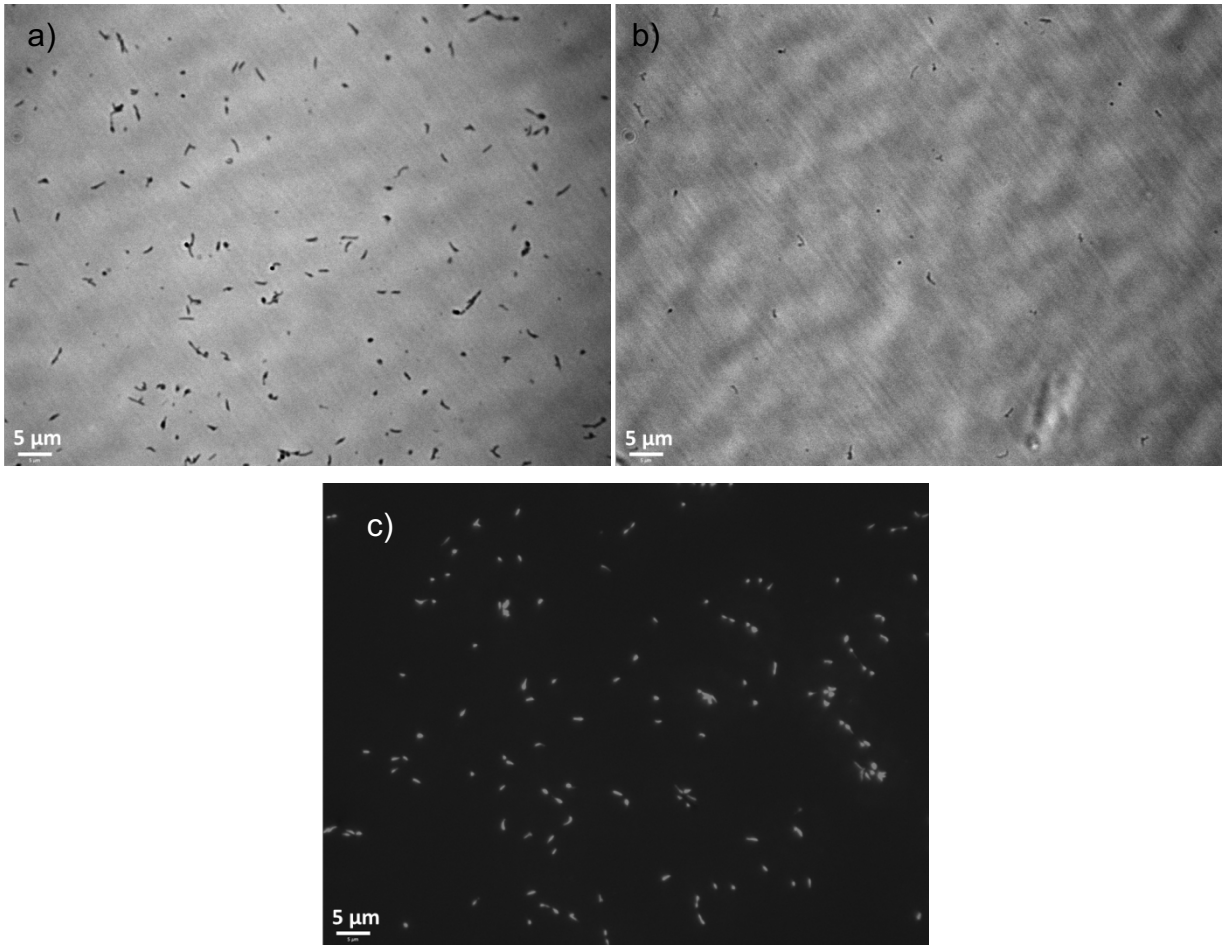

Figure 2.9. Live *M. pneumoniae* cells adhered to (a) 3'-sialyllactose conjugated and (b) PAH grafted coverslips and (c) DAPI staining on 3'-sialyllactose conjugated coverslips.

Conclusion

Here, we have reported a strategy to conjugate carbohydrates to surfaces using poly(PFPA) brushes reacted with hydrazine. This simple and straightforward approach is both highly efficient and convenient, and allows conjugation of simple and complex carbohydrates. By backfilling with a NBA chromophore, we confirmed a ligation efficiency of about 80% for various carbohydrates, which is comparable to that observed in solution.[24] Using a minimal amount of carbohydrate, we were able to effectively produce surface grafted glycopolymers where all the conjugation is through the reducing end, which mimics cell-surface glycans. This method also retains biological activity of the conjugated saccharides, using only mild processing conditions. The biorecognition and bioactivity as well as evidence for successful conjugation were confirmed through fluorescent tagged WGA binding and *M. pneumoniae* attachment to the sialyllactose conjugated surface. This methodology offers a simplified approach to fabricate carbohydrate microarrays using diverse sugar structures for high throughput screening without laborious derivatization and purification steps of the carbohydrate.

References

1. Lienkamp, K.; Noe, L.; Breniaux, M.-H.; Lieberwirth, I.; Groehn, F.; Wegner, G., *Macromolecules* **2007**, 40, 2486-2502.

2. Brown, J. M.; Xia, J.; Zhuang, B. Q.; Cho, K.-S.; Rogers, C. J.; Gama, C. I.; Rawat, M.; Tully, S. E.; Uetani, N.; Mason, D. E.; Tremblay, M. L.; Peters, E. C.; Habuchi, O.; Chen, D. F.; Hsieh-Wilson, L. C., *PNAS* **2012**, 109, 4768-4773.

3. Freeze, H. H., *Nat. Rev. Genet*. **2006**, 7, 537-551.

4. Bohorov, O.; Andersson-Sand, H.; Hoffmann, J.; Blixt, O., *Glycobiology* **2006**, 16, 21C-27C.

5. Gerland, B.; Goudot, A.; Ligeour, C.; Pourceau, G.; Meyer, A.; Vidal, S.; Gehin, T.; Vidal, O.; Souteyrand, E.; Vasseur, J.-J.; Chevolot, Y.; Morvan, F., *Bioconjugate Chem*. **2014**, 25, 379-392.

6. Ruhela, D.; Riviere, K.; Szoka, F. C., Jr., Bioconjugate Chem. 2006, 17, 1360-1363.

7. Rinaudo, M., *Polymers* **2010**, 2, 505-521.

8. Bigge, J. C.; Patel, T. P.; Bruce, J. A.; Goulding, P. N.; Charles, S. M.; Parekh, R. B., *Anal. Biochem*. **1995**, 230, 229-238.

9. Moroney, S. E.; D'Alarcao, L. J.; Goldmacher, V. S.; Lambert, J. M.; Blattler, W. A., *Biochemistry* **1987**, 26, 8390-8398.

10. Flinn, N. S.; Quibell, M.; Monk, T. P.; Ramjee, M. K.; Urch, C. J., *Bioconjugate Chem*. **2005**, 16, 722-728.

11. Wang, S.; Oommen, O. P.; Yan, H.; Varghese, O. P., *Biomacromolecules* **2013**, 14, 2427-2432.

12. Wang, Z.; Chinoy, Z. S.; Ambre, S. G.; Peng, W.; McBride, R.; de Vries, R. P.; Glushka, J.; Paulson, J. C.; Boons, G.-J., *Science* **2013**, 341, 379-383.

13. Kilcoyne, M.; Gerlach, J. Q.; Kane, M.; Joshi, L., *Anal. Methods* **2012**, 4, 2721-2728.

14. Yu, K.; Lai, B. F. L.; Foley, J. H.; Krisinger, M. J.; Conway, E. M.; Kizhakkedathu, J. N., *ACS Nano* **2014**, 8, 7687-7703.

15. Godula, K.; Bertozzi, C. R., *J. Am. Chem. Soc*. **2012**, 134, 15732-15742.

16. Appelhans, D.; Klajnert-Maculewicz, B.; Janaszewska, A.; Lazniewska, J.; Voit, B., *Chem. Soc. Rev*. **2015**, 44, 3968-3996.

17. Chen, Q.; Han, B.-H., *J. Polym. Sci., Part A: Polym. Chem*. **2009**, 47, 2948-2957.

18. Wang, X.; Wang, L.; Yang, S.; Zhang, M. M.; Xiong, Q.; Zhao, H.; Liu, L., *Macromolecules* **2014**, 47, 1999-2009.

19. Martinez, G.; Fernandez-Garcia, M.; Sanchez-Chaves, M., *J. Polym. Sci., Part A: Polym. Chem*. **2005**, 43, 18-27.

20. Ladmiral, V.; Mantovani, G.; Clarkson, G. J.; Cauet, S.; Irwin, J. L.; Haddleton, D. M., *J. Am. Chem. Soc*. **2006**, 128, 4823-4830.

21. Kumar, A.; Ujjwal, R. R.; Mittal, A.; Bansal, A.; Ojha, U., *ACS Appl. Mater. Interfaces* **2014**, 6, 1855-1865.

22. Bae, Y.; Fukushima, S.; Harada, A.; Kataoka, K., *Angew. Chem., Int. Ed*. **2003**, 42, 4640-4643.

23. Ganguly, T.; Kasten, B. B.; Bucar, D.-K.; MacGillivray, L. R.; Berkman, C. E.; Benny, P. D., *Chem. Commun*. **2011**, 47, 12846-12848.

24. Godula, K.; Bertozzi, C. R., *J. Am. Chem. Soc*. **2010**, 132, 9963-9965.

25. O'Shannessy, D. J.; Wilchek, M., *Anal. Biochem*. **1990**, 191, 1-8.

26. Zhi, Z.-L.; Powell, A. K.; Turnbull, J. E., *Anal. Chem*. **2006**, 78, 4786-4793.

27. Hoypierres, J.; Dulong, V.; Rihouey, C.; Alexandre, S.; Picton, L.; Thebault, P., *Langmuir* **2015**, 31, 254-261.

28. Brooks, K.; Razavi, M. J.; Wang, X.; Locklin, J., ACS Nano 2015, 9, 10961-10969.

29. Arnold, R. M.; Sheppard, G. R.; Locklin, J., *Macromolecules* **2012**, 45, 5444-5450.

30. Bielecki, R. M.; Doll, P.; Spencer, N. D., *Tribol. Lett*. **2013**, 49, 273-280.

31. Arnold, R. M.; McNitt, C. D.; Popik, V. V.; Locklin, J., *Chem. Commun*. **2014**, 50, 5307-5309.

32. Waites, K.; Atkinson, T. P., *Curr. Infec.t Dis. Rep.* **2009**, 11, 198-206.

33. Roberts, D. D.; Olson, L. D.; Barile, M. F.; Ginsburg, V.; Krivan, H. C., *J. Biol. Chem*. **1989**, 264, 9289-9293.

34. Kasai, T.; Nakane, D.; Ishida, H.; Ando, H.; Kiso, M.; Miyata, M., *J. Bacteriol*. **2013**, 195, 429-435.

35. Tully, J. G.; Whitcomb, R. F.; Clark, H. F.; Williamson, D. L., *Science* **1977**, 195, 892-894.

36. Brittain, W. J.; Minko, S., *J. Polym. Sci. Part A: Polym. Chem*. **2007**, 45, 3505-3512.

37. Zhu, Y.; Zajicek, J.; Serianni, A. S., *J. Org. Chem*. **2001**, 66, 6244-6251.

38. Dirksen, A.; Dirksen, S.; Hackeng, T. M.; Dawson, P. E., *J. Am. Chem. Soc*. **2006**, 128, 15602-15603.

39. Thygesen, M. B.; Munch, H.; Sauer, J.; Cló, E.; Jørgensen, M. R.; Hindsgaul, O.; Jensen, K. J., *J. Org. Chem*. **2010**, 75, 1752-1755.

40. Orski, S. V.; Fries, K. H.; Sheppard, G. R.; Locklin, J., *Langmuir* **2009**, 26, 2136-2143.

41. Miura, Y., *J. Polym. Sci., Part A: Polym. Chem*. **2007**, 45, 5031-5036.

CHAPTER 3

NEW SURFACE BOUND CARBOHYDRATE ARRAYS USED TO EXAMINE THE ATTACHMENT AND GLIDING MOTILITY OF *MYCOPLASMA PNEUMONIAE*

Chen, Li; Williams, Caitlin; Sheppard, Edward; Locklin, Jason; Krause, Duncan. Accepted by *Molecular Microbiology*. Reprinted here with permission of publisher.

Abstract

Mycoplasma pneumoniae is a common cause of human respiratory tract infection, which binds glycoprotein receptors having sialic acid residues via the P1 adhesin protein. Here, we explored the impact of sialic acid presentation on *M. pneumoniae* adherence and gliding on surfaces chemically functionalized with α-2,3- and α-2,6-sialyllactose ligated individually or in combination to a polymer scaffold in precisely controlled densities. A higher receptor density threshold was required for gliding than adherence, and receptor density influenced gliding frequency but not gliding speed. Both α-2,3- and α-2,6-sialyllactose supported *M. pneumoniae* adherence, but gliding was only observed on the former. Finally, gliding on α-2,3-sialyllactose was inhibited by α-2,6-sialyllactose when both were conjugated on the same surface, suggesting that both moieties bind P1 despite the inability of the latter to support gliding. Our results using this new surface bound carbohydrate array indicate the nature and density of host receptor moieties profoundly influences *M. pneumoniae* gliding, which could affect pathogenesis and infection outcome. Furthermore, precise functionalization of polymer scaffolds shows great promise for further analysis of sialic acid presentation and *M. pneumoniae* adherence and gliding.

Introduction

Mycoplasma pneumoniae is a small, cell wall-less bacterium with a minimal genome and limited biosynthetic capabilities and causes bronchitis and atypical or "walking" pneumonia in humans.[1] *M. pneumoniae* is responsible for up to 40% of community-acquired pneumonia in both adults and children,[2] and infections can lead to prolonged respiratory disorders, including asthma and chronic obstructive pulmonary disease.[3, 4] As a respiratory pathogen *M. pneumoniae* engages innate immune defenses but often avoids triggering an effective adaptive immune response,[5] resulting in poor clearance of the organism, chronic infection, and reinfection.[4]

M. pneumoniae adherence and gliding motility are essential for colonization of the airway mucosa and are mediated by a multifunctional, membrane-bound cell extension, the terminal or attachment organelle.[6] The terminal organelle is complex, with eleven distinct substructures evident by electron cryotomography.[7] Most relevant to the current study are the protein knobs that line the outer surface of the terminal organelle at its distal end and correspond to P1 adhesin complexes.[8-10] The terminal organelle constitutes the gliding motor,[11] but the gliding mechanism is unique and poorly understood.[12] A gliding model based on electron cryotomography analysis asserts that conformational changes in the terminal organelle interior mobilize P1 adhesin complexes to treadmill on the mycoplasma surface.[7, 10] Consistent with a direct role for P1 in gliding, P1-specific monoclonal antibodies detach gliding but not static mycoplasmas from an inert surface.[13]

M. pneumoniae engages sialylated glycoproteins as receptors for adherence to respiratory epithelium, based on the inhibition of mycoplasma attachment *in vitro* by pretreatment of host tissue with neuraminidase to remove terminal sialic acid residues.[14] Sialylated serum glycoproteins in mycoplasma growth media enable *M. pneumoniae* attachment to the plastic

surface of cell culture flasks, and mycoplasma binding to sialylated receptors can be modeled using glycoproteins alone.[15] Sialylated glycoproteins having α-2,3 linkages, such as fetuin and laminin, but not those having α-2,6 linkages, such as human plasma fibronectin and fibrinogen, support *M. pneumoniae* attachment to inert surfaces.[15] Furthermore, pre-treatment with neuraminidase or competition with soluble laminin, α-2,3-sialyllactose, or other synthetic sialylated compounds having α-2,3-linked sialic acid, significantly reduces *M. pneumoniae* attachment[14] and subsequent gliding on sialylated glycoproteins.[16] Significantly, α-2,6-sialyllactose and synthetic sialylated compounds with α-2,6-linked sialic acid also inhibit binding and gliding, but require higher concentrations to do so.[15, 16] Thus *M. pneumoniae* receptor specificity is nuanced, particularly *in vivo* where diverse sialic acid linkages and other modifications are found, and as such is perhaps similar to the better characterized binding of influenza virus hemagglutinins to sialylated receptors.[17]

In the current study, we used a precisely tunable model system to explore further the interaction of *M. pneumoniae* with sialylated receptor populations *in vitro*. This model employed a protocol for surface-grafted glycopolymer construction[18] that allowed us to control the oligosaccharide chemical presentation and surface grafting density. The surface density of sialylated residues influenced *M. pneumoniae* gliding frequency but not gliding speed. And while both α-2,3- and α-2,6-sialyllactose supported *M. pneumoniae* adherence to an inert surface, gliding motility was only observed on the former. However, when α-2,6- and α-2,3-sialyllactose were both conjugated to the surface, the former inhibited gliding on the latter. Our results demonstrate that differences in receptor environment affect gliding capability, which could influence the outcome of airway colonization in the human host. Elucidating the dynamics of

mycoplasma – host receptor interactions will lead to a better understanding of pathogenesis and persistence in *M. pneumoniae* the human airway.

Experimental

Chemically functionalized surfaces

All glass coverslip substrates with grafted poly(PFPA) brushes were fabricated as described previously.[18] Hydrazide linkages for conjugating reducing sugars to the poly(PFPA) were generated by incubating the poly(PFPA)-grafted substrates in dimethylformamide (DMF) containing hydrazine monohydrate and trimethylamine. We controlled the density of hydrazide linkers by replacing various percentages of hydrazine with ethanolamine hydrochloride. These were allowed to react with the poly(PFPA) substrates for 2 h at room temperature, rinsed with DMF, and dried under a stream of nitrogen. To conjugate the sialyllactose, the disaccharide sodium salt (Carbosynth) (10 mM) and aniline (100 mM) were dissolved in 100 mM sodium acetate buffer (pH 4.5). The hydrazine/ethanolamine-modified substrates were incubated with the sialyllactose solutions in a moisture chamber for 24 h, rinsed with water, and dried under a stream of nitrogen.

To quantify the percentage of hydrazide on poly(PFPA) surfaces, coverslips prepared in parallel were incubated with *p*-nitrobenzaldehyde (0.03 mmol) dissolved in DMF/water (1:1 vol/vol) and then aniline (0.3 mmol) and the pH adjusted to 4.5 with 2 M HCl. After 2 h the substrates were rinsed with DMF, water, DMF again, and then dried under a stream of nitrogen. The absorbance of conjugated *p*-nitrobenzaldehyde on each quartz substrates was measured by UV-vis spectrometry and surface hydrazide percentages calculated by comparing the absorbance of hydrazine/ethanolamine-modified substrates with that of substrates modified with 100%

hydrazine. The corresponding density was calculated by $d = \frac{A}{\varepsilon \cdot 1000} N_a$, where A is absorbance, ε is the extinction coefficient of chromophore at λ_{max}, and N_a is Avogadro's number.

M. pneumoniae culture

We grew *M. pneumoniae* wild-type strain M129 (38) for 72 h at 37°C in tissue culture flasks in SP4 medium[19] containing fetal bovine serum (FBS). When cultures reached mid-log phase (pH 6.9-7.1), the growth medium was removed and the culture vessels were washed three times with phosphate buffered saline (PBS; pH 7.2). Mycoplasmas were then scraped from the surface into PBS and harvested by centrifugation at 20,000 × *g* for 20 min at 4°C. The resulting pellets were washed once with PBS by centrifugation, suspended in modified SP4 medium (mSP4; no FBS and phenol red), plus 5% ovalbumin (Sigma-Aldrich), syringe-passaged ten times using a 25 gauge needle to disperse the cells, and syringed-filtered twice through a 0.45µm filter to remove cell clumps.

Analysis of M. pneumoniae binding and gliding

M. pneumoniae cell suspensions of 10^7-10^8 color-change units[20] in 600-µl volumes and prepared as described above were added to each pre-treated chambered coverglass well and incubated 1 h at 37°C.[21] The culture medium was removed, each well was washed three times with mSP4 to remove unattached mycoplasmas, and 600 µl mSP4 plus 3% gelatin was added per well. We examined coverglasses by using a DM IRB inverted microscope (Leica Microsystems) and captured images with a digital charge-coupled-device camera (Hamamastsu Photonics K.K.). Images were analyzed using Openlab version 5.5.0 (PerkinElmer). We quantified binding by direct microscopic counts from phase contrast images. For direct microscopic counts, we analyzed 10 fields of view from three replicates, counting only individual mycoplasma cells and excluding occasional clumps of cells. Neuraminidase (Sigma-Aldrich) treatments were done for

1 hour at 37°C , using 0.5units per well for all assays, following sugar functionalization. We assessed gliding motility as described previously.[22] Briefly, we captured time-lapse movies for mycoplasma cultures maintained at 37°C in an incubator chamber surrounding the microscope (Solent Scientific). We calculated gliding speed for individual cells over a minimum of 20 uninterrupted frames at a constant time interval along a collision-free cell path, with paths tracked using Openlab software. We used those measurements to calculate average gliding frequency for a minimum of 200 cells, and gliding speed for a minimum of 100 cells, per experimental treatment per experiment. Results are presented as the means and positive standard errors of the mean for each treatment from three independent experiments.

Statistics

Data on cell attachment and gliding percentage were analyzed in SigmaPlot (systat Software) by multivariate analysis of variance followed by Holm-Sidak post hoc pairwise comparisons.

Results and Discussion

Surface-grafted glycopolymer and quantification method

We used hydrazine to connect various reducing sugars with poly(PFPA) scaffold which has been described previously. Poly(PFPA) was first spin-coated on (3-aminopropyl)trimethoxysilane (APTMS) modified substrates where some of the ester moieties react with amine on the surface to form covalent bond. Then hydrazine and ethanolamine with various ratios were conjugated to the polymeric scaffold leaving reactive handles, hydrazide, for the further carbohydrate functionalization, 3'- and 6'-sialyllactose specifically (Figure 1). To probe the chemical modifications in each individual steps, ellipsometry, DSA and FTIR were employed to detect thickness, hydrophobicity and chemical changes of the thin polymer film,

respectively. Table A.1 shows the thickness and contact angle changes of each functionalization steps in five selected ratios of hydrazine and ethanolamine, 0.1%, 0.5%, 1%, 2.5% and 100% respectively. One average, hydrophilic glycosurface with thickness of ~10 nm was built on ~15 nm poly(PFPA) hydrophobic films through hydrazine linker. The morphologies of each surface in different steps were measured using AFM, shown in Figure A.1, all of which demonstrate smooth and featureless topologies with a root mean squared (RMS) roughness ~1 nm. The chemical changes of polymer films monitored by FTIR are shown in Figure A.2. The disappearance of ester carbonyl stretch at 1785 cm^{-1} and fluorinated aromatic ring C=C stretch at 1525 cm^{-1} and C-F stretch at 1005 cm^{-1} upon hydrazine/ethanolamine conjugation indicate the formation of a amide linkage with a clear appearance of amide I peaks at 1655 cm^{-1}, and amide II peak at 1530 cm^{-1} for 100% hydrazine conjugation while at 1560 cm^{-1} for 0.5% hydrazine/ethanolamine conjugation. Amide II band is believed to be due to the coupling of N-H bending and C-N stretching vibration which are strongly perturbed by H bonding.[23] The H-bond is mainly formed by NH…C=O in 100% hydrazine conjugation case while by NH…O-H in ethanolamine dominated conjugation case, resulting in the shift of amide II peak.

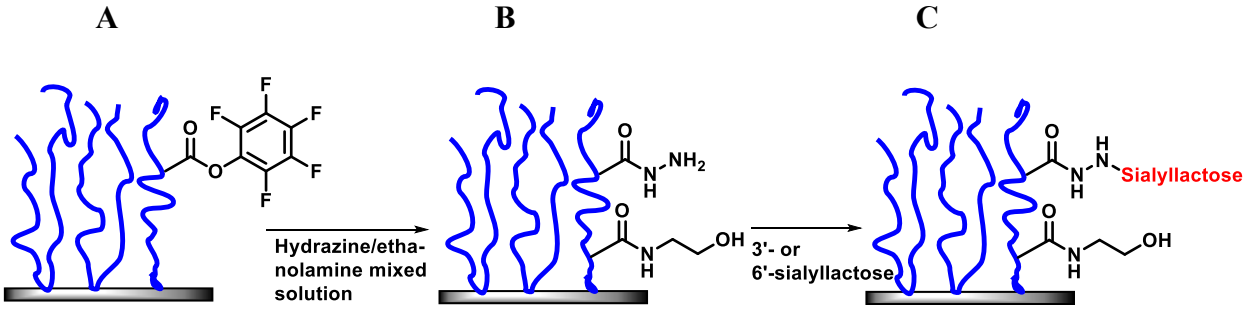

Figure 3.1. Schematic representation of poly(PFPA) brushes conjugated to glass. (**A**), with the subsequent conjugation of hydrazine at various ratios with competing ethanolamine (**B**), dictating the density of hydrazide available for (**C**) ligation with the reducing end of sialyllactose.

Several different ratios of hydrazine/ethanolamine solution were prepared to conjugate poly(PFPA) scaffold, giving rise to poly(acryloyl hydrazide-co-*N*-hydroxylethyl acrylamide) (poly(AH-co-HEAA)) coated surface where varied amounts of PAH moiety is the reactive handle for carbohydrate modification. Due to different reactivity towards aminolysis where hydrazine is expected to be more nucleophile than ethanolamine, the ratios of conjugated hydrazine, which is poly(acryloyl hydrazide) (PAH), is not expected to be the same with feeding ratios. Here we used *p*-nitrobenzaldehyde (NBA), a UV-active dye with an extinction coefficient ε of 23283±59 $M^{-1}\cdot cm^{-1}$ at 330 nm, to quantify the density of PAH on the surface. Through imine formation, NBA covalently binds to PAH moiety in the copolymer. Using equation 1, where d is the functional density in molecules/cm^2, A is absorbance, ε is the extinction coefficient of chromophore at λ_{max}, and Na is Avogadro's number, the conjugated NBA functional density can be estimated, equivalent to PAH moiety density. For example, NBA conjugated substrate that was fully functionalized with hydrazide gives an average UV-vis absorbance of 0.125 at 330 nm, yielding the total PAH density of 3.3×10^{15} molecules/cm^2.

$$d = \frac{A}{\varepsilon \cdot 1000} N_a \qquad (1)$$

By comparing the calculated PAH density with that of 100% hydrazine conjugation, the fully functionalized PAH substrate, the ratio of PAH in poly(AH-co-HEAA) can be figured. A calibration curve in a range of 0.1% to 1% hydrazine (in solution) is demonstrated in Figure 2, giving a linear relationship of PAH percentage on surface (y%) and hydrazine percentage in solution (x%) in equation 2. Using equation 2, the conjugated hydrazide ratio, PAH%, can be estimated with a known percentage of hydrazine in the mixed solution. Table 1 shows the estimated PAH% on surface corresponding to the five selected ratios of hydrazine in solution.

$$y = 19.7817x\% + 0.26817 \qquad (2)$$

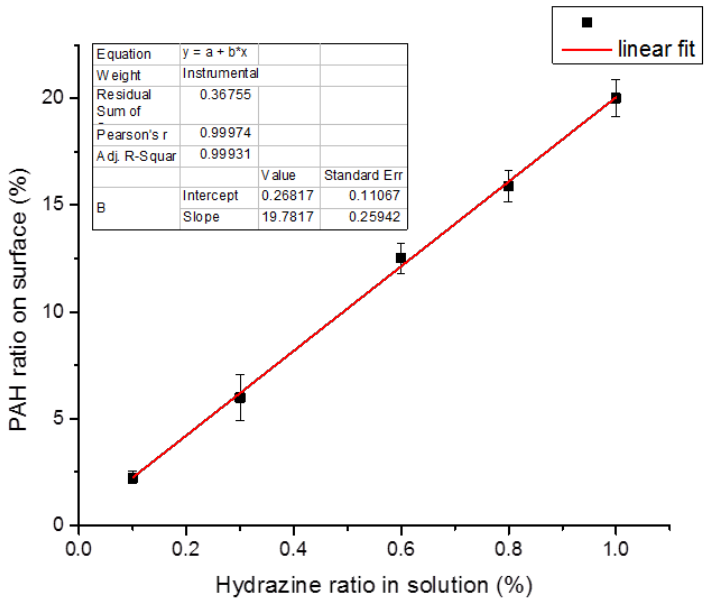

Figure 3.2. PAH ratio on surface is proportional to hydrazine ratio in solution in the range of 0.1% to 1% and the fitted linear relationship is $y\%=19.7817x\%+0.26817$ with a R^2 value of 0.99931.

Table 3.1. PAH%, 3'-SL% and corresponding density quantifications

Hydrazine% in sln	PAH% on surface	3'-SL% on surface	3'-SL density (molecules/cm^2)
0.1%	2%	1.6%	5.4×10^{13}
0.5%	10%	8%	2.7×10^{14}
1%	20%	16%	5.4×10^{14}
2.5%	40%	32%	1.1×10^{15}
100%	100%	80%	2.7×10^{15}

We used the same strategy discussed above to quantify the remaining PAH% after carbohydrate conjugation. NBA conjugation was repeated on substrates that previously reacted with carbohydrate. This work had been done in our previously published paper, indicating nearly

80% carbohydrate coverage in a fully functionalized PAH substrate.1 We assume the ratio of PAH on surface doesn't significantly affect carbohydrate ligation efficiency; therefore, all the substrates with varied percentages of PAH were estimated to yield similar carbohydrate ligation efficiency of 80%. Under this assumption, 3'-SL% and 3'-SL density can be simply calculated in each case, shown in Table 2. Since the only difference of 3'-SL and 6'-SL is the sialic acid displayed position either in an α-2, 3 linkage (3'-SL) or α-2, 6 linkage(6'-SL), the chemical reactivity is not expected to be drastically altered. Thus, 6'-SL shares the same carbohydrate coverage and density results with 3'-SL.

M. pneumoniae attachment to sialyllactose-functionalized surfaces

Sialylated glycoproteins receptors are significantly important in *M. pneumoniae* colonizing human airway and in vitro proxied thereof.[14, 24] This also encompasses mycoplasma gliding on inert surfaces, and likely on epithelial surfaces, although this has only been observed indirectly.[16, 25, 26] The gliding motility requires repeated binding and release of receptors to effect sustained movement across the surface.[27, 28] *M. pneumoniae* exhibits higher binding affinity in suspension for sialic acid having α-2,3 linkages over α-2,6 linkages,[16] but the nature of surface-bound receptor recognition in *M. pneumoniae* attachment and gliding is otherwise poorly understood and likely influenced by variability in the local receptor environment. The previously-used glycoprotein physisorption method offers a convenient and easy model to study *M. pneumoniae*-receptor interactions. However, this method has several significant limitations, such as the poorly defined actual amount of glycoprotein receptors bound to the surfaces, and little to no control over carbohydrate linkages, composition, or arrangement. To solve all of these limitations, we recently proposed a versatile methodology for ligating saccharides at the reducing end to poly(PFPA)-coated substrates through hydrazine linker.[18]

Using this approach, 3'- and 6'-SL were ligated onto surface at densities ranging from 1.6% to 80%, shown in Table 1. Figure 3 demonstrate cells attachment on 3'- and 6'-SL surfaces with various receptor densities. Both 3'- and 6'-SL supported *M. pneumoniae* in a concentration-dependent manner. Attachment to 3'-SL at densities of 16%, 32% and 80% was statistically comparable to that seen with SP4 growth media control and binding saturation was observed at 16% 3'-SL. On the hand, attachment to 6'-SL was significant but substantially lower than for 3'-SL and never achieved the levels seen for SP4 control. This is consistent with both the lower binding affinity reported for *M. pneumoniae* and 3'-SL in suspension[16] and the higher levels of 3'-SL required to inhibit *M. pneumoniae* attachment to laminin.[15] All these attachments were believed to be directly related to the present sialic acid receptors on the surface, because only very minimal attachments (less than 10 cells per field) were observed on poly(PFPA) scaffold with 100% ethanolamine or hydrazine (no sialyllactose; data not shown).

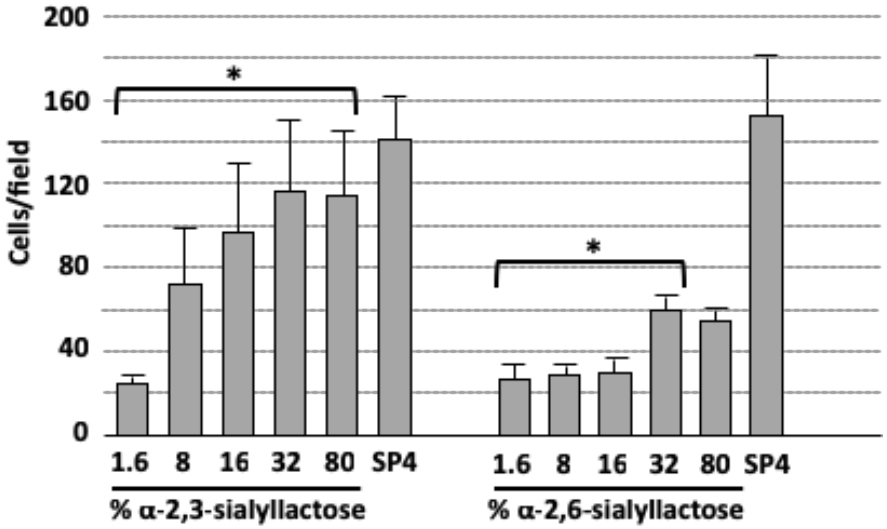

Figure 3.3. *M. pneumoniae* attachment to slides chemically functionalized with α-2,3- or α-2,6-sialyllactose, as indicated. Each bar represents the mean and positive standard error of the mean for total cell counts at a given sialyllactose percentage for three separate experiments. SP4,

chamber slides coated with SP4 growth medium as a positive control. * $P < 0.001$ for cell numbers on 1.6% α-2,3-sialyllactose relative to the higher α-2,3-sialyllactose percentages; ** $P < 0.001$ for cell numbers on 32% and 80% α-2,6-sialyllactose relative to the lower α-2,6-sialyllactose percentages; *** $P < 0.001$ for cell numbers on SP4 relative to all percentages of α-2,6-sialyllactose.

Neuraminidase is a class of glycoside hydrolase enzymes that can cleave the glycosidic linkages of sialic acids (or neuraminic acids). Treatment 3'- and 6'-SL with neuraminidase resulted in significantly decreased attachment, confirming the specificity for the sialic acids (Figure 4). Increasing the amount of neuraminidase or treatment time did not yield further reduced attachments (data not shown). The residual *M. pneumoniae* attachment to neuraminidase-treated sialyllactose probably indicates its binding to the remaining lactose after removal of sialic acid residues, based upon the previous report on low level of mycoplasma binding to lactosylceramide.[29]

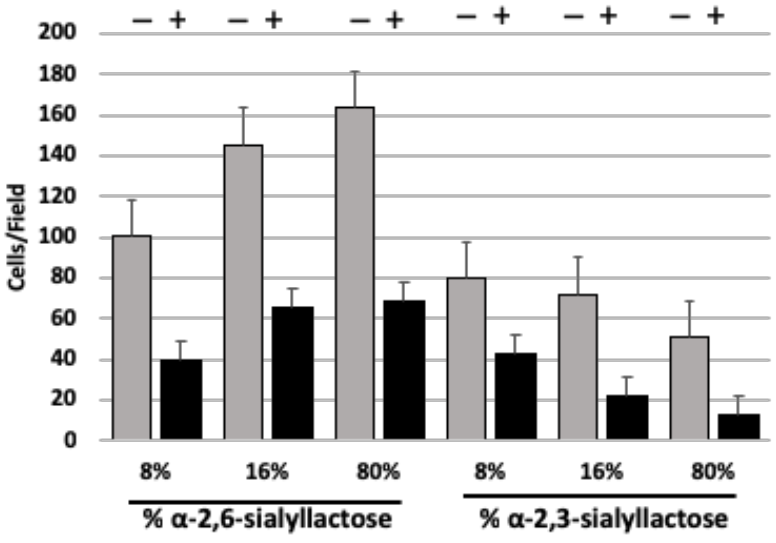

Figure 3.4. *M. pneumoniae* attachment to slides functionalized with sialyllactose with and without pre-treatment with neuraminidase. Each bar represents the mean and positive standard

error of the mean for attached cells for three separate experiments. SP4, data for chamber slides coated with serum glycoproteins in SP4 growth medium, which served as a positive control. + / -, with or without neuraminidase pre-treatment ($P < 0.001$).

M. pneumoniae gliding on sialyllactose-functionalized surfaces

Only 3'-SL supported M. pneumoniae gliding motility and no gliding was observed on surfaces with 6'-SL at any concentrations, or on 3'-SL following pre-treatment with neuraminidase (data not shown). Shown in Figure 5, there was no gliding cell on surface with a 3'-SL ligation density lower than 8%, despite the significant level of attachment noted in Figure 3. Gliding was prominent at densities of 8% and higher. Gliding frequency generally followed an increasing trend from 8% to 32%. Mean gliding speed for all cells measured was 0.28-0.30 μm/sec for all 3'-SL densities that supported gliding, tracking 200 cells per ratio in triplicate. The observed gliding threshold are consistent with the two-step model of gliding motility for *M. pneumoniae*,[28] where the "catch and release" interaction that is believed to occurs between P1 adhesin complex and sialylated receptors occurs repeatedly during gliding across the surface. The P1 complex appears to engage both α-2,3 and α-2,6-sialyl receptors, supported by the capability of either in solution to competitively inhibit receptor binding by M. pneumoniae, resulting in their detachment from the surface,[16] and by our attachment data in Figure 3 and 4. However, sialic acid linked α-2,3 but not α-2,6 may trigger a secondary recognition event, such as a conformational change in the adhesin complex, resulting in engagement of the bound adhesin complex in treadmilling, and initiation of gliding. *M. pneumoniae* attachment may be similar in this respect to the two-step initial and tight binding described for gliding by *Mycoplasma mobile*.[27] If sialic acid linked α-2,3 is too sparse, insufficient P1 adhesin engage to drive cells movement and gliding motility. In this study, no gliding occurred on 3'-SL

functionalized surfaces having sialic acid densities below an estimated 0.54 residues/nm^2. It should be noted that the poly(PFPA) matrix extends into three-dimensional space, but we did not consider depth in our sialyllactose density estimate for two reasons. First, we recorded thickness of the coating for dehydrated matrices, and the depth of the dehydrated matrix will vary with extent of conjugation. Second, the average conjugation efficiency with different saccharides may vary from 80% to 90%, and it is unknown if conjugation is uniform throughout the depth of the film or may reflect steric inhibition within the matrix.

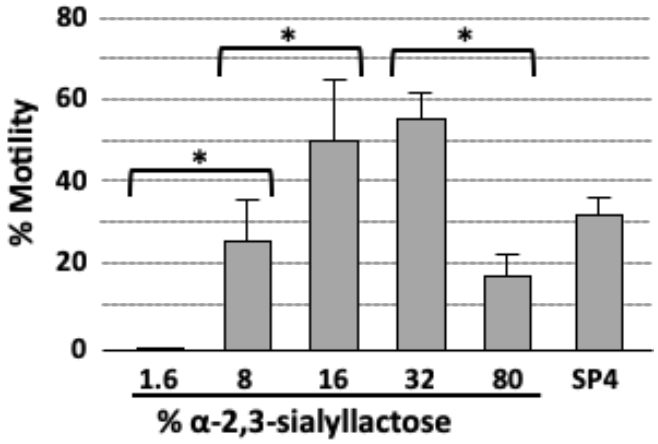

Figure 3.5. Gliding frequency for *M. pneumoniae* cells attached to chemically functionalized slides with α 2-3 sialyllactose. Each bar represents the mean and positive standard error of the mean for gliding frequency for three separate experiments. SP4, data for chamber slides coated with serum glycoproteins in SP4 growth medium, which served as a positive control. *P<0.001 for the indicated sialyllactose densities.

Another interesting phenomenon we observed is that mycoplasma gliding frequency increased with 3'-SL density but only to a point (Figure 5). At the highest density tested 80%, *M. pneumoniae* gliding frequency decreased relative to the maximum gliding frequencies observed at lower sialyllactose densities. This reduction might reflect an avidity issue, where too many

adhesin complexes are engaged and therefore unavailable to sustain cell movement via treadmilling. In contrast, gliding speed did not change with receptor densities.

Competing receptors on 3'-sialyllactose surfaces

It has been reported that sialic acid linked both α-2,3 and α-2,6 are expressed on the surface of human bronchial epithelial cells differentiated *in vitro*.[30] However, the relative distribution of each linkage type reportedly varies in different regions of intact airways.[31] In all cases, it is clear that the airway mucosa presents a heterogeneous array of sialylated and other oligosaccharides, with *M. pneumoniae* likely to encounter sialic acids in diverse linkages and relative abundance. In order to explore how this diversity might affect M. pneumoniae attachment and gliding behavior, we conjugated both 3'- and 6'-SL to poly(PFPA) scaffold at different ratios, shown in Table 2. We also prepared poly(PFPA) surfaces in parallel with competing ethanolamine, in the manner described in Table 1, to allow direct comparison on an equivalent density of 3'-SL alone. In each case, the additional conjugated 6'-SL on 3'-SL surfaces significantly reduced both the level of mycoplasma attachment and the gliding frequency (Figure 6) below that observed on 3'-SL alone at the same density. We believe this inhibition is competition by 6'-SL for putative binding by P1 adhesin complexes engaged with 3'-SL and therefore contributing to cell movement. This likely interplay between P1 adhesin and sialic acids having diverse linkages and presentations on airway epithelium could have a profound impact on mycoplasma localization and mobilization in different regions of the conducting airways, depending on the relative abundance of each sialyl linkage.

Table 3.2. M. pneumoniae attachment and gliding motility on surface having 3'- and 6'-SL conjugated individually and in combination at the indicated ratios

3'- : 6'-SL in solution	Resulting 3'- : 6'-SL on surface (%)	Cells per field[b]	Gliding frequency (%)[c]
NA[a]	27:0	178.7±35.6	63
1:1	27:27	116.7±20.6	10
1:2	27:53	92.7±13.1	6
NA	14:0	121±22.5	17
1:5	14:66	82.3±10.8	1
0:100	0:80	62.9±7.4	0

[a]NA, not applicable; amount of 3'-SL conjugated was controlled by varying the hydrazine/ethanolamine ratio, as in Table 1, rather that its ratio to 6'-SL

[b]$P<0.001$ for differences between 27:0 and 27:27 or 27:53; $P<0.03$ for differences between 14:0 and 14:66

[c]$P<0.001$ for differences between 27:0 and 27:27 or 27:53; $P<0.05$ for differences between 14:0 and 14:66

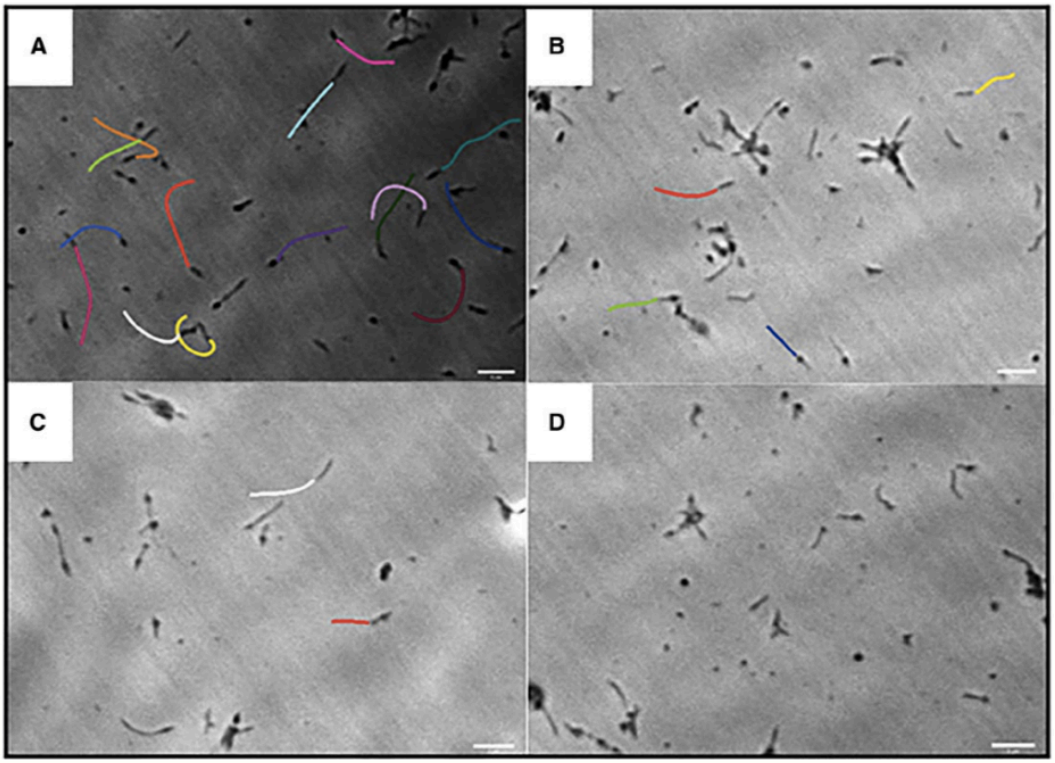

Figure 3.6. Gliding tracks (recorded at 1 frame/sec for 20-30 sec) for M. pneumoniae attached to slides functionalized with 3'- and 6'-sialyllatose at different ratios. 1:0 (A), 1:1 (B), 1:2 (C), and 1:5 (D).

Conclusion

A versatile and controllable strategy for conjugating oligosaccharides to a poly(PFPA) matrix was applied in *M. pneumoniae* attachment and gliding motility under different environment with various ligands and densities. By manipulating the ligated densities, cells attachments and gliding were found to be increasing depending on the densities of conjugated sialyllactose residues. A threshold and gliding frequency maximum were also observed in this study, indicating the influence of receptors distribution and avidity issue. Furthermore, gliding on 3'-SL surfaces was inhibited by the addition of 6'-SL, which might correlates to the P1 adhesin complexes. This proposed new surface bound carbohydrates array shows excellent promise and should allow analysis of receptor specificity beyond linkage alone to reflect the

diversity that can exist in conformational flexibility and presentation. We anticipate this approach will allow us to incorporate variations in the spacer length, as well as the composition, modifications and combination of oligosaccharides. As glycan analysis reveals more information about the surface environment of the airway mucosa it will be possible to define further how the receptor environment influences *M. pneumoniae* attachment and gliding behavior and infection outcome.

References

1. Himmelreich, R.; Hilbert, H.; Plagens, H.; Pirkl, E.; Li, B.-C.; Herrmann, R., *Nucleic Acids Res*. **1996**, 24 (22), 4420-4449.

2. Waites, K. B.; Atkinson, T. P., *Curr. Infect. Dis. Rep*. **2009**, 11 (3), 198-206.

3. Nisar, N.; Guleria, R.; Kumar, S.; Chand Chawla, T.; Ranjan Biswas, N., *Postgrad. Med. J*. **2007**, 83 (976), 100-4.

4. Waites, K. B.; Balish, M. F.; Atkinson, T. P., Future Microbiol. 2008, 3 (6), 635-48.

5. Atkinson, T. P.; Balish, M. F.; Waites, K. B., *FEMS Microbiol. Rev*. **2008**, 32 (6), 956-73.

6. Biberfeld, G.; Biberfeld, P., *J. Bacteriol*. **1970**, 102 (3), 855-61.

7. Henderson, G. P.; Jensen, G. J., *Mol. Microbiol*. **2006**, 60 (2), 376-85.

8. Layh-Schmitt, G.; Podtelejnikov, A.; Mann, M., *Microbiology* **2000**, 146 (Pt 3), 741-7.

9. Nakane, D.; Adan-Kubo, J.; Kenri, T.; Miyata, M., *J. Bacteriol*. **2011**, 193 (3), 715-22.

10. Krause, D. C.; Chen, S.; Shi, J.; Jensen, A. J.; Sheppard, E. S.; Jensen, G. J., *Mol. Microbiol*. **2018**, 108 (3), 306-318.

11. Hasselbring, B. M.; Krause, D. C., *J. Bacteriol*. **2007**, 189 (20), 7442-9.

12. Miyata, M., Cell Motility, Springer: **2008**; pp 137-175.

13. Seto, S.; Kenri, T.; Tomiyama, T.; Miyata, M., *J. Bacteriol*. **2005**, 187 (5), 1875-7.

14. Sobeslavsky, O.; Prescott, B.; Chanock, R. M., *J. Bacteriol*. **1968**, 96 (3), 695-705.

15. Roberts, D. D.; Olson, L. D.; Barile, M. F.; Ginsburg, V.; Krivan, H. C., *J. Biol. Chem*. **1989**, 264 (16), 9289-93.

16. Kasai, T.; Nakane, D.; Ishida, H.; Ando, H.; Kiso, M.; Miyata, M., *J. Bacteriol*. **2013**, 195 (3), 429-35.

17. Ji, Y.; White, Y. J.; Hadden, J. A.; Grant, O. C.; Woods, R. J., *Curr. Opin. Struct. Biol*. **2017**, 44, 219-231.

18. Chen, L.; Leman, D.; Williams, C. R.; Brooks, K.; Krause, D. C.; Locklin, J., *Langmuir* **2017**, 33 (35), 8821-8828.

19. Tully, J. G.; Whitcomb, R. F.; Clark, H. F.; Williamson, D. L., *Science* **1977**, 195 (4281), 892-4.

20. Purcell, R. H.; Taylor-Robinson, D.; Wong, D.; Chanock, R. M., *J. Bacteriol*. **1966**, 92 (1), 6-12.

21. Dajani, A. S.; Clyde, W. A., Jr.; Denny, F. W., *J. Exp. Med*. **1965**, 121, 1071-86.

22. Bredt, W., Pathol. *Microbiol. (Basel)* **1968**, 32 (6), 321-6.

23. Lee, H. S.; Wang, Y. K.; Hsu, S. L., *Macromolecules* **1987**, 20 (9), 2089-2095.

24. Manchee, R. J.; Taylorro.D, *J. Bacteriol*. **1969**, 98 (3), 914.

25. Jordan, J. L.; Chang, H. Y.; Balish, M. F.; Holt, L. S.; Bose, S. R.; Hasselbring, B. M.; Waldo, R. H.; Krunkosky, T. M.; Krause, D. C., *Infect. Immun*. **2007**, 75 (1), 518-522.

26. Prince, O. A.; Krunkosky, T. M.; Krause, D. C., *Infect. Immun*. **2014**, 82 (2), 579-86.

27. Nagai, R.; Miyata, M., *J. Bacteriol*. **2006**, 188 (18), 6469-6475.

28. Miyata, M.; Hamaguchi, T., *Front. Microbiol*. **2016**, 7, 960.

29. Krivan, H. C.; Olson, L. D.; Barile, M. F.; Ginsburg, V.; Roberts, D. D., *J. Biol. Chem*. **1989**, 264 (16), 9283-8.

30. Kogure, T.; Suzuki, T.; Takahashi, T.; Miyamoto, D.; Hidari, K. I. P. J.; Guo, C. T.; Ito, T.; Kawaoka, Y.; Suzuki, Y., *Glycoconjugate J*. **2006**, 23 (1-2), 101-106.

31. Shinya, K.; Ebina, M.; Yamada, S.; Ono, M.; Kasai, N.; Kawaoka, Y., *Nature* **2006**, 440 (7083), 435-6.

CHAPTER 4

SUFEX-BASED STRATEGIES FOR THE PREPARATION OF FUNCTIONAL PARTICLES AND CATION EXCHANGE RESINS

Chen, Li; Kassick, Andrew; Kovaliov, Marina; Mathers, Robert; Locklin, Jason; Averick, Saadyah. Accepted by *Chemical Communications*. Reprinted with permission of publisher.

Abstract

Strong acid cation (SAC) exchange resins are valuable polymeric materials with broad applicability across various industries and academic disciplines. While their method of production via electrophilic sulfonation has been well established, this approach is also characterized by a strongly acidic waste stream and a lack of control over sulfonic acid density and substitution distribution. In this manuscript, we report a method for achieving a predictable and reproducible number of sulfate acid sites for strong acid cation (SAC) exchange resins by employing a mild SuFEx-based reagent system to effect the hydrolysis of fluorosulfonated polymer beads. In addition to maintaining their overall structure and morphology, the resultant poly(hydrogen sulfate) beads effectively demonstrate their utility as cation exchange resins in ion-capture experiments. Furthermore, their polyfluorosulfonated precursors have also proven to be suitable substrates for traditional SuFEx-type click reactions in both small molecule and protein immobilization applications.

Introduction

Ion exchange resins are a versatile class of polymeric materials that have a number of important industrial and medical applications ranging from water treatment and compound purification to drug delivery and catalysis.[1-5] Among the most widely employed ion exchange resins are crosslinked styrene/divinylbenzene (DVB) copolymers bearing highly ionizable sulfonic acid moieties known as strong acid cation (SAC) exchange resins. SAC resins are typically prepared via the post-polymerization modification of DVB-crosslinked polystyrene beads with excess concentrated sulfuric acid at elevated temperatures, normally over 100 °C,[6] resulting in the installation of the requisite sulfonic acid functionality for cationic exchange. While this protocol is effective for producing SAC exchange resins, generation of acidic, sulfate-rich waste streams require inconvenient neutralization procedures that pose environmental concerns.[7-9] This methodology also installs an unpredictable sulfonic acid density and substitution distribution, since the only way to manipulate these parameters is by varying sulfuric acid reaction time. A more benign synthetic approach to SAC resins involves the direct preparation of sulfonic acid containing crosslinked polystyrenes from sulfonated monomers; however, given the challenges associated with this strategy, namely the poor solubility of the hydrophilic monomers in styrene-DVB mixtures, an alternative, environmentally-friendly and controllable method could have wide-ranging impact.

An interesting approach to address this issue has emerged from our recent efforts to expand upon the synthetic applications of the sulfur(VI) fluoride exchange (SuFEx) reaction developed by Sharpless and coworkers.[10] SuFEx chemistry harnesses the unique reactivity displayed by traditionally inert sulfonyl fluorides and fluorosulfonates toward *N*- and *O*-nucleophiles as well as silyl ethers in the presence of amidine or guanidine bases to arrive at the

corresponding sulfonamide, sulfonate, or sulfate products (Scheme 4.1). This innovative "click" reaction technology has demonstrated its utility in numerous scientific disciplines including polymer synthesis, surface chemistry, drug discovery/medicinal chemistry, and protein functionalization.[11-16] Our most recent endeavor concerning SuFEx methodology focused on its application to the post-polymerization modification of sulfonyl fluoride containing polymer brushes for the efficient functionalization of surfaces.[15,17] During the course of these studies, it was discovered that when TBS-protected benzyl or allyl alcohols, such as TBS-pyrenemethanol (**1**), were exposed to sulfonyl fluorides under standard SuFEx conditions, they did not afford the expected benzyl or allyl sulfonates, but rather were hydrolyzed to the corresponding sulfonic acids (Scheme 4.2).[17] This observation encouraged our further investigation into fluorosulfonate polymer hydrolysis as a means to arrive at poly(hydrogen sulfate) materials with the potential to act as SAC exchange resins. We therefore sought to prepare DVB-crosslinked polystyrene beads bearing fluorosulfonate moieties such as **2** and explore mild hydrolysis conditions to yield desired hydrogen sulfate variants of type **3** (Scheme 4.3). This approach is particularly advantageous as the exact proportion of sulfate groups present in the polymer backbone can be controlled by the initial selection of monomer ratios while avoiding the use of harshly acidic reaction conditions.

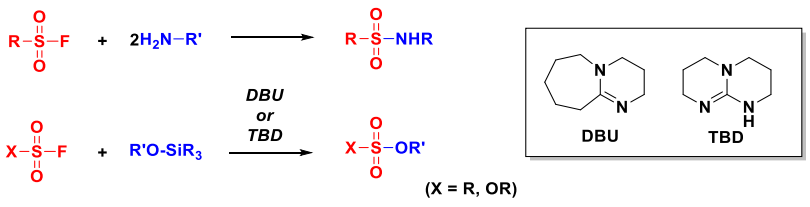

Scheme 4.1. General scheme for the Sulfur(VI) Fluoride Exchange (SuFEx) reaction

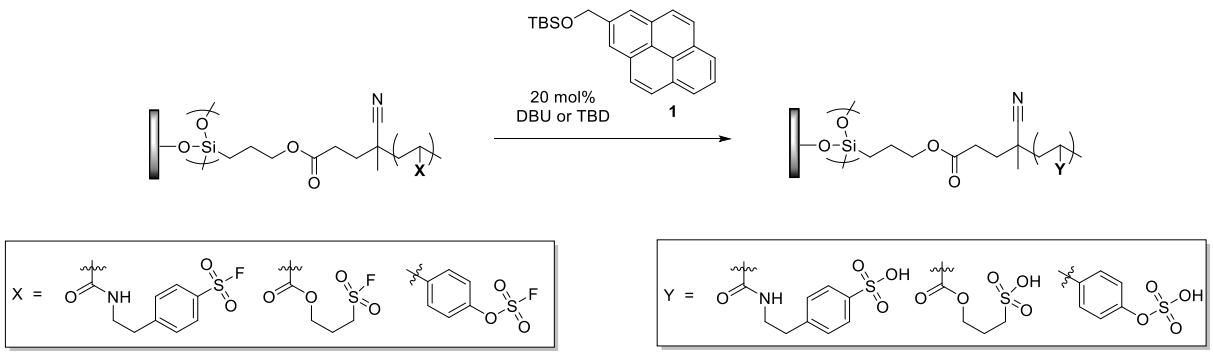

Scheme 4.2. Unexpected SuFEx-based hydrolysis of sulfonyl fluorides and fluorosulfonates with benzyl silyl ethers

In addition to ion exchange, polymeric microspheres also play an important role in many other applications, such as solid-support catalysis, liquid chromatography and enzyme immobilization.[18-20] The functional groups on the beads, whether introduced directly in the monomer or via post-polymerization modification, are crucial to the applications mentioned above. In general, beads with low dispersity, versatile functionality, and a defined and reproducible amount of functional groups are of great interest. For these reasons, we also explored using the fluorosulfonated beads **2** as a polymer support to introduce several different functionalities via SuFEx click chemistry. Herein, we report an operationally simple approach to a novel class of SAC exchange resins, and also demonstrate a versatile platform for the fabrication of polymer particles that have utility in a variety of applications.

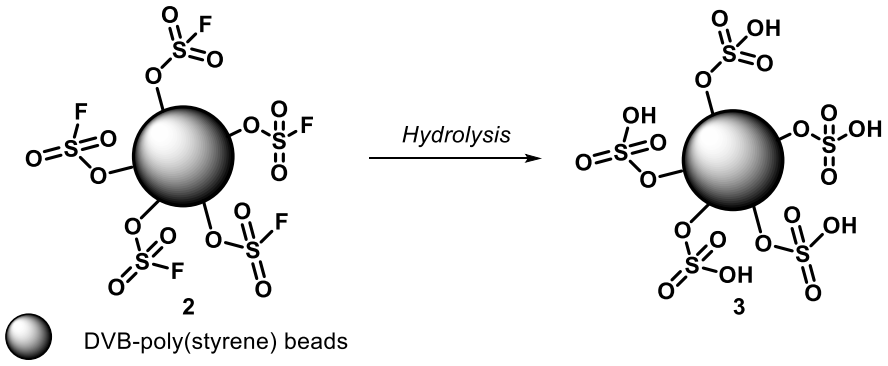

Scheme 4.3. Crosslinked polysulfuric acids via the hydrolysis of fluorosulfonated polymer beads

Experimental

Materials

Styrene and divinylbenzene were purchased from Sigma-Aldrich (St. Louis, MO) and were passed through basic alumina prior to use. Sodium dodecyl sulfate (SDS) was obtained from Invitrogen (Carlsbad, CA). 1,8-Diazabicyclo[5.4.0]undec-7-ene (DBU), triazabicylcodecene (TBD), and ammonium persulfate were purchased from Sigma-Aldrich (St. Louis, MO). *N, N*-Dimethylformamide (DMF) was purchased from ACROS Organics (Morris Plains, NJ). PVA, phenol, *tert*-butyldimethylchlorosilane, and imidazole were obtained from Sigma-Aldrich (St. Louis, MO). Methanol and 2-propanol were purchased from Pharmco-AAPER (Shelbyville, KY). Water was purified via a Millipore Synergy water purification system. 4-Vinylphenyl sulfofluoridate (VPSF) was prepared from 4-acetoxystryrene, sourced from ACROS Organics (Morris Plains, NJ), according to the literature procedure.[17] The enzymes used in this work were *Thermomyces Lanuginosus* lipase (lipozyme® TL) or green fluorescent protein (GFP) as a control. All reagents and solvents were used as received unless otherwise noted.

Emulsion polymerization of VPSF and 10 wt% DVB

A 25 mL Schlenk flask equipped with a stir bar was charged with SDS (89 mg) and 6 mL of H_2O. The resulting clear, colorless solution was treated with $(NH_4)_2S_2O_8$ (53 mg). A mixture of VPSF monomer **5** (1.58 g) and DVB (0.175 g) was then added slowly dropwise via pipette to the solution under vigorous stirring. The now milky white reaction mixture was thoroughly degassed with N_2 for 30 min then heated at 50 °C for 18 h with constant stirring. Saturated aqueous NaCl (30 mL) was added to the resulting thick, white suspension. The mixture was triturated and filtered. The collected solid was washed with H_2O (2 × 20 mL) and MeOH (2 × 20 mL) then suspended in 20 mL of DMF. The suspension was added dropwise to a solution of 1:1 MeOH/H_2O (300 mL). The mixture was filtered and the solid was washed with H_2O (3 × 20 mL) and MeOH (3 × 20 mL). The white solid was dried on a Buchner funnel under vacuum to provide 1.35 g of the desired polymeric material.

Emulsion polymerization of styrene/VPSF (90:10) and 10 wt% DVB

A 25 mL Schlenk flask equipped with a stir bar was charged with SDS (89 mg) and 6 mL of H_2O. The resulting clear, colorless solution was treated with $(NH_4)_2S_2O_8$ (55 mg). A 90:10 mixture of styrene (1.42 g) and VPSF monomer **5** (0.158 g) containing 10 wt% DVB (0.175 g) was then added slowly dropwise via pipette to the solution under vigorous stirring. The milky white reaction mixture was thoroughly degassed with N_2 for 30 min then heated at 50 °C for 18 h with constant stirring. Saturated aqueous NaCl (30 mL) was added to the resulting thick, white suspension. The mixture was triturated and filtered. The collected solid was washed with H_2O (2 × 20 mL) and MeOH (2 × 20 mL) then suspended in 20 mL of DMF. The suspension was added dropwise to a solution of 1:1 MeOH/H_2O (300 mL). The mixture was filtered and the

solid was washed with H_2O (3 × 20 mL) and MeOH (3 × 20 mL). The white solid was dried on a Buchner funnel under vacuum to provide 1.40 g of the desired polymeric material.

Emulsion polymerization of styrene/VPSF (70:30) and 10 wt% DVB

A 25 mL Schlenk flask equipped with a stir bar was charged with SDS (89 mg) and 6 mL of H_2O. The resulting clear, colorless solution was treated with $(NH_4)_2S_2O_8$ (55 mg). A 70:30 mixture of styrene (1.11 g) and VPSF monomer **5** (0.474 g) containing 10 wt% DVB (0.176 g) was then added slowly dropwise via pipette to the solution under vigorous stirring. The milky white reaction mixture was thoroughly degassed with N_2 for 30 min then heated at 50 °C for 18 h with constant stirring. The resulting white suspension was cooled to ambient temperature and quenched with saturated aqueous NaCl (30 mL). The mixture was triturated and filtered. The collected solid was washed with H_2O (2 × 20 mL) and MeOH (2 × 20 mL) then dissolved in 20 mL of DMF (with sonication). The solution was added dropwise to a solution of 1:1 MeOH/H_2O (300 mL). The resulting precipitate was filtered and washed with H_2O (3 × 20 mL) and MeOH (3 × 20 mL). The collected material was dried on a Buchner funnel under vacuum to provide 1.45 g of a white solid.

Suspension polymerization of styrene/VPSF (90:10) and 10 wt% DVB

A 250 mL round bottomed flask was charged with 100 mg PVA and 70 mL of H_2O. The mixture was heated at 65 °C to dissolve the PVA. The resulting clear, colorless solution was cooled to ambient temperature whereupon a solution of styrene (8.1 g), VPSF monomer **5** (0.9 g), 10 wt% DVB (1.0 g), and benzoyl peroxide (100 mg) was added slowly dropwise under vigorous stirring (900 rpm). The resulting suspension was heated at 90 °C for 18 h with constant stirring. The reaction was cooled to ambient temperature then added to ~400 mL of ^{i}PrOH with

stirring. The precipitate was filtered, washed several times with ^{i}PrOH (3 x 50 mL), and dried under reduced pressure to obtain 7.5 g of a white solid.

Suspension polymerization of styrene/VPSF (70:30) and 10 wt% DVB

A 250 mL round bottomed flask was charged with 100 mg PVA and 70 mL H_2O. The mixture was heated at 65 °C to dissolve the PVA. The resulting clear, colorless solution was cooled to ambient temperature whereupon a solution of styrene (6.3 g), VPSF monomer **5** (2.7 g), 10 wt% DVB (1 g), and benzoyl peroxide (100 mg) was added dropwise under vigorous stirring (900 rpm). The resulting suspension was heated at 90 °C for 18 h with constant stirring. The reaction was cooled to ambient temperature then added to ~400 mL of ^{i}PrOH with stirring. The precipitate was filtered, washed several times with ^{i}PrOH (3 x 50 mL), and dried under reduced pressure to obtain 2.3 g of a white solid.

Suspension polymerization of VPSF and 10 wt% DVB

A 250 mL round bottomed flask was charged with 70 mg PVA and 50 mL H_2O. The mixture was heated at 65 °C to dissolve the PVA. After cooling to ambient temperature, a solution of VPSF monomer **5** (6.3 g), 10 wt% DVB (0.7 g), and benzoyl peroxide (70 mg) was added slowly dropwise under vigorous stirring (800 rpm). The resulting suspension was heated at 90 °C for 45 h with constant stirring. The reaction was cooled to ambient temperature then added to ~350 mL of ^{i}PrOH with stirring. The precipitate was filtered, washed several times with ^{i}PrOH (4 x 50 mL), and dried to obtain 6.54 g of a white solid.

Deprotection of DVB-crosslinked styrene/VPSF beads

KOH hydrolysis: Fluorosulfonated polymer beads (100 mg) were suspended in 5 mL of aqueous 2M KOH in a scintillation vial equipped with a magnetic stir bar, and the reaction was stirred vigorously at 85 °C for 2 d. The mixture was treated with several drops of 2M HCl

aqueous solution, and then centrifuged to obtain white powders, which were further washed with water and ethanol. Products were subsequently dried in a vacuum oven at 80 °C.

TBD-catalyzed hydrolysis: Fluorosulfonated polymer beads (100 mg) were dispersed in 5 mL of anhydrous acetonitrile, and then TBS-benzyl alcohol (10 eq to VPSF in beads) and TBD catalyst (20 mol% to VPSF in beads) were added to the dispersion. The mixture was stirred at 70 °C overnight, followed by centrifuge and washed with ethanol. Products were subsequently dried in a vacuum oven.

Synthesis of TBS-Phenol

Phenol (2.00 g, 21.25 mmol), *tert*-butyldimethylchlorosilane (3.36 g, 22.31 mmol), and imidazole (3.18 g, 46.75 mmol) were dissolved in 25 mL of anhydrous dichloromethane (DCM), and the reaction was maintained overnight at ambient temperature. The mixture was extracted with water (2X) and brine. The organics were then dried over anhydrous $MgSO_4$, filtered and concentrated. ^{1}H NMR (300MHZ, $CDCl_3$) δ: 7.23 (m, 2H), 6.98 (t, 1H), 6.88 (d, 2H), 1.01 (s, 9H), 0.22 (s, 6H). ^{13}C NMR δ: 155.63, 129.35, 121.25, 120.11, 25.69, 18.20, -4.42.

Methylene Blue dye staining

Methylene blue (10.0 mg) was dissolved in 10 mL deionized water, which was then added to protected and deprotected beads and sonicated for 1 min. The beads were separated from methylene blue solution through vacuum filtration, and then thoroughly washed with water and methanol.

TBS-Phenol and fluorosulfonated polymer beads click reaction

SuFEx beads with different compositions (50 mg) were suspended in 5 mL of anhydrous DMF. TBS-Phenol (10 equiv) and 20 mol% DBU were then added to the solution, and the reaction was maintained at 60 °C for 24 h. Several drops of 2M HCl aqueous solution was added

to the mixture, and then centrifuged to obtain white product. After washing with ethanol twice, the powders were dried in vacuum oven overnight.

Immobilization of Lipase/GFP

Immobilization was performed using 33 mg of protein per gram of wet support. A suspension of 7:3 sty/VPSF containing 10 wt% DVB (24 mg) in 4 mL of PBS buffer was treated with 40 μL of lipase (20 mg/mL) or 20 μL of GFP (40 mg/mL). The suspension was gently mixed with a Barnstead/Thermolyne LABQUAKE shaker for 24 hours at ambient temperature. After immobilization the suspension was filtered, and the supported lipase was washed several times with distilled water.

Enzyme activity was determined by measuring the increase in absorbance at 405 nm produced by the released *p*-nitrophenol in the hydrolysis of *p*-nitrophenyl palmitate (p-NPP). *p*-NPP stock solution (1 mM) was prepared, first *p*-NPP was dissolved in 3 mL isopropanol and 50 mL of 0.01 M potassium phosphate buffer (pH 7.4) (3% Triton X-100) was added. A volume of 500 μL of buffered *p*-NPP solution was added to 50 μL protein/beads solution (0.002 mg/mL enzyme), and 450 μL of 0.01 M potassium phosphate buffer was added. The mixture was incubated for 20 min at 37 °C. The samples were filtered and the *p*-nitrophenol (*p*-NP) release was monitored at 405 nm in 96-well Nunc clear polystyrene plate on a BioTek Cytation 3 plate reader. A blank sample was always used containing distilled water instead of enzyme solution.

Characterization

Infrared spectra were taken using a Thermo-Nicolet model 6700 spectrometer equipped with a variable angle grazing angle attenuated total reflection (GATR-ATR) accessory (Harrick Scientific) at 64 scans with 4 cm^{-1} resolution. Beads morphology images were taken on a FEI Inspec F FEG scanning electron microscope at 20 kV. Measurements of beads size and zeta

potential were performed using a Zetasizer Nano Series (Malvern) with dynamic light scattering (DLS). Elemental analysis for C, H, S, and F was performed on 20 mg of original (**7a-c**) and KOH or TBD/TBS-benzyl alcohol treated beads (**10a-c**) by Atlantic Microlab, Inc. (Norcross, GA). C, H and S were analyzed by combustion using automatic analyzers, while F was analyzed by flask combustion followed by ion chromatography.

Results and Discussion

Our investigation into the feasibility of this SuFEx-based hydrolysis approach commenced with the synthesis of several DVB-crosslinked polymer substrates possessing varied degrees of fluorosulfonation. As illustrated in Scheme 4.4, the desired polymers were obtained via two different polymerization methods. Emulsion polymerization was first employed to generate polymers **6a-c** by slow treatment of a vigorously stirred aqueous solution of sodium dodecyl sulfate (SDS) and $(NH_4)_2S_2O_8$ with a mixture composed of 10 wt% DVB and different ratios of styrene (**4**) and the previously described arylfluorosulfonate monomer, 4-vinylphenyl sulfofluoridate (VPSF, **5**).[17] Identical monomer ratios were then utilized for the suspension polymerization of styrene and VPSF whereby mixtures of **4** and **5** containing the radical initiator benzoyl peroxide and 10 wt% DVB were slowly added to an aqueous solution of 0.3% polyvinyl alcohol (PVA) to arrive at an additional three DVB-crosslinked polymers **7a-c**. While the composition of the respective polymers was the same, the method by which they were prepared allowed for control over their particle size as emulsion polymerization generally results in smaller polymer beads than those formed by suspension polymerization.

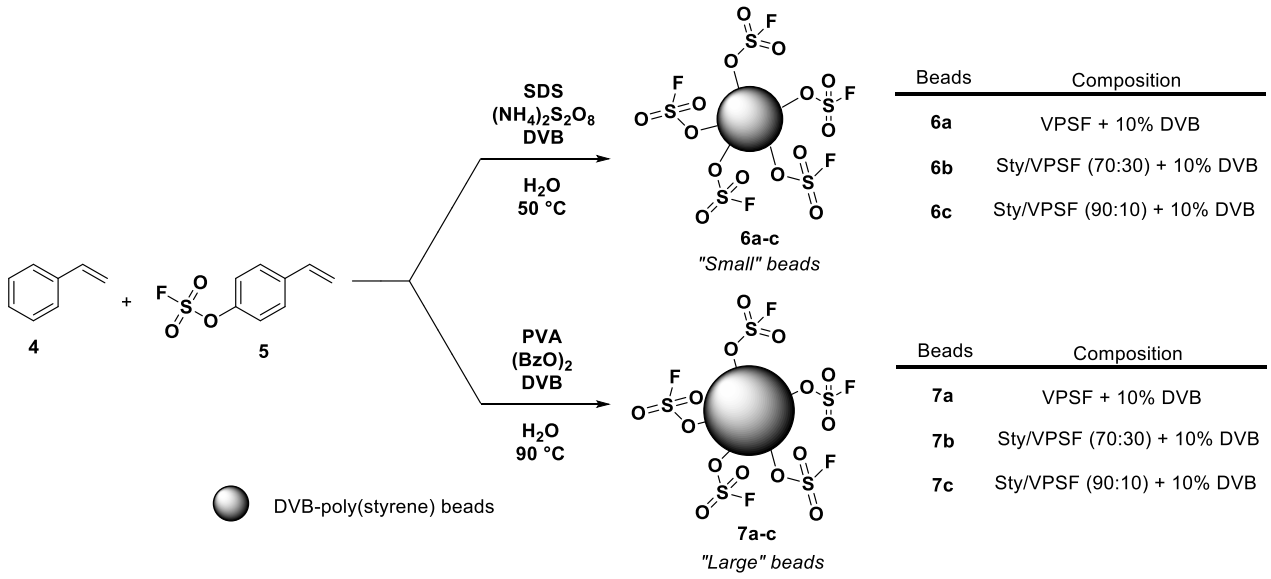

Scheme 4.4. Synthesis of DVB-crosslinked fluorosulfonated polymer substrates via emulsion and suspension polymerization

With sufficient quantities of the fluorosulfonated polymers **6a-c** and **7a-c** in hand, attention was then focused on their conversion to the corresponding polysulfuric acids. Application of our previously reported sulfonyl fluoride hydrolysis conditions involving benzyl silyl ethers and strong organic amine bases was anticipated to furnish the desired hydrolysis products **9a-c** and **10a-c** as outlined in Scheme 4.5.[17] Treatment of small and large beads **6a** and **7a** with TBS-benzyl alcohol **8** in the presence of substoichiometric amounts of triazabicylcodecene (TBD) at 70 °C resulted in the near complete conversion to the desired sulfuric acid bearing polystyrenes as determined by IR spectroscopy. As can be seen from Figure 4.1, the strong absorption band at 1450 cm^{-1}, indicative of the asymmetric S=O stretching of fluorosulfonates, disappeared after ~ 12 h at 70 °C while a prominent new peak appeared at 1045 cm^{-1} corresponding to the formation of a hydrogen sulfate product. The TBD-catalyzed hydrolysis of polymer beads **6b** and **7b**, composed of 7:3 styrene/VPSF, demonstrated similar reactivity but to a lesser extent as a mixture of both flurorosulfonate starting material and

hydrogen sulfate product was observed (Figure 4.2). FTIR spectra for the reaction of polymer beads **6c** and **7c** did not show significant conversion to the desired hydrolyzed products (Figure 4.3). This is likely due to the poor solubility of polystyrene in acetonitrile,[21] the most effective solvent for the TBD-catalyzed transformation. As the percentage of polystyrene in the copolymer composition increases the observed reaction extent decreases. Orthogonal confirmation of deprotection efficacy was obtained via elemental analysis for beads **7a-c** (Table 4.1) where TBD-catalyzed hydrolysis conditions resulted in near quantitative conversion of fluorosulfonates into hydrogen sulfate products in all cases.

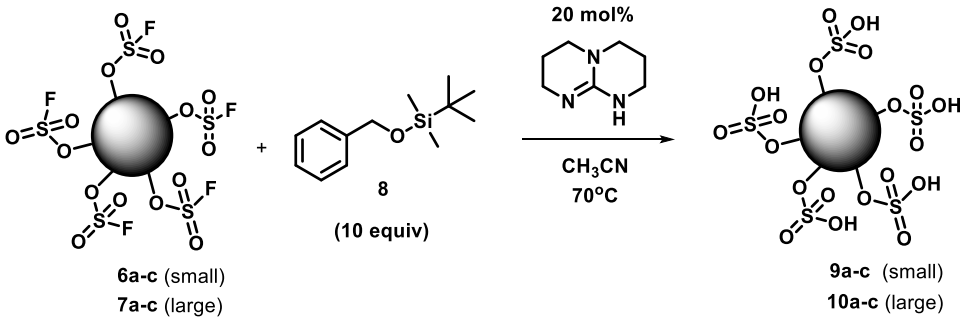

Scheme 4.5. TBD-catalyzed hydrolysis of fluorosulfonated polymer beads

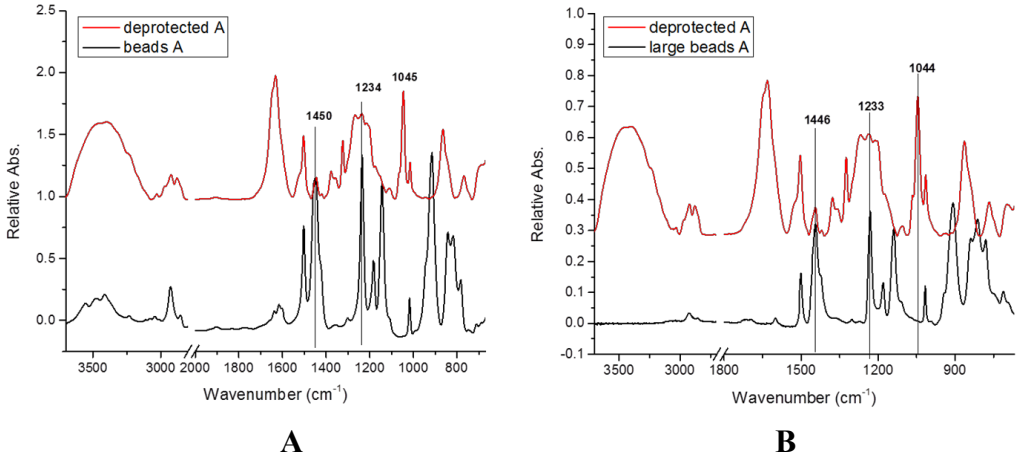

Figure 4.1. IR analysis of TBD-catalyzed hydrolysis reactions. (A) Small fluorosulfonated polymer beads **6a** (B) Large fluorosulfonated polymer beads **7a**.

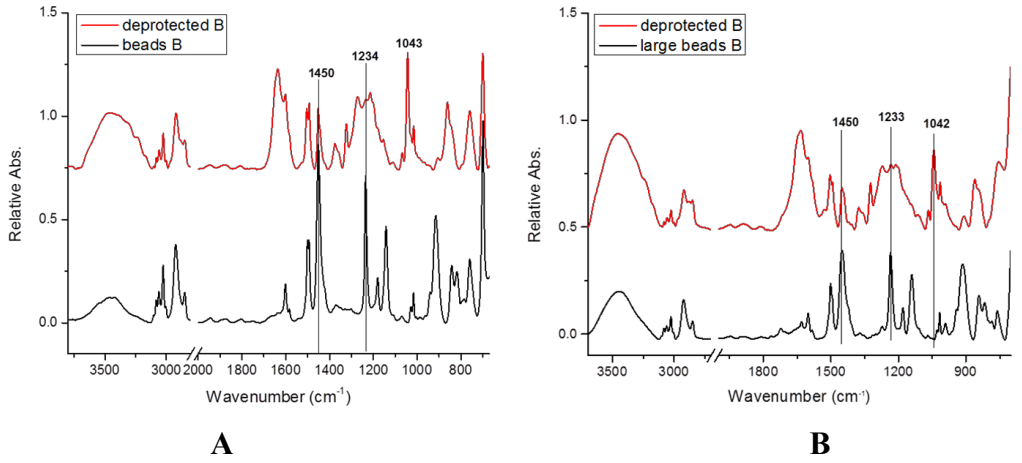

Figure 4.2. IR analysis of TBD-catalyzed hydrolysis reactions. (A) Small fluorosulfonated polymer beads **6b** (B) Large fluorosulfonated polymer beads **7b**.

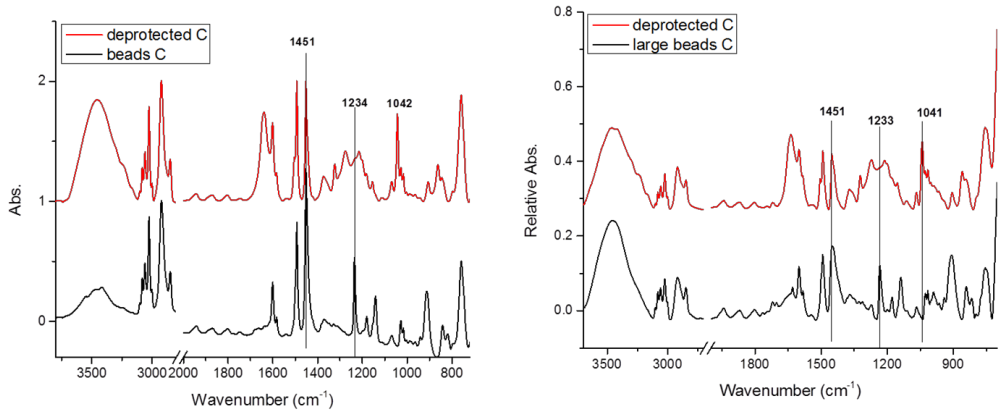

Figure 4.3. IR analysis of TBD-catalyzed hydrolysis reactions. (A) Small fluorosulfonated polymer beads **6c** (B) Large fluorosulfonated polymer beads **7c**.

Table 4.1. Elemental analysis of large fluorosulfonated beads **7a-c** and corresponding hydrolyzed resins **10a-c**

	C%	H%	S%	F%	Conversion [b]
7a	52.3	4.1	14.1	8.1	
7b	73.2	6.1	5.9	3.5	
7c	86.4	7.1	1.7	1.1	
			2M KOH at 85 °C		
10a	52.6	4.1	13.9	7.7	5%
10b	74.1	6.2	5.8	3.2	9%
10c	86.7	7.3	1.7	1.0	9%
			TBS-benzyl alcohol/TBD at 70 °C		
10a	55.2	5.8	9.7	1.5	81%
10b	73.9	6.9	3.7	trace [a]	~100% [c]
10c	85.0	7.6	1.5	trace [a]	~100% [c]

[a] Trace: < 0.25%; [b] Conversion = [F%(original) – F%(deprotected)]/ F%(original); [c] Full conversion within limit of detection (less than 0.25% F).

Fluorosulfonate hydrolysis to the corresponding sulfuric acids was also speculated to occur under basic aqueous conditions. To test this hypothesis, 50 mg of small and large polymer beads were suspended in 5 mL of 2 M KOH and maintained at 85 °C for 2 days (Scheme 4.6). After reaction, the resulting solids were collected by centrifugation, washed with H_2O and EtOH, and characterized via FTIR (Figure 4.4). As observed with the TBD-mediated hydrolysis conditions, polymers **6a** and **7a**, containing only DVB-crosslinked VPSF **5**, resulted in near complete hydrolysis as evidenced by the disappearance of the characteristic S=O absorption band at 1450 cm^{-1} and the appearance of a prominent new peak at 1053 cm^{-1} and 1051 cm^{-1} for **6a** and **7a**, respectively, corresponding to the formation of hydrogen sulfates **9a** and **10a**. Polymer beads **6b** and **7b**, composed of 7:3 styrene/VPSF, demonstrated modest reactivity under the same conditions with FTIR analysis revealing a mixture of flurorosulfonate starting material and hydrogen sulfate product (Figure 4.5). However, elemental analysis did not show significant conversion to the desired products (Table 4.2), potentially indicating surface hydrolysis of the polymeric resins under aqueous KOH conditions.

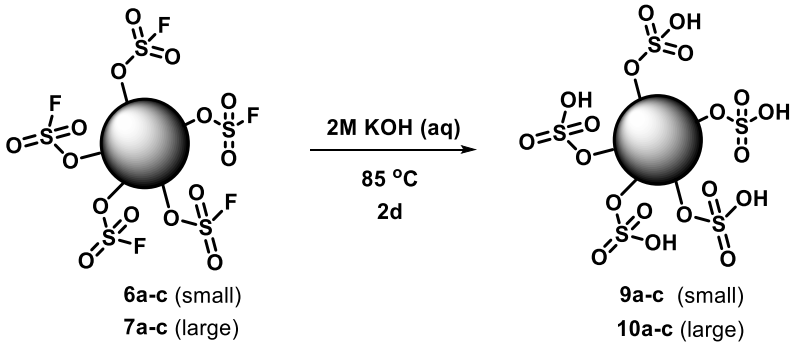

Scheme 4.6. Base-mediated hydrolysis of fluorosulfonated polymer beads

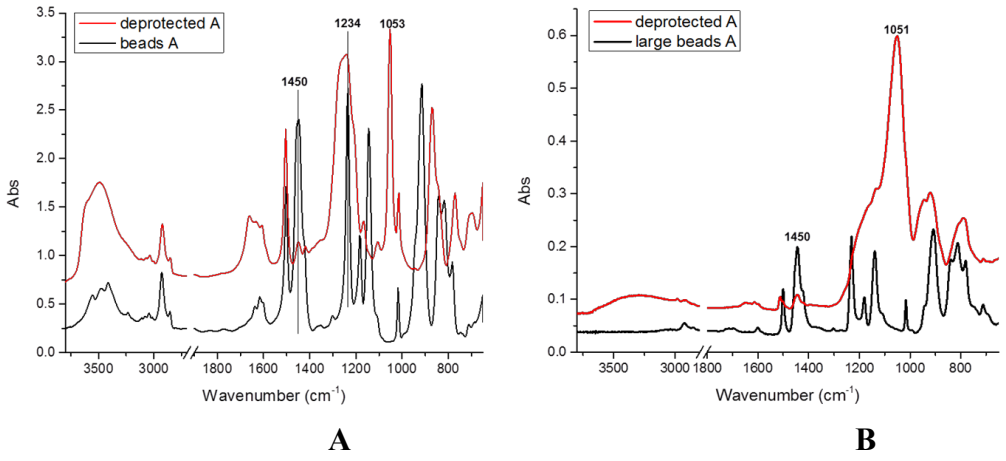

Figure 4.4. IR analysis of KOH-mediated hydrolysis reactions. (A) Small fluorosulfonated polymer beads **6a** and (B) Large fluorosulfonated polymer beads **7a**.

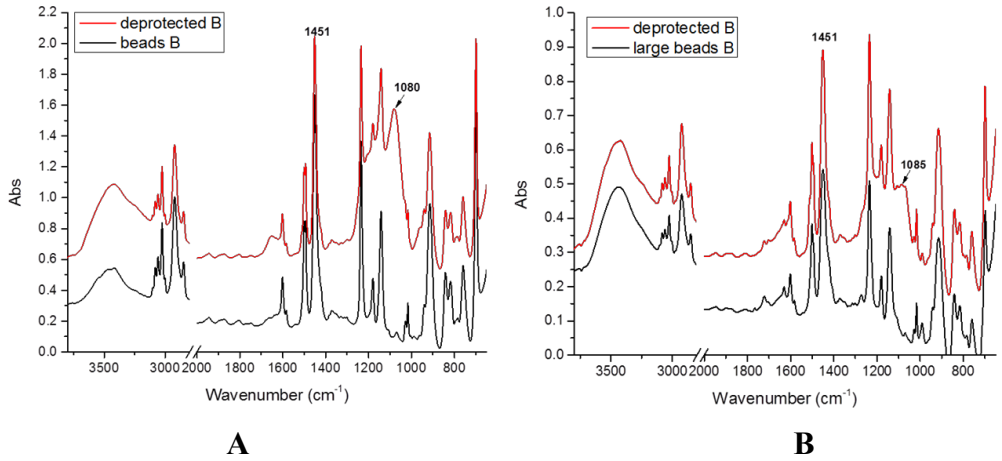

Figure 4.5. IR analysis of KOH hydrolysis reactions. (A) Small fluorosulfonated polymer beads **6b** (B) Large fluorosulfonated polymer beads **7b**.

Further characterization of the polymer beads obtained from these basic hydrolysis experiments was achieved via zeta potential, dynamic light scattering (DLS), and scanning electron microscopy (SEM). Zeta potential and DLS measurements obtained for the parent fluorosulfonate polymer beads **6a-c** and the corresponding hydrolyzed particles **9a-c** are presented in Table 4.2. Parent beads **6a-c** exhibited a negative zeta potential value of –30 mV

most likely due to residual surface adsorbed SDS from the emulsion polymerization conditions. The remaining data for small beads **9a-c** shows zeta values ranging from –38 mV to –28 mV, respectively, which is consistent with the presence of highly ionizable sulfate moieties. The observed zeta potential variability correlates with the percentage of sulfate moiety incorporation as hydrolyzed polymer beads derived from precursors containing greater amounts of VPSF displayed a more negative surface charge. Negligible change was observed in the case of beads **9c** which possessed the lowest percentage of VPSF monomer. Strong, negative zeta potentials also suggest moderately stable particles with a lower propensity for aggregation. Particle size determinations via DLS revealed a diameter of 120 nm for polymer beads **6a** containing only DVB-crosslinked VPSF **5** while polymers **6b** and **6c** containing 30% and 10% VSPF, respectively, were significantly smaller measuring 67 and 80 nm in diameter. Hydrolyzed variants **9a-c**, as expected, displayed larger diameters than the parent. Due to difficulty in identifying a suitable solvent to suspend large beads **7a-c**, no zeta potential or DLS measurements were obtained for these examples.

Table 4.2. Zeta potential and DLS data for fluorosulfonated polymers **6a-c** and hydrolyzed products **9a-c**

Entry	Polymer	Original diameter (nm)	Hydrolyzed diameter (nm)	Zeta potential (mV)
a	**6a**	120		-30
b	**6b**	67		-30
c	**6c**	80		-30
d	**9a**		153	-38
e	**9b**		111	-33
f	**9c**		118	-28

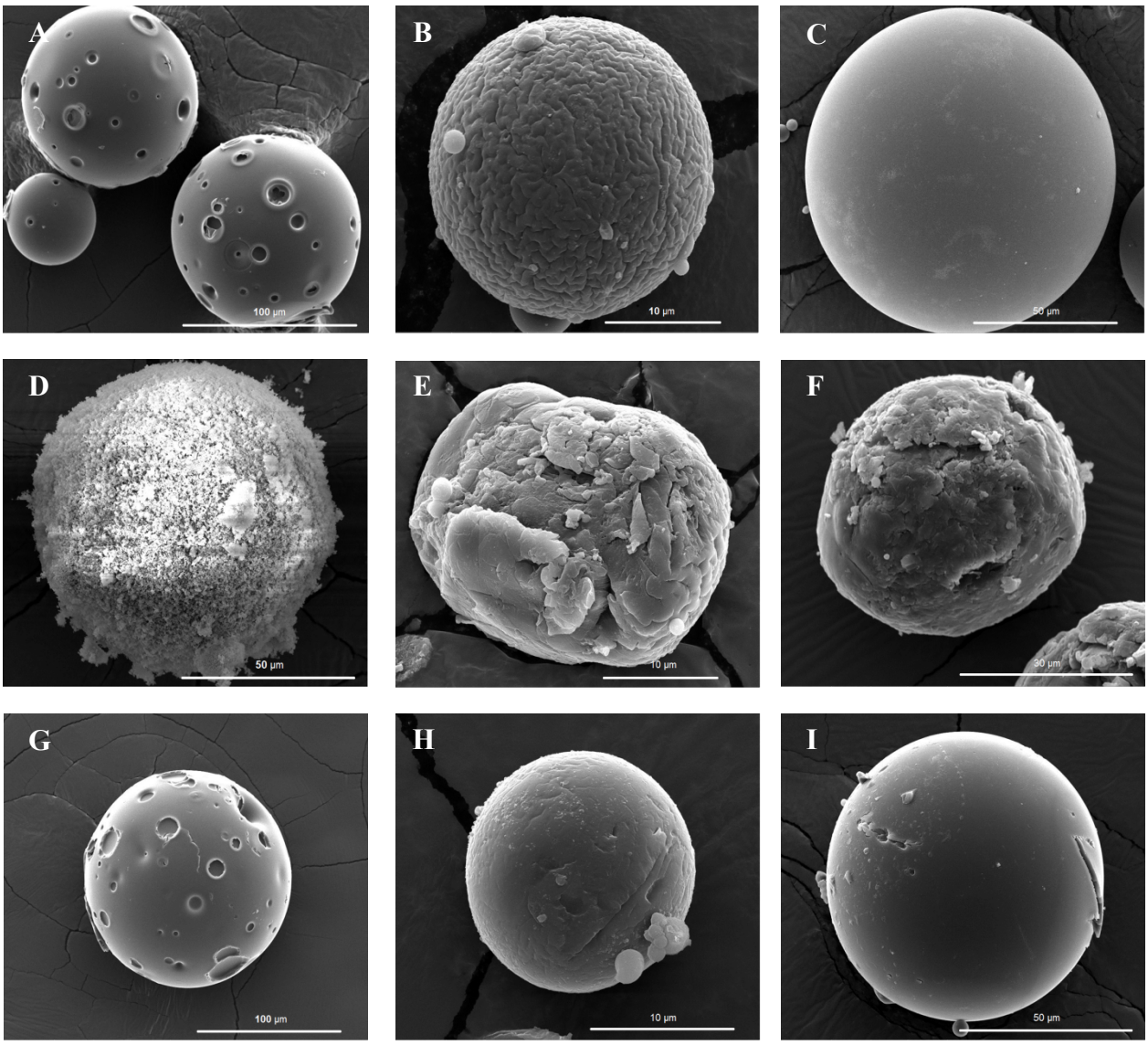

Figure 4.6. Scanning electron micrographs of original and deprotected large fluorosulfonated beads. (A-C) Large fluorosulfonated beads **7a-c** before deprotection, (D-F) deprotected beads from aqueous base hydrolysis, and (G-I) deprotected beads via TBD-catalyzed hydrolysis.

The morphology of large fluorosulfonate beads under different treatments were studied using scanning electron microscopy (Figure 4.6). Parent fluorosulfonate polymer beads were all spherical particles ranging from 10 to 100 µm in diameter. Subtle differences were observed at the outer surface of the particles, where large beads **7a** showed several surface defects and **7b** had a "wrinkling skin" that likely originates from the immiscibility of the monomers and

oligomers during the polymerization process (Figure 4.6A-C). Both beads **7b** and **7c** are composed of styrene and VPSF monomers, however, the majority of large beads **7c** are much smoother due to the relatively low percentage of VPSF in the beads. In comparing the two different hydrolysis conditions, the KOH treatment yielded damaged particles with significant etching that either presented a hairy microstructure (Figure 4.6D) or cracked holes (Figure 4.6E-F). On the other hand, the TBS-benzyl alcohol/TBD treatment is much milder, and maintains the intact particles with only a few surface defects or cracks (Figure 4.6G-I). These can be explained by the basicity of the solution and the agitation and heating time. Aqueous 2M KOH solution is more basic than the millimolar TBD, resulting in more etching. The milder TBD conditions not only resulted in more intact spherical resins, but also afforded a superior amount of sulfate groups based on FTIR and elemental analysis.

To evaluate the ability of these hydrolyzed polymeric products to serve as SAC exchange resins, a simple ion capture experiment was performed employing large beads and the synthetic cationic dye, methylene blue. Fluorosulfonated polymer beads **7a-c** and the corresponding hydrolyzed particles **10a-c**, prepared via both KOH-mediated and TBD-catalyzed routes, were treated with a 1 mg/mL solution of methylene blue in deionized water. After gentle shaking, the beads were separated from the solution by vacuum filtration, and then thoroughly washed with water and methanol. As illustrated in Figure 4.7, the parent compounds **7a-c** did not retain any blue coloring while the images of the hydrolyzed products **10a-c** indicate the successful capture of the cationic methylene blue dye. The amount of color retained by the new cation exchange resins qualitatively correlates to the percentage of sulfate moieties present on the polymer beads. The beads containing greater amounts of VPSF displayed a darker blue color. Moreover, resins obtained via TBD-catalyzed hydrolysis (Figure 4.7A) exhibit a darker coloring compared to their

base-mediated hydrolysis counterparts (Figure 4.7B) most likely due to the more complete level of hydrolysis achieved with TBD-catalysis over aqueous KOH conditions.

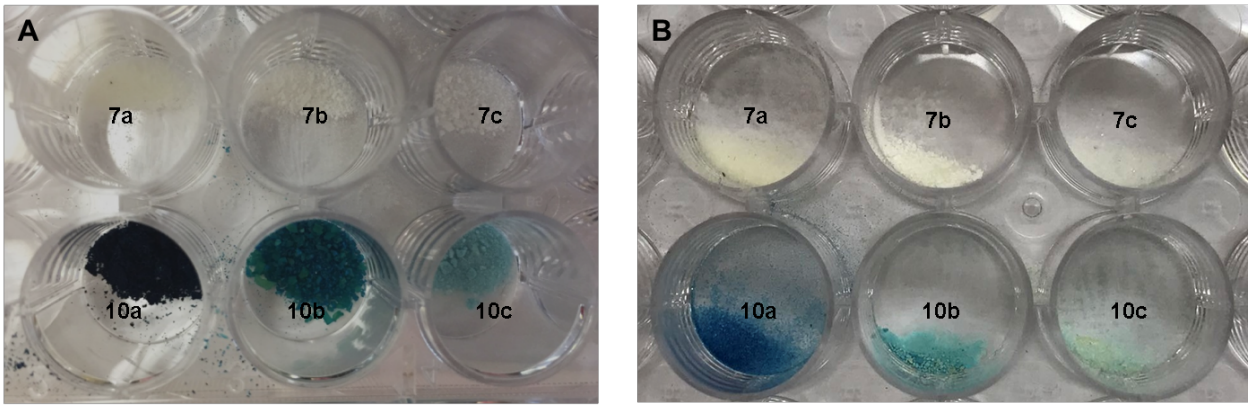

Figure 4.7. Methylene blue capture experiment. (A) Parent and hydrolyzed DVB-crosslinked polymer beads obtained via TBD-catalyzed hydrolysis following aqueous methylene blue treatment. (B) Parent and hydrolyzed DVB-crosslinked polymer beads obtained via aqueous basic hydrolysis following aqueous methylene blue treatment.

Next, the ion exchange capacity (IEC) of hydrolyzed beads **10a-c** was investigated to gain a quantitative measure of sulfuric acid functionalization. IECs were determined via a standard titration protocol and compared to theoretically established values (Table 4.3). [6] Resins **10a-c** were found to exhibit IEC values of 2.7, 1.2, and 0.45 mequiv g^{-1}, respectively. As predicted, resins derived from polymers with lower amounts of VPSF, displayed correspondingly lower IECs. These results show a reasonable correlation between the theoretically calculated IEC values as well as literature values for similar sulfonated resins.[6] It is also confirmed that resin IEC can be directly controlled by the initial monomer ratio allowing for the predictable and reproducible incorporation of acidic functionality. Overall, these preliminary results effectively demonstrate the utility of poly(hydrogen sulfate) beads as cation exchange resins.

Table 4.3. Ion exchange capacities (IEC) for hydrolysed beads **10a-c**

	IEC (mequiv/g)		Composition (% wt of VPSF)	
	Calculated	Measured	Theoretical	Experimental [a]
10a	3.5	2.7	90	89
10b	1.7	1.2	27	39
10c	0.53	0.45	9	11

[a] Calculated from elemental analysis results

In addition to demonstrating their ability to undergo hydrolysis in the presence of aqueous or organic amine bases to arrive at SAC exchange resins, polyfluorosulfonate precursors **6** and **7** have also proven to be suitable substrates for traditional SuFEx-type click reactions. Both large and small beads with different compositions obtained from suspension and emulsion polymerization, respectively, were treated with a simple silyl-protected reacting partner, *tert*-butyldimethylsilyl phenol **11**, in the presence of 20 mol% DBU at 60 °C (Scheme 4.7). Under these standard SuFEx reaction conditions, the desired phenyl sulfate product **12** was formed as detected by IR spectroscopy (Figure 4.8-10). All beads in different compositions resulted in the appearance of two new peaks, ~1415 and ~1216 cm^{-1}, that originate from the formed phenyl sulfate groups. Polymer beads containing a lower amount of VPSF, such as beads **6c** and **7c**, showed weaker signals in FTIR spectra (Figure 4.10) due to fewer conjugation sites.

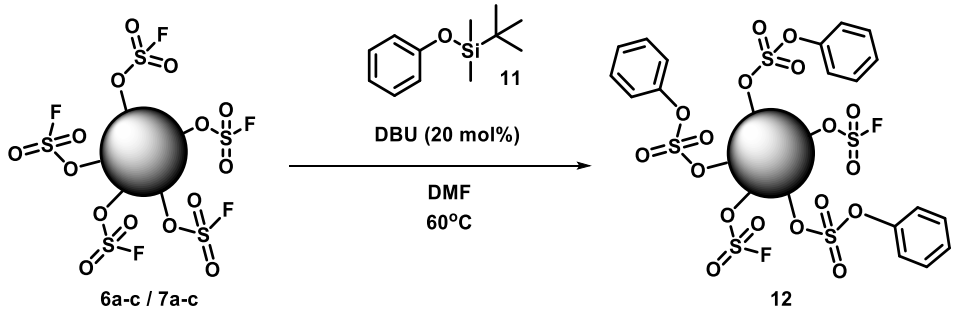

Scheme 4.7. TBS-phenol SuFEx click on fluorosulfonated polymer beads

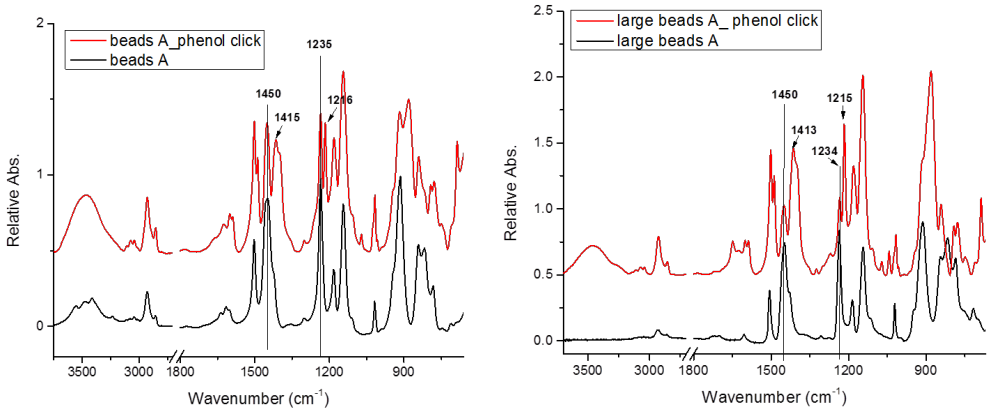

A **B**

Figure 4.8. IR analysis of TBS-phenol click reactions. (A) Small fluorosulfonated polymer beads **6a** (B) Large fluorosulfonated polymer beads **7a**.

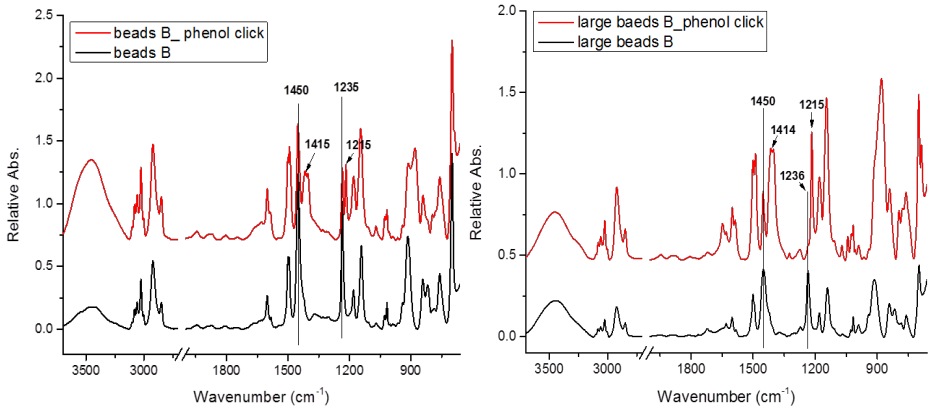

A **B**

Figure 4.9. IR analysis of TBS-phenol click reactions. (A) Small fluorosulfonated polymer beads **6b** (B) Large fluorosulfonated polymer beads **7b**.

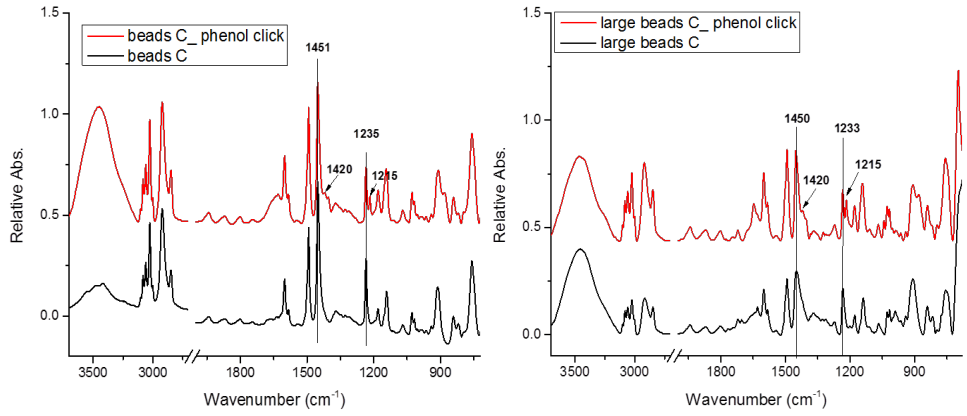

A **B**

Figure 4.10. IR analysis of TBS-phenol click reactions. (A) Small fluorosulfonated polymerbeads **6c** (B) Large fluorosulfonated polymer beads **7c**.

Given the observed compatibility with SuFEx reaction conditions, we attempted to further extend the scope of our DVB-crosslinked fluorosulfonated beads by utilizing them as a support for the immobilization of enzymes. Enzyme immobilization has become a popular strategy to more effectively harness the excellent selectivity and specificity exhibited by enzymes for industrial applications.[22-25] By enabling enzyme recycling, enhancing stabilization, and allowing for easy separation from reaction mixtures, enzyme immobilization presents distinct advantages over the use of soluble enzymes for biocatalytic transformations.[26,27] Recently, we demonstrated the utility of SuFEx reaction technology for protein-polymer bioconjugation through the chemoselective functionalization of the commercially available enzyme, bovine serum albumin (BSA).[16] For the present investigation, we sought to evaluate the potential of our new fluorosulfonated polymers to immobilize lipase from the thermophilic fungus, *Thermomyces lanuginosus* (TL), and subsequently test the activity of the resultant conjugate. Lipase was chosen for this study as this protein class is quite robust under a wide

range of conditions and reaction media, has a broad specificity accepting very different substrates, and can catalyze many reactions.[28-33]

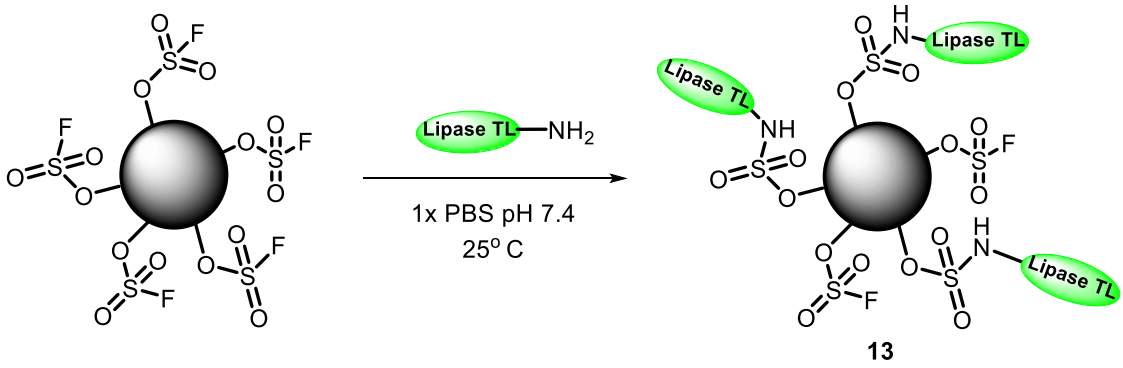

Scheme 4.8. Immobilization of lipase TL on fluorosulfonated polymer beads

The previously described SuFEx ligation chemistry[16] was then employed to modify the DVB-crosslinked styrene/VPSF (7:3) beads with lipase TL and also with green fluorescent protein (GFP) as a control (Scheme 4.8). The reaction of DVB-crosslinked styrene/VPSF beads with lipase TL was carried out by gently mixing the two reagents in aqueous buffer solution (pH = 7.4). The resulting protein-polymer conjugate **13** was then purified by filtration and subsequent washing with distilled water. Lipolytic activity of immobilized lipase on DVB-crosslinked fluorosulfonated beads (sty/VPSF-TL) was determined spectrophotometrically by using *p*-nitrophenyl palmitate (*p*-NPP) as substrate and compared to both lipase in solution (TL) and immobilized GFP (sty/VPSF-GFP). While the immobilized lipase conjugate **13** exhibited lower activity than the native lipase (Figure 4.11), further optimization of the immobilization conditions and enzyme loading could be investigated to enhance enzymatic activity and will be the subject of a future study.

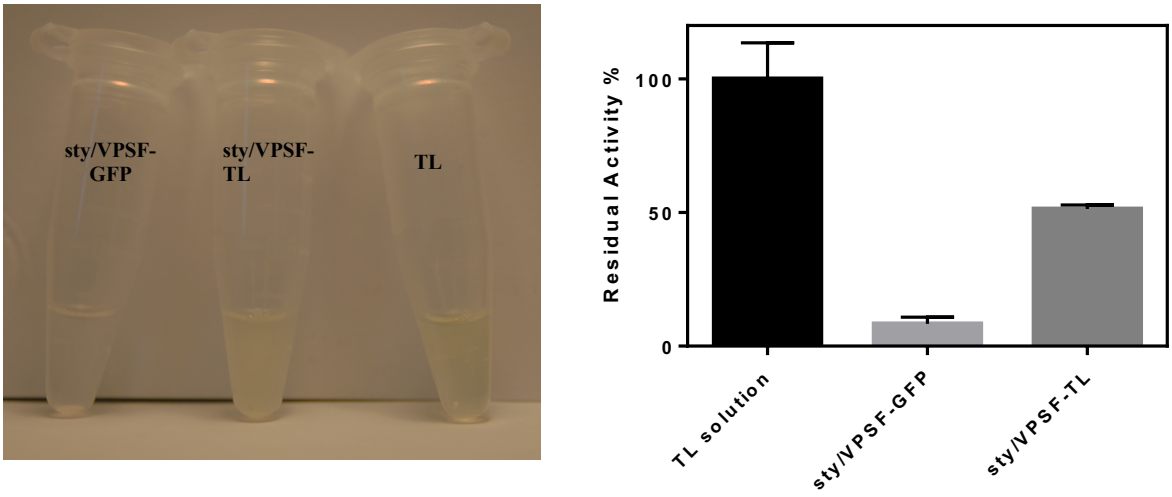

Figure 4.11. Lipolytic activity of native lipase TL versus immobilized lipase-polymer hybrid (sty/VPSF-TL).

Conclusion

In summary, we have discovered an operationally simple and controllable strategy for the fabrication of SAC exchange resins. Mild SuFEx-based hydrolysis conditions allowed for the installation of a predictable and reproducible number of sulfate acid sites while maintaining the overall structure and morphology of the parent beads. The resulting hydrolyzed beads effectively demonstrated their capability as cation exchange resins in dye capture experiments where the relative exchange capacity of the various resins, reflected in the amount of color retained, qualitatively correlated to the percentage of incorporated sulfate moieties. In addition, the precursor DVB-crosslinked polystyrene beads bearing fluorosulfonate moieties were shown to undergo conventional SuFEx chemistry using aromatic silyl ethers and protein-polymer bioconjugation with lipase. These materials and methodology offer a feasible and versatile approach to fabricate multifunctional polymer-supported beads, which are useful across various applications of chemistry and biology.

References

1. Alexandratos, S. D., *Ind. Eng. Chem. Res.* **2009**, *48*, 388-398.

2. Gelbard, G., *Ind. Eng. Chem. Res.* **2005**, *44*, 8468-8498.

3. Elder, D. P., *J. Chem. Ed.* **2005**, *82*, 575.

4. Wheaton, R. M.; Anderson, R. E., *J. Chem. Ed.* **1958**, *35*, 59.

5. Srikanth, M. V.; Sunil, S. A.; Rao, N. S.; Uhumwangho, M. U.; Ramana Murthy, K. V., *J. Sci. Res.* **2010**, *2*, 597-611.

6. Pepper, K. W., *J. Appl. Chem.* **1951**, *1*, 124-132.

7. Lens, P. N. L.; Visser, A.; Janssen, A. J. H.; Pol, L. W. H.; Lettinga, G., *Crit. Rev. in Env. Sci. Technol.* **2010**, *28*, 41-88.

8. Mahmood, Q.; Zheng, P.; Cai, J.; Hayat, Y.; Hassan, M. J.; Wu, D.-l.; Hu, B.-l., *J. of Zhejiang Univ.-SCIENCE A* **2007**, *8*, 1126-1140.

9. Colleran, E.; Finnegan, S.; Lens, P., *Antonie van Leeuwenhoek* **1995**, *67*, 29-46.

10. Dong, J.; Krasnova, L.; Finn, M. G.; Sharpless, K. B., *Angew. Chem. Int. Ed.* **2014**, *53*, 9430-9448.

11. Dong, J.; Sharpless, K. B.; Kwisnek, L.; Oakdale, J. S.; Fokin, V. V., *Angew. Chem. Int. Ed.* **2014**, *53*, 9466-9470.

12. Oakdale, J. S.; Kwisnek, L.; Fokin, V. V., *Macromolecules* **2016**, *49*, 4473-4479.

13. Li, S.; Beringer, L. T.; Chen, S.; Averick, S., *Polymer* **2015**, *78*, 37-41.

14. Brooks, K.; Yatvin, J.; McNitt, C. D.; Reese, R. A.; Jung, C.; Popik, V. V.; Locklin, J., *Langmuir* **2016**, *32*, 6600-6605.

15. Yatvin, J.; Brooks, K.; Locklin, J., *Angew. Chem. Int. Ed.* **2015**, *54*, 13370-13373.

16. Li, S.; Cohen-Karni, D.; Beringer, L. T.; Wu, C.; Kallick, E.; Edington, H.; Passineau, M. J.; Averick, S., *Polymer* **2016**, *99*, 7-12.

17. Brooks, K.; Yatvin, J.; Kovaliov, M.; Crane, G. H.; Horn, J.; Averick, S.; Locklin, J., *Macromolecules* **2018**, *51*, 297-305.

18. Haag, R.; Roller, S., *Top. Curr. Chem.* **2004**, *242*, 1–42

19. Miletic, N.; Vukovic, Z.; Nastasovic, A.; Loos, K., *J. Mol. Catal. B: Enzym.* **2009**, *56*, 196–201.

20. Ugelstad, J.; Søderberg, L.; Berge, A.; Bergstrøm, J., *Nature* **1983**, *303*, 95-96.

21. Gündüz, S.; Dinçer, S., *Polymer* **1980**, *21*, 1041-1046.

22. Zdarta, J.; Meyer, A.; Jesionowski, T.; Pinelo, M., *Catalysts* **2018**, *8*, 92.

23. Bernal, C.; Rodríguez, K.; Martínez, R., *Biotechnol. Adv.* **2018**, *36*, 1470-1480.

24. Garcia-Galan, C.; Barbosa, O.; Hernandez, K.; Santos, J.; Rodrigues, R.; Fernandez-Lafuente, R., *Molecules* **2014**, *19*, 7629-7645.

25. C. Rodrigues, R.; Hernandez, K.; Barbosa, O.; Rueda, N.; Garcia-Galan, C.; C. S. dos Santos, J.; Berenguer-Murcia, A.; Fernandez-Lafuente, R., *Curr. Org. Chem.* **2015**, *19*, 1707-1718.

26. Sigurdardóttir, S. B.; Lehmann, J.; Ovtar, S.; Grivel, J.-C.; Negra, M. D.; Kaiser, A.; Pinelo, M., *Adv. Synth. Catal.* **2018**, *360*, 2578-2607.

27. Cui, J.; Feng, Y.; Lin, T.; Tan, Z.; Zhong, C.; Jia, S., *ACS Appl. Mater. Interfaces* **2017**, *9*, 10587-10594.

28. Jaeger, K. E.; Eggert, T., *Curr. Opin. Biotechnol.* **2002**, *13*, 390-397.

29. Villeneuve, P.; Muderhwa, J. M.; Graille, J.; Haas, M. J., *J. Mol. Catal. B: Enzym.* **2000**, *9*, 113-148.

30. Lozano, P.; Garcia-Verdugo, E.; V. Luis, S.; Pucheault, M.; Vaultier, M., *Curr. Org. Synth.* **2011**, *8*, 810-823.

31. Ghanem, A., *Tetrahedron* **2007**, *63*, 1721-1754.

32. Hernandez, K.; Garcia-Galan, C.; Fernandez-Lafuente, R., *Enzyme Microb. Technol.* **2011**, *49*, 72-78.

33. Kovaliov, M.; Cheng, C.; Cheng, B.; Averick, S., *Polym. Chem.* **2018**, *9*, 4651-4659.

CHAPTER 5

PREPARATION AND CHARACTERIZATION OF MONOFUNCTIONAL SULFURIC, PHOSPHONIC ACID RESINS AND BIFUNFUNCTIONAL PHOSPHONIC/SULFURIC ACID RESINS ON FLUOROSULFONATED POLYSTYRENE SUPPORTS

Chen, Li; Averick, Saadyah; Locklin, Jason. To be submitted to *Langmuir*.

Abstract

In this work, the preparation and characterization of monofunctional phosphonic and sulfuric acid, and bifunctional phosphonic/sulfuric acid ion exchange resins (P-, S- and PS-IERs) using our recently reported fluorosulfonated polystyrene supports were presented. These resins were fabricated by a new click reaction — Sulfur(VI) Fluoride Exchange (SuFEx), yielding sulfuric acid, and phosphate ester containing resins. The phosphonate ester resins were then hydrolyzed by bromotrimethylsilane and methanol to produce P-IERs. The sorption capacity of monofunctional sulfuric acid resins for Ni(II), Cu(II), Mg(II), and Fe(III) was investigated in 0.04 M HNO_3 solution. Efficient Fe(III) retention was observed, but little to no divalent ions were complexed with S-IERs. To explore the impact of sulfuric acid ligand on P-IERs, separate installation method based on SuFEx click was employed to yield bifunctional phosphonic/sulfuric acid resins. Each type of resins was characterized by infrared spectrometry, scanning electron microscopy, and the determination of acid capacity. The total Fe(III) sorption capacity of S-, P-, and PS-IERs were studied in 0.04, 1, and 4 M nitric acid solution. P-IERs complexed ~3.4 mg Fe(III) per gram of resins in 0.04M HNO_3 solution, outperforming the sorption capacities of either S- or PS-IERs.

Introduction

Polymer beads are composed of crosslinked polymer networks with functional ligands on the surface designed to function as catalysts in organic synthesis, solid absorbents in separation and purification, or ion-selective complexants. These microbeads are often fabricated via suspension polymerization of styrene- or methacrylate-based monomers. Introducing various ligands to the beads, such as amines, thiols, different acids or bases, and macrocycles, these polymer-supported agents can be applied to desired fields.[1]

Ion exchange resins (IERs) are classified as strong/weak acid cation or strong/weak base anion exchange resins depending on the functional ligands. Strong acid IERs are usually fabricated by covalent immobilization of sulfonic acid moieties to a cross-linked polystyrene microbeads.[2] Because of the insoluble solid phase and affinity to ions, IERs are widely used in water treatment and hydrometallurgy.[3] By incorporating chelating groups into the microbeads, it is possible to selectively bind to targeted ions. These chelating IERs include iminodiacetate, bipyridine, phosphonic acid, aminothiophosphonate, picolylamine, etc.[4-6]

Phosphorus-containing resins have been reported as an important class of chelating IERs in many literatures because of the coordinating ability of the phosphoryl oxygen and its structure, allowing metal ions chelation.[7] The selectivity towards heavy metals can be varied by manipulating the structure of phosphorus ligands, such as phosphoric, phosphonic, phosphinic acids or phosphonate ester. Phosphonic acid IERs have demonstrated high metal ion uptake and selectivity towards Fe(III), U(VI), Yb(III), and Mn(II).[8] It is also extensively studied with other ligands conjugated on the same beads. Studies also showed that multiple ligands on the resin could complex much greater amount of heavy metal species than either one alone.[9] The mechanism involved in this bifunctional IERs can be explained as a coupling of an access

mechanism and a recognition mechanism, where one ligand permits all ions contacting the matrix rapidly and the other selectively coordinates a targeted metal ion.[10] The introduction of sulfonic acid has been proved to provide efficient access mechanism due to its hydrophilicity that permits rapid entry of metal ions into the matrix.[9] Various chemical formulas of bifunctional phosphonic/sulfonic acid resins (Figure 5.1) were explored in terms of its selectivity and applications. Different strategies were used to fabricate these bifunctional (di)phosphonic/sulfonic acid resins. For example, resin A in Figure 5.1 involves phosphorylation of crosslinked chlorinated styrene resins by Arbuzov reactions, and then sulfonation by 90% sulfuric acid at elevated temperature of at least 100 °C. Resins B and C are generally synthesized by copolymerization of phosphorous containing monomer, usually phosphonate ester species due to its solubility, and styrene-based monomer, followed by the hydrolysis of phosphonate ester and sulfonation by concentrated sulfuric acid. These contemplated resins shown in Figure 5.1 demonstrated different selectivity towards heavy metals, absorptivity, and kinetics. However, all can be used to separate polyvalent metal ions such as Eu(III), Am(III), and Fe(III) by both ion exchange and coordination mechanisms. It is believed that the phosphonic acid groups in these resins particularly bind to metal cations having a valence of +3 or greater, whereas the sulfonic acid moieties primarily bind to water molecules and prevent the beads from collapsing in concentrated acid or metal ions solution. In the presence of sulfonic acid groups, these resins were examined to have superior metal removal efficiency, selectivity, and fast kinetics for polyvalent metal cations relative to monofunctional sulfonic or phosphonic acid resins.

We recently reported an operationally simple and controllable strategy for the fabrication of sulfuric acid IER using mild SuFEx-based condition without concentrated sulfuric acid.[11] SuFEx, sulfur(VI) fluoride exchange reaction, was first introduce by Sharpless and his

coworkers.[12] It describes the reactions between sulfonyl fluoride (-SO_2F) or fluorosulfonate (-OSO_2F) and a silyl ether, forming sulfonate or sulfate linkages in the presence of amidine or guanidine bases.[13] However, when it comes to benzyl or allyl alcohol derivatized silyl ether, such as *tert*-butyldimethylsilyl (TBS)-protected benzyl alcohol, the fluorosulfonate groups are hydrolyzed to form corresponding sulfuric acids.[14] Using this reaction, sulfuric acid groups were introduced to fluorosulfonated polystyrene resins. To the best of our knowledge, it was the first report on sulfuric acid containing strong acid IERs, and there is no work done on the metal complexing properties of sulfuric acid IERs.

In addition, this new click reaction, SuFEx, also offers a new avenue to fabricate phosphorous containing chelating IERs. Compared to conventional phosphorylation method, such as Friedel-Crafts reaction with $PCl_3/AlCl_3$ followed by oxidation of concentrated nitric acid,[8] or Arbuzov reaction with reflux of phosphite derivatives, SuFEx usually yield the targeted molecules under mild condition without high temperature which could potentially damage the microbeads. Here, we proposed to first conjugate TBS-protected phosphonate ester to fluorosulfonated polystyrene microbeads under mild condition followed by the cleavage of ester to form phosphonic acid containing chelating resins. This alternative method was then evaluated by metal chelating measurement on the resulting phosphonic acid IERs. As mentioned earlier, the introduction of sulfonic acid can further improve the metal complexing capability of phosphonic acid IERs due to the access mechanism introduced by sulfonic acid ligands. In comparison, the impact of sulfuric acid ligands on phosphonic acid IERs was also investigated in this work. An effective strategy for making bifunctional phosphonic/sulfuric acid resins was described and investigated on its chemical composition, beads morphology, acid capacity and metal complexing capability.

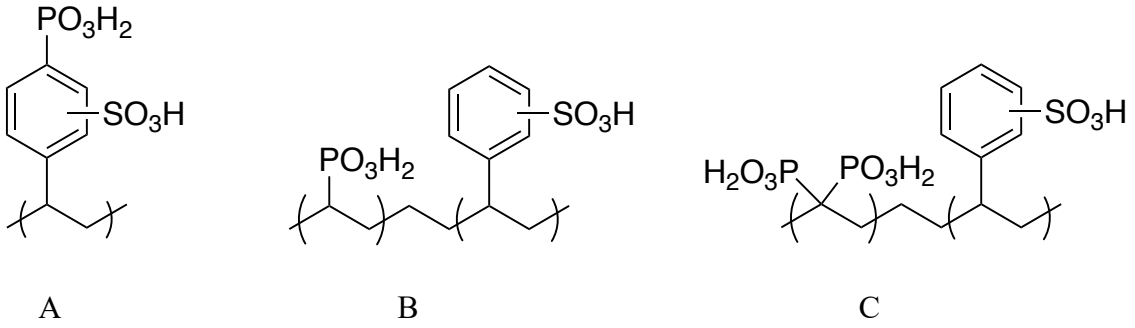

A B C

Figure 5.1. Structures of common bifunctional phosphonic/sulfonic acid resins: monophosphonic/sulfonic acid both linking to the same repeating benzene ring (A), monophosphonic/sulfonic acid linking to separate polymer repeating units (B), and diphosphonic/sulfonic acid also called Diphonix® resin (C)

Experimental

Materials

Acetonitrile was distilled from CaH_2 and stored in molecular sieves. Imidazole was recrystallized from dichloromethane (DCM) at room temperature. TBS-benzyl alcohol was synthesized following previous reported methods.[11] Styrene and fluorosulfonated styrene containing polymer beads were fabricated following previous reported approach.[11] All other reagents were purchased from VWR, TCI, or Sigma-Aldrich and used as received unless noted.

Synthesis of TBS-(diethyl 4-hydroxyphenylphosphonate)

Diethyl 4-hydroxyphenylphosphonate. The synthesis of precursor diethyl 4-hydroxyphenylphosphonae was adapted from previous reported method.[15] 4-bromophenol (5 g, 20 mmol), $NiBr_2$ (0.51 g, 2.32 mmol) catalyst and 5 mL mesitylene were placed in an oven-dried three neck round bottle. The mixture was then vigorously stirred under N_2 atmosphere at 170 °C for 2 h, followed by dropwise addition of triethylphosphite (7.2 g, 43.5 mmol). After another 4 h

stirring at 170 °C, the mixture was passed through celite, dissolved in ether and extracted with 10% NaOH aqueous solution twice. The aqueous layer was washed with ether twice and acidified with concentrated HCl acid. Then it was extracted with ether three times, followed by $MgSO_4$ treatment, rotary evaporator and high vacuum. The yellowish liquid was purified through flash chromatography (hexane : ethyl acetate) to yield a colorless liquid, which was then recrystallized in DCM to yield white powder. NMR was shown in SI.

TBS-(diethyl 4-hydroxyphenylphosphonate). Diethyl 4-hydroxyphenylphosphonate (4.5 g, 19.5 mmol), *tert*-butyldimethylchlorosilane (3.1 g, 20.6 mmol), and imidazole (2.9 g, 42.5 mmol) were dissolved in 40 mL DCM, and the mixture was stirred at 35 °C overnight. The crude product was washed with H2O three times and brine once and dried with $MgSO_4$. The residual solvent was removed by rotary evaporator under vacuum to yield colorless liquid. NMR was shown in SI.

Fabrication of sulfuric acid containing polymer beads (Sulfated ion exchange resin)

Sulfated IER was fabricated through deprotection of fluorosulfonate groups on styrene-based resins, using our recently reported SuFEx-based condition.[11] 0.5 g fluorosulfonated beads (styrene : fluorosulfonated styrene 7:3 w/w with 10% crosslinker divinyl benzene), 1.5 g TBS-benzyl alcohol (5 eq to SO_3F in beads), and 0.2 g TBD catalyst (20 mol%) were dispersed in 10 mL anhydrous acetonitrile, and stirred at 70 °C overnight. The beads were separated by vacuum filtration, washed with acetonitrile, 2 M HCl solution, H_2O, and ethanol, and then dried at 80 °C in vacuum oven before use.

Fabrication of phosphonic acid containing polymer beads (Phosphonated ion exchange resin)

0.5 g fluorosulfonated beads, 1 g TBS-(diethyl 4-hydroxyphenylphosphonate) (2 eq to SO_3F in beads), and 82 mg TBD catalyst (20 mol%) were dispersed in 10 mL anhydrous

acetonitrile, and stirred at 70 °C overnight. The beads were separated by vacuum filtration, washed with acetonitrile, and ethanol, and then dried at 80 °C in vacuum oven. Bromotrimethylsilane (TMS-Br)/MeOH was employed to deprotect diethylphosphonate, yielding phosphonic acid ligands. In detail, 5 mL 5% TMS-Br in acetonitrile was added to the previously treated beads, stirred at room temperature for 2 h. The solvent was removed by rotary evaporator under vacuum. 5 mL methanol was then added to the beads, stirred at room temperature for another 2 h. The final product was separated by vacuum filtration, washed with methanol, 2 M HCl solution, H_2O, and ethanol, and then dried at 80 °C in vacuum oven before use.

Fabrication of bifunctional phosphonic/sulfuric acid polymer beads (Phosphonated/sulfated ion exchange resin)

1 g fluorosulfonated beads, ~ 0.5 g TBS-(diethyl 4-hydroxyphenylphosphonate) (0.5 eq to SO_3F in beads) and 21 mg TBD catalyst (20 mol%) were dispersed in 20 mL anhydrous acetonitrile, and stirred at 70 °C overnight. The beads were separated by vacuum filtration, washed with acetonitrile, and ethanol, and then dried at 80 °C in vacuum oven. Bromotrimethylsilane (TMS-Br)/MeOH was employed to deprotect diethylphosphonate, yielding phosphonic acid ligands. The leftover SO_3F was deprotected using TBS-benzyl alcohol method with details shown above.

Acid capacity measurement

~ 0.1 g acid ion exchange resins fabricated using methods above were reacted with 15.00 mL ~ 0.05 M NaOH solution overnight. 10.00 mL of the solution was then separated by syringe filter, and titrated with standardized ~ 0.05 M HCl solutions with several drops of 0.1% methyl orange as indicators. Using the following equation, acid capacity of different resins can be calculated:

$$acid\ capacity = \frac{(15\ mL\ NaOH) \times M(NaOH) - 1.5 \times (volume\ of\ titrated\ HCl) \times M(HCl)}{Weight\ of\ dried\ resins\ (g)}$$

Metal ions adsorption analysis

50 mg of S- or P-IERs were dried at 80 °C in vacuum oven overnight before the loading tests. Resins were preconditioned with 5 mL of 0.04, 1 or 4 M nitric acid solution in a scintillation vial for 15 min. Then, 5 mL of 50 ppm Fe(III), Mg(II), Cu(II), or Ni(I) containing solution was added to the vial. The suspension was stirred at room temperature for about 20 h, followed by filtration to separate solution from beads. The filtered solution was sent to Agricultural & Environmental Services Laboratories (ASEL) of University of Georgia for the metal analysis by inductively coupled plasma – mass spectrometry (ICP-MS). Metal ion analysis was carried out with bifunctional PS-IERs that gave same amount of P element with 50 mg P-IERs. P elemental analysis was also conducted by ASEL. About 50 mg of P- or PS-IERs were first digested in fluorocarbon tubes in a microwave at 200 °C under pressure, and then measured by ICP-MS. Several important parameters, metal adsorptivity%, distribution coefficient (*D*), and metal complexes concentration (*Q*), were calculated to evaluate metal ion uptake by different IERs in this study, shown below.

$$Adsorptivity\% = \frac{c_0 - c_t}{c_0} \times 100\%$$

$$D = \frac{c_0 - c_t}{c_t} \times \frac{V}{m}\ (mL/g)$$

$$Q = \frac{(c_0 - c_t)V}{m}\ (mg/g)$$

where c_0 and c_t is the concentration of metal ions before and after resins treatment, respectively; V is the total volume of solution; m is the dry weight of resins used in the study.

Characterization

Infrared spectra were taken using a Thermo-Nicolet model 6700 spectrometer equipped with a variable angle grazing angle attenuated total reflection (GATR-ATR) accessory (Harrick Scientific) at 64 scans with 4 cm^{-1} resolution. Beads morphology images were taken on a FEI Inspec F FEG scanning electron microscope at 10 kV. Elemental analysis for P and the concentration of metal ions were measured by ASEL.

Results and Discussion

The synthesis of resins used in this study is summarized in Scheme 5.1. Synthesis of the sulfated resins (S-IER) has been reported in detail recently.[11] Phosphonated resins (P-IER) were fabricated using SuFEx click reaction, followed by bromotrimethylsilane deprotection to yield phosphonic acid functionalities. Unlike Arbuzov-type reaction commonly used to install phosphonate ester onto chlorinated beads,[15, 16] SuFEx reaction is generally under milder condition without high temperature reflux. To evaluate the impact of sulfuric acid moiety on the performance of P-IER, bifunctional phosphonic/sulfuric acid resins (PS-IER) were also fabricated and studied in this work. Combining the two strategies employed to fabricate S- and P-IER, it was first partially functionalized with phosphonic acid and then residual fluorosulfonate groups were deprotected, resulting two acidic functional groups immobilized on the same beads. Another strategy, shown in Scheme B.1, was first used in the preliminary study. Both sulfonate and phosphonate ligands were conjugated to parent beads in one pot using TBS-benzyl alcohol and TBS-phosphonate mixtures, followed by the deprotection of phosphonate ester. However, we found the disappearance of sulfuric acid groups in FTIR after the treatment with TMS-Br and MeOH (Figure B.1).

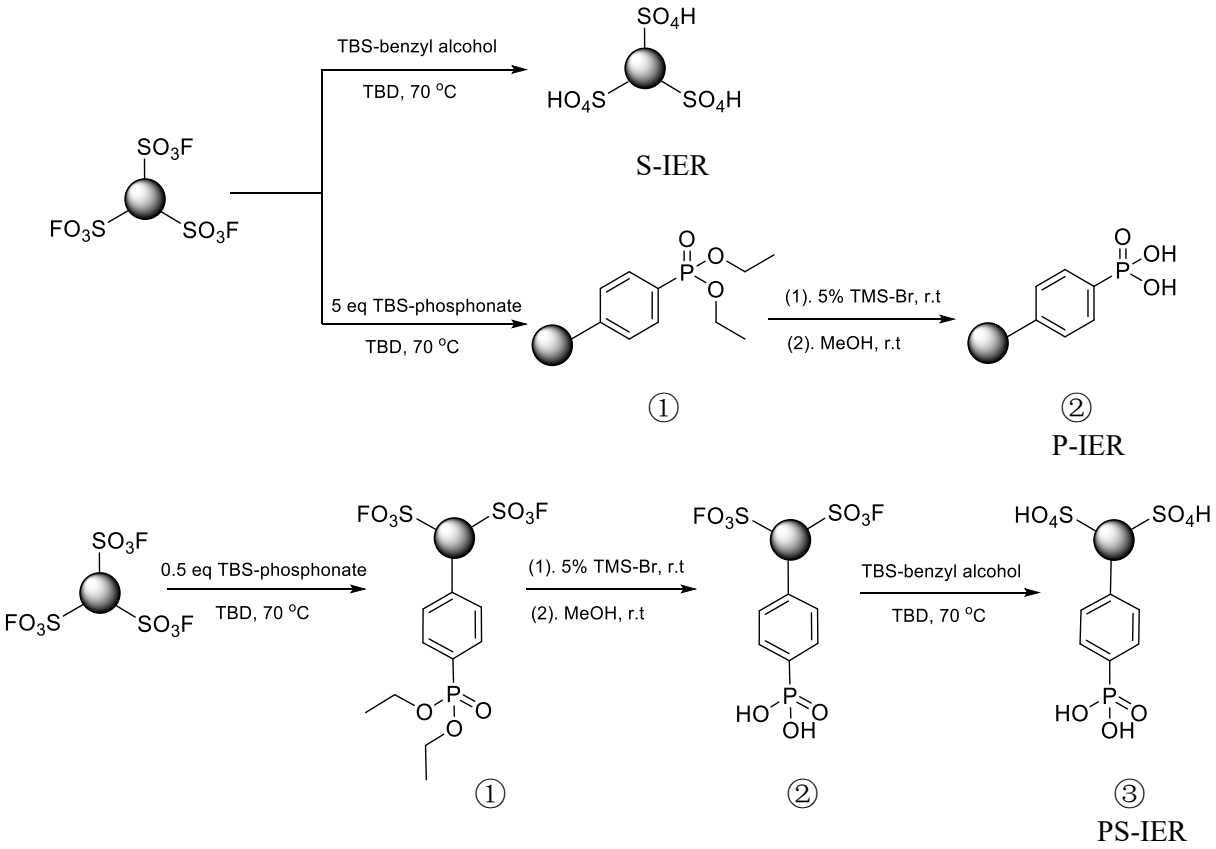

Scheme 5.1. Preparation of monofunctional sulfated, phosphonated, and bifunctional sulfated/phosphonated polymer resins

To confirm the successful modification, each resin was characterized with FTIR. In Figure 5.2, P-IER was analyzed, showing three characteristic bands at 1184, 1218 and 1252 cm^{-1} associated with PO_3 asymmetric stretch[17] in P-IER ① beads, and 1184, 1218 and 1238 cm^{-1} in P-IER ② beads. The P=O stretch was downshifted to 1238 cm^{-1} after the hydrolysis of phosphonate ester, which is consistent with previous report.[9] Another noticeable difference between P-IER ① and ② spectra was the diminish of the broad peak at 1053 cm^{-1}, corresponding to the P—O—C of phosphonate ester groups. The assignment of IR indicated the conjugation of phosphonate functional groups and its fully hydrolyzed phosphonic acid formationalities. For bifunctional PS-IER, Figure 5.3 demonstrated similar PO_3 asymmetric

stretches at 1181 and 1216 cm^{-1}, and the third band appeared in Figure 5.1 might be overlapped with its neighboring band. In addition, a characteristic band at 1040 cm^{-1} associated with sulfate groups[11, 14] appeared in PS-IER, proving the presence of sulfuric acid on the resins.

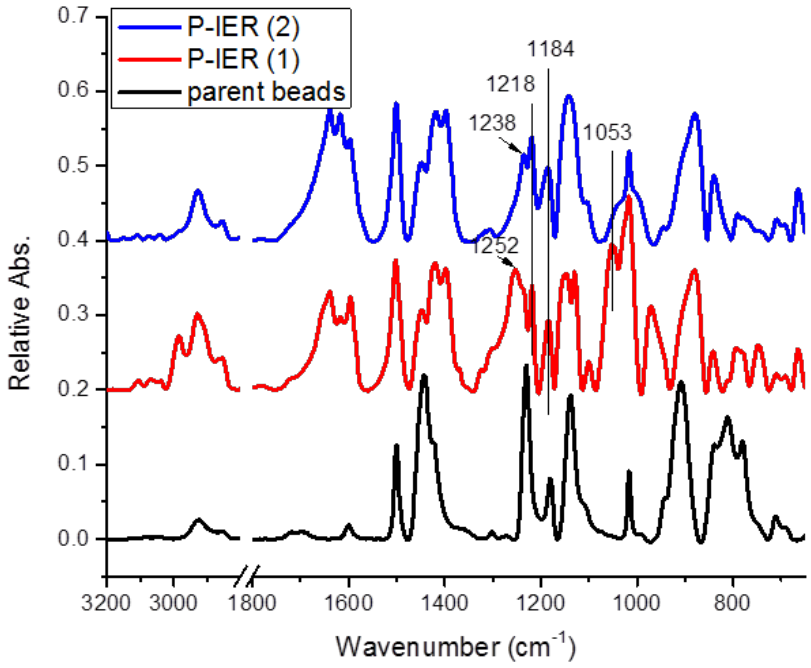

Figure 5.2. IR spectra of polymer-supported phosphonate ester and phosphonic acid as KBr pellet forms

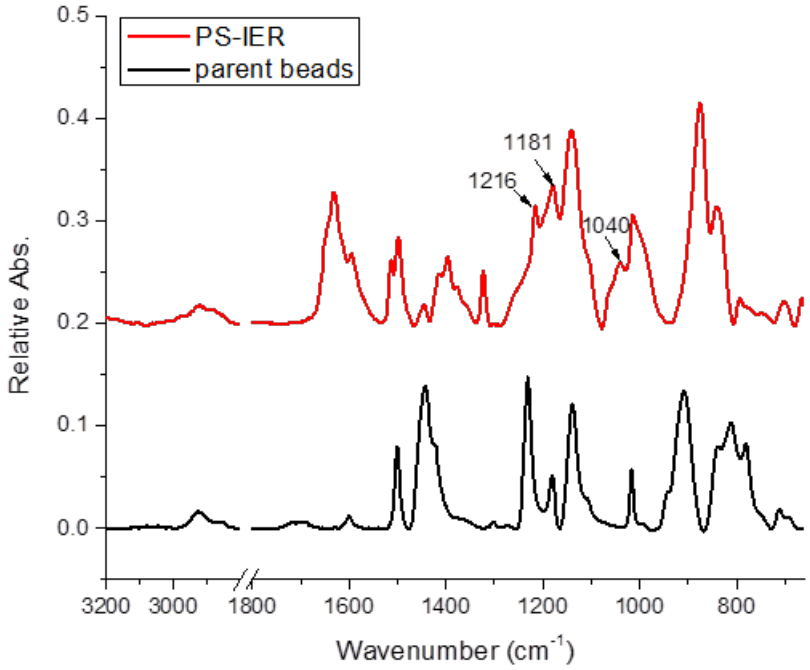

Figure 5.3. IR spectra of bifunctional phosphonic/sulfuric acid polymeric microbeads as KBr pellet form

The morphologies of different resins were characterized using SEM, shown in Figure 5.4. Images of fully sulfuric acid resins were studied previously[11] and no graphs were shown here. These fluorosulfonated polymeric beads were all spherical particles ranging from 40 to 70 μm in diameter. Both original beads and phosphonated beads had very smooth surfaces and almost no significant difference can be observed on parent and phosphonic acid resins in Figure 5.4A and B. In Figure 5.4C, bifunctional PS-IERs had much more small debris attached to the particle surface. This might be due to the extra sulfation step, longer vigorous agitation and processing time, leading to a small amount of damaged beads debris. Since most of the microbeads we observed on PS-IERs held intact spherical structures, this proposed multiple processing steps for the fabrication of PS-IER were believed to be effective and feasible. That is to say, using SuFEx-based strategies, monofunctional sulfuric or phosphonic acid resins and bifunctional

phosphonic/sulfuric resins can be achieved with intact microbeads structures under relatively mild conditions.

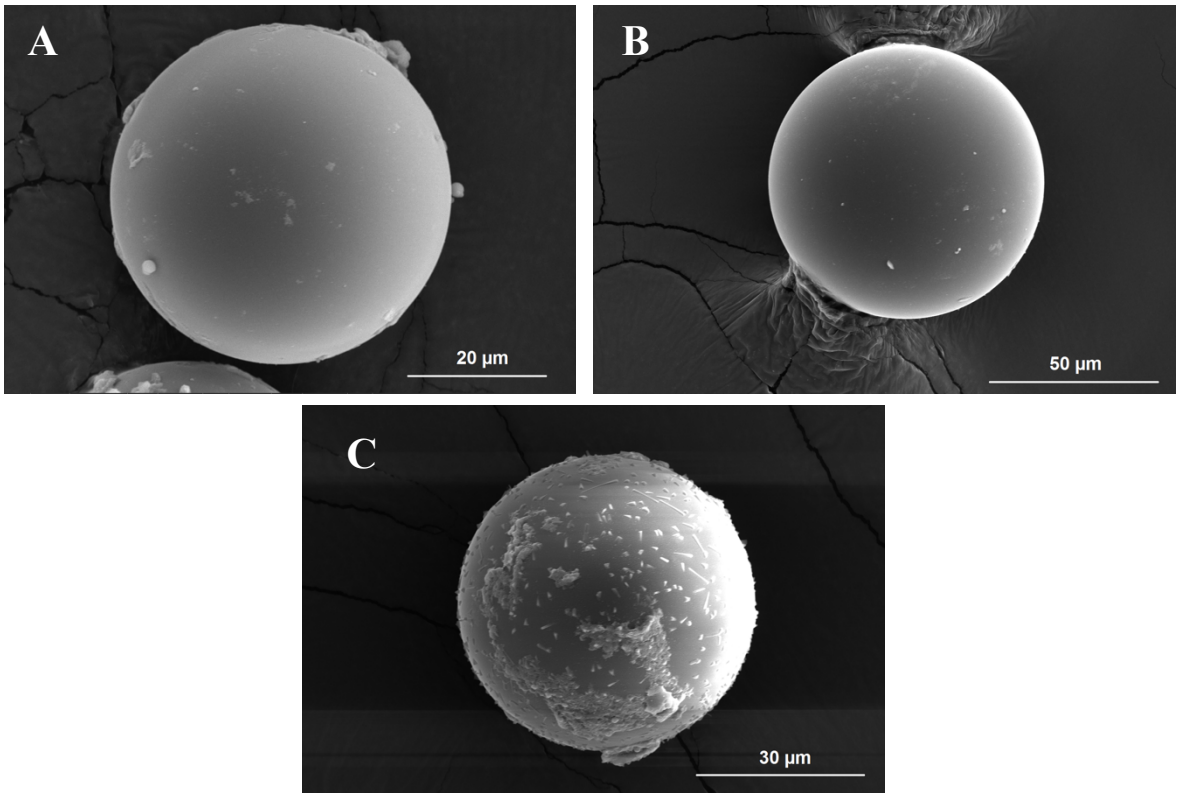

Figure 5.4. Scanning electron micrographs of original fluorosulfonated polystyrene beads (A), functionalized phosphonic acid beads (B), and bifunctional phosphonic/sulfuric acid beads (C)

Then, acid capacities of three different resins fabricated in this work were investigated using a standard titration protocol.[18] As shown in Table 5.1, the capacity of fully sulfated and phosphonated resins are 1.2 and 2.3 meq/g respectively, and the former is nearly half of the latter. This is consistent with the acidity ratio of phenylsulfate and phenylphosphonic acid which is 1:2. Using this theoretical acidity ratio and capacity of PS-IERs, the ratio of ligated sulfuric and phosphonic acid could be estimated. In this case, 0.5 eq PS-IERs, meaning 0.5 eq of TBS-phosphonate ester was reacted with parent beads in the first step, yielded an acid capacity of 1.75 meq/g, roughly 46% and 54% of reactive sites linked to phosphonic and sulfuric acid groups

respectively. Comparing phosphorous elemental analysis of P-IERs and PS-IERs, similar ratio of phosphonic and sulfuric acid ligands was calculated on 0.5 eq PS-IERs. Both methods estimated almost 1:1 of phosphonic and sulfuric acid ligand in 0.5 eq PS-IERs.

Table 5.1. Acid capacities of different resins used in this study

Resins	S-IER	P-IER	PS-IER[1]
Capacity (meq/g)	1.2	2.3	1.75

[1] 0.5 eq phosphonate ester conjugated PS-IER

As a new strong acid ion exchange resins, S-IERs, it has not been investigated on metal adsorption performance. We picked several divalent and trivalent metallic ions including Ni(II), Cu(II), Mg(II), and Fe(III) and loaded with 50 mg S-IERs in 0.04 M nitric acid solution. Note that the S-IERs tested here were fabricated using 90% fluorosulfonated polystyrene resins, which was different from 30% used in the latter study. The results were shown in Table 5.2. Except 56% Fe(III) was complexed, the rest divalent ions showed little to no affinity to S-IERs. The metallic ions affinity or selectivity on S-IERs can be concluded in this order: Fe(III) ≫ Mg(II) > Cu(II) ≈ Ni(II). For a non-chelating ion exchange resin, its selectivity or affinity to ions usually depend on the diameter of ions, metal ions valance and the free volume in water swelling state.[19] Fe(III) is the smallest metal ions in the selected four ions with highest valance, which explains the absorbed amount of Fe(III) ions was the highest. Since S-IERs are strong acid IERs, proton in solution has significant competition with metal ions interaction especially in very acidic 0.04 M nitric acid solution whose pH was about 1.4. Consequently, metal ions with low valance and relatively larger size had little to no adsorption by S-IERs in the case of Ni(II), Mg(II), and Cu(II).

Table 5.2. Metal ions complexing abilities of sulfuric acid IERs

Metal ions	Absorptivity %	D (mL/g)	Q(mg/g)
Ni(II)	0	0	0
Cu(II)	0	0	0
Mg(II)	8.4	18	0.4
Fe(III)	56	253	2.8

Furthermore, we evaluated heavy metal complexing abilities of each resins including monofunctional S- and P-IERs, and bifunctional 0.8 eq and 0.5 eq PS-IERs. Here, Fe(III) was chosen as a target heavy metal ion. The presence of iron in copper electrowinning electrolyte solution would significantly decrease the current efficiency, because it diverts electricity from copper plating by oxidation or reduction of iron itself at the anode or cathode.[4] In addition, small amount of iron is also a big challenge for producing high purity nickel and cobalt due to its similar aqueous chemical properties and electro-potentials with nickel or cobalt.[20, 21] Therefore, iron must be removed from the process liquors before or during electrolysis. Phosphonic acid IERs are well-known chelating resins used to remove trace iron from copper, nickel or cobalt solutions, such as commercially available Monophos® and Diphonix® resins. To test the complexing property of ligated phosphonic acid by new SuFEx strategy, we first evaluated P-IERs performance on Fe(III) adsorptivity in different acidic aqueous solutions. Figure 5.5A showed a decreasing adsorptivity% trend with the increasing acidity of solution. The highest Fe(III) removal efficiency 68% was observed in 0.04 M nitric acid solution. The distribution ratios of P-IERs shown in Figure 5.5B, were relatively higher than other reports,[22-24] and maximum *D* was nearly 400 mL/g in 0.04 M HNO_3 solution. In comparison, a non-chelating IER, S-IER, was also evaluated, and it generally complexed smaller amount of Fe(III) ions. This was attributed to the higher metal ion capture ability - two exchangeable sites in phosphonic acid

ligand while only one in sulfuric acid ligand. Besides, in a chelating ion exchange resins, the stability constant of chelating groups with metal ions also represents the affinity to metal ions.

Inspired by commercially available bifunctional phosphonic/sulfonic acid chelating IERs, the impact of additional sulfuric acid on P-IERs was investigated by conducting the same Fe(III) complexing experiments. Two types of PS-IERs with different phosphonic to sulfuric acid ratios were studied. 0.8 eq PS-IERs had higher phosphonic to sulfuric acid ratio than 0.5 eq PS-IERs. Figure 5.5 demonstrated the ion complexing capability of PS-IERs. Compared to fully functionalized P-IERs, lower Fe(III) adsorptivity% was observed and significant decrease was seen on distribution coefficient and metal complexes concentration. Because of its hydrophilicity and nonselective metal access, sulfonic acid greatly increased phosphonated resins chelating capacity and efficiency on Fe(III) adsorption.[24] However, the introduction of sulfuric acid into the matrix did not enhance the kinetics of complexation, and it decreased Fe(III) adsorptivity% in all acidic solution instead, compared with P-ISRs. This might correlate to the ligands distribution structure on the resins surface, shown in Figure 5.6. The conjugated phenylphosphonic acid has longer side chain than sulfuric acid. Consequently, ions more likely first interact with phosphonic acid, which probably also block sulfuric acid sites since the amount of phosphonic acid was equal or larger than sulfuric acid in the two fabricated PS-IERs. That is to say, due to the higher free volume of phosphonic acid, sulfuric acid ligands failed to offer rapid access mechanism to cations in solution when they first contacted the polymer matrix. Similar or better adsorptivity% was demonstrated in Figure 5.5A on PS-IERs relative to S-IERs, which might be due to the stronger iron affinity of phosphonic acid than sulfuric acid ligands. Since much more PS-IERs were loaded to reach same amount of P element with 50 mg P-IERs,

its distribution coefficient and metal complex concentration were much lower than the two monofunctional resins.

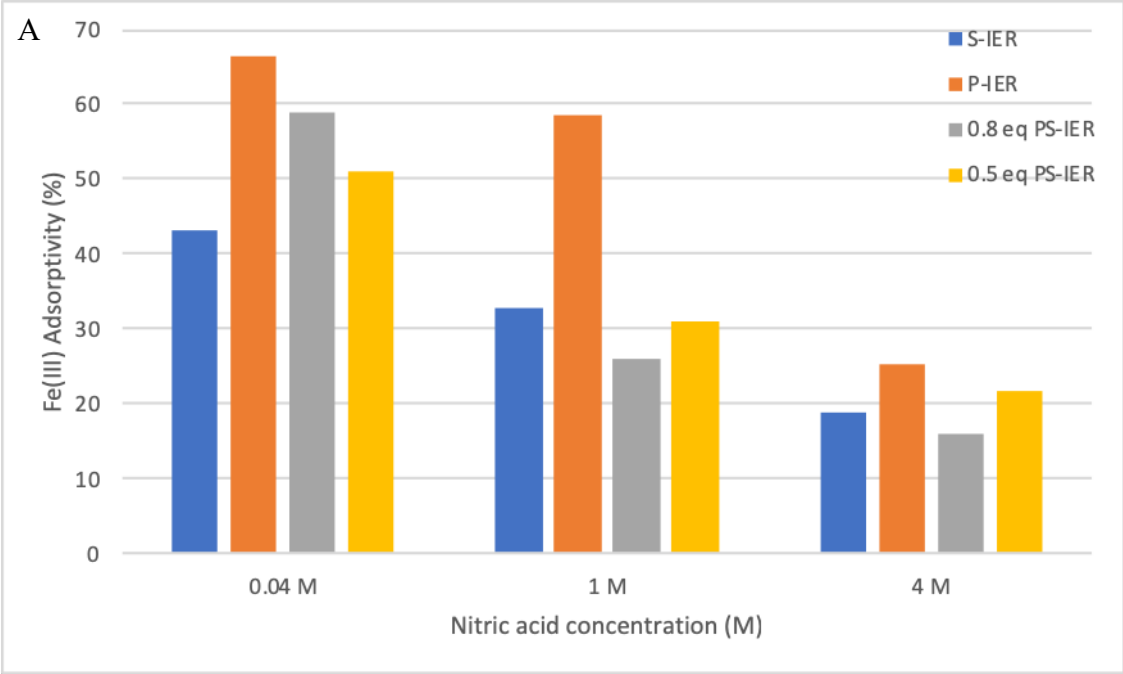

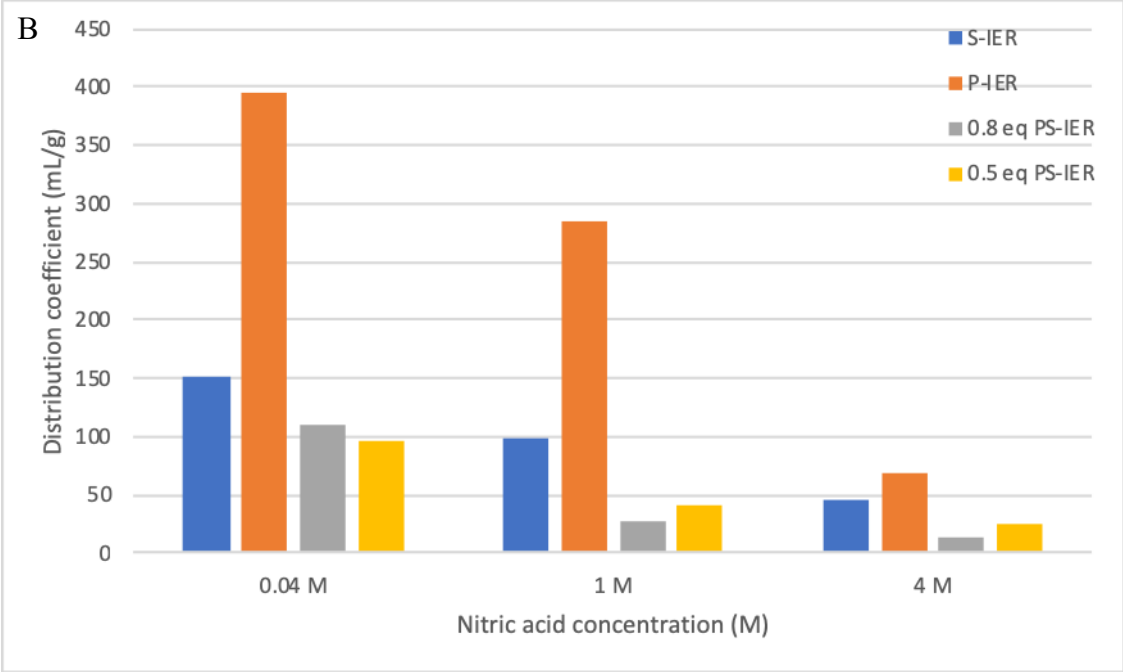

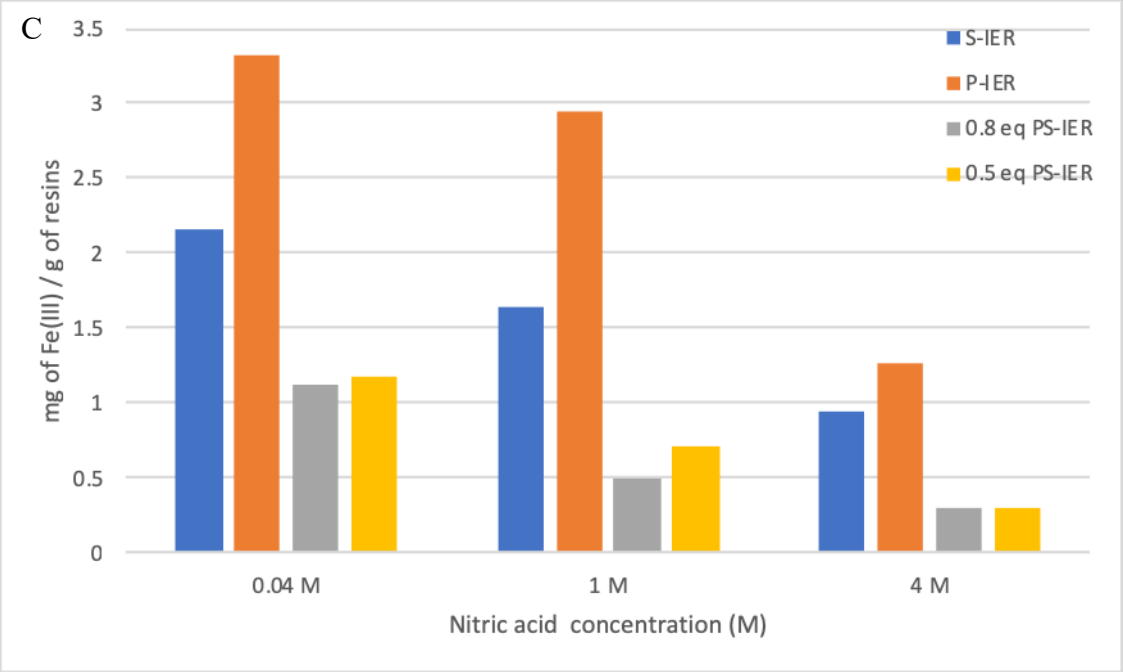

Figure 5.5. Iron uptake adsorptivity (A), distribution ratio (B), and iron loaded (mg/g resin) (C) for various resins in 0.04, 1, and 4 M nitric acid solution

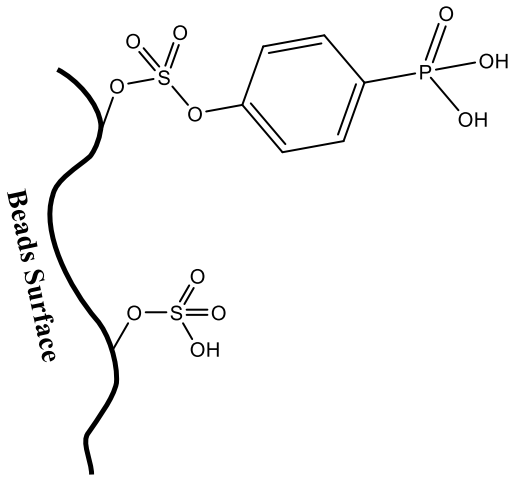

Figure 5.6. Possible ligands distribution on bifunctional phosphonic/sulfuric acid resins surface

Conclusion

The proposed new strategy for preparation of phosphonic acid containing resins on our recently reported versatile fluorosulfonated polystyrene supports was fully investigated on its

chemical composition, surface morphology, and Fe(III) ions adsorption performance. Adsorptivity% decreased with the increased acidity of solution. Inspired by commercially available phosphonic/sulfonic acid chelating resins, the newly reported sulfuric acid ligand was introduced to the phosphonic acid resins by two separate installation steps. Unlike the dual mechanism present in phosphonic/sulfonic acid resins, the additional sulfuric acid groups were found to decrease its adsorptivity% compared to fully functionalized phosphonic acid resins. It is apparent that much more work is needed to fully understand the mechanism and metal adsorption kinetic and selectivity of sulfuric acid ion exchange resins.

References

1. Alexandratos, S. D.; Crick, D. W., *Ind. Eng. Chem. Res.* **1996,** *35* (3), 635-644.

2. Pepper, K. W., *J. Appl. Chem.* **1951,** *1* (3), 124-132.

3. Alexandratos, S. D., *Ind. Eng. Chem. Res.* **2008,** *48* (1), 388-398.

4. McKevitt, B.; Dreisinger, D., *Hydrometallurgy* **2009,** *98* (1-2), 116-121.

5. Popa, A.; Davidescu, C.-M.; Negrea, P.; Ilia, G.; Katsaros, A.; Demadis, K. D., *Ind. Eng. Chem. Res.* **2008,** *47* (6), 2010-2017.

6. Wolowicz, A.; Hubicki, Z., *Chem. Eng. J.* **2012,** *197*, 493-508.

7. Clearfield, A., *J. Alloy Compd.* **2006,** *418* (1-2), 128-138.

8. Egawa, H.; Yamabe, K.; Jyo, A., *J. Appl. Polym. Sci.* **1994,** *52* (8), 1153-1164.

9. Alexandratos, S. D.; Trochimczuk, A. W.; Crick, D. W.; Horwitz, E. P.; Gatrone, R. C.; Chiarizia, R., *Macromolecules* **1996,** *29* (3), 1021-1026.

10. Alexandratos, S. D.; Shelley, C. A.; Horwitz, E. P.; Chiarizia, R., *Solvent Extr. Ion Exc.* **1998,** *16* (4), 951-966.

11. Kassick, A. J.; Chen, L.; Kovaliov, M.; Mathers, R. T.; Locklin, J.; Averick, S., *Chem. Commun.* **2019**.

12. Dong, J. J.; Krasnova, L.; Finn, M. G.; Sharpless, K. B., *Angew. Chem. Int. Ed.* **2014,** *53* (36), 9430-9448.

13. Yatvin, J.; Brooks, K.; Locklin, J., *Chem-Eur J.* **2016,** *22* (46), 16348-16354.

14. Brooks, K.; Yatvin, J.; Kovaliov, M.; Crane, G. H.; Horn, J.; Averick, S.; Locklin, J., *Macromolecules* **2018,** *51* (2), 297-305.

15. Lejeune, N.; Dez, I.; Jaffres, P. A.; Lohier, J. F.; Madec, P. J.; Santos, J. S. D., *Eur. J. Inorg. Chem.* **2008,** (1), 138-143.

16. Abderrahim, O.; Ferrah, N.; Didi, M. A.; Villemin, D., *J. Radioanal. Nucl. Chem.* **2011,** *290* (2), 267-275.

17. Demadis, K. D.; Katarachia, S. D., *Phosphorus. Sulfur.* **2004,** *179* (3), 627-648.

18. Stine, C. L., Polymer-Supported 14-Crown-4 and Bifunctional Resins for Selective Metal Ion Complexation: Synthesis and Characterization. **2002**.

19. Wang, C. C.; Chang, C. Y.; Chen, C. Y., *Macromol. Chem. Physic.* **2001,** *202* (6), 882-890.

20. Wang, G. X.; Zhao, Y. C.; Yang, B.; Song, Y. F., *Hydrometallurgy* **2018,** *176*, 69-72.

21. Song, Y. F.; Wang, G. X.; Yang, B.; Wang, Y. M., *Hydrometallurgy* **2018,** *180*, 246-253.

22. Fila, D.; Hubicki, Z.; Kolodynska, D., *Adsorption* **2019,** *25* (3), 367-382.

23. Azarudeen, R. S.; Ahamed, M. A. R.; Jeyakumar, D.; Burkanudeen, A. R., *Iran Polym. J.* **2009,** *18* (10), 821-832.

24. Xue, S. S.; Gula, M. J.; Harvey, J. T.; Horwitz, E. P., *Miner. Metall. Proc.* **2001,** *18* (3), 133-137.

CHAPTER 6

CONCLUSIONS AND FUTURE OUTLOOK

Conclusions

In this dissertation, postpolymerization modification (PPM) and click chemistry were utilized to design and generate multifunctional polymeric interfaces catering to desired applications. New methodologies for fabricating glycopolymer-coated surfaces and (chelating) cation exchange resins were developed and studied. In chapter 1, a literature review presenting each related techniques and applications was discussed. Various currently employed coating techniques and polymer brushes fabrication methods were first introduced. A brief review on the combination of PPM and click reactions was also presented with examples of several important polymer materials. A new type of click reaction, sulfur(VI) fluoride exchange (SuFEx), was highlighted among other common examples, focusing on the current development. Finally, the development of glycopolymer and ion exchange resins was outlined, illustrating strategies and some applications.

Chapter 2 presented a new approach to generate glycopolymer modified substrates through PPM on poly(PFPA) platform. Employing hydrazine linker, various reducing saccharides were able to efficiently immobilize to polymer surface with evidence of bioactivity retaining. Only minimal amount of carbohydrates was needed to achieve over 80% ligation efficiency, examined by *p*-nitrobenzaldehyde backfilling on several randomly selected saccharides. Furthermore, a lectin (wheat germ agglutinin) and a bacterium (*M. pneumoniae*) were used to successfully demonstrated the retain of ligated biomolecules' activity. Overall, this

simplified methodology offered an effective and versatile avenue to fabricate carbohydrate arrays to mimic glycan presentation on cell surface.

Subsequently, Chapter 3 applied the glycosurface method introduced in Chapter 2 to mimic glycan display in human epithelial cells, in regards to attachment and gliding motility of *M. pneumoniae*, a major cause of "walking" pneumonia. Both 3'- and 6'-sialyllactose were found to support attachment, but gliding motility was only found in the former. Also, a general increasing trend with ligated sialyllactose density was observed on the attachment of *M. pneumoniae*. Using this tunable model system, a receptor density threshold was found for gliding frequency, which was also influenced by avidity issue. Besides, it was demonstrated that the presence of 6'-sialyllactose hindered the gliding motility on 3'-sialyllactose ligated polymer surface. This precise glycopolymer model showed excellent promise in studying receptor specificity beyond linkage alone to reflect the diversity that can exist in conformational flexibility and presentation.

In Chapter 4, a new type of polymer beads precursor was examined to create different polymer-supported reagents, mainly focusing on the formation of strong acid cation exchange resins. When treated with SuFEx-based condition containing TBS-benzyl alcohol, these fluorosulfonated polystyrene beads generated sulfate functionalities on the beads. The formed sulfated polymer beads were further characterized with FTIR and zeta-potential, revealing the formation of anionic sulfate groups. Mild SuFEx condition allowed for the installation of a predictable and controllable number of sulfate groups, maintaining an intact structure and morphology compared to its parent beads. In addition, the resulting sulfated beads were shown to be an effective cation exchange resin by acid capacity measurement and dye capture

experiments. Other molecules were also modified on the parent beads using SuFEx click reaction to demonstrate the versatility of this new polymer beads precursor.

Chapter 5 applied that fluorosulfonated polystyrene supports and sulfuric acid resins (S-IERs) fabrication method discussed in Chapter 4 to the preparation of monofunctional phosphonic acid and bifunctional phosphonic/sulfuric acid ion exchange resins (P- and PS-IERs). Resins were fully characterized by FTIR and SEM, demonstrating the presence of phosphonate and sulfate ligands in the beads, and the retain of intact spherical structure for all three fabricated IERs. P-IERs demonstrated the best Fe(III) sorption capacity, followed by S-IERs and PS-IERs. Newly-reported sulfuric acid resins showed strong affinity to Fe(III) and little to no affinity to divalent metal ions, such as Ni(II), Mg(II), and Cu(II) in acidic solution

Future Work

This dissertation has outlined the utility of postpolymerization modification on different polymer interfaces, combining with click chemistry, to create (multi)functional polymer materials for desired applications. While glycopolymer coating on poly(PFPA) scaffold demonstrated great promise in analysis of gliding motility on 3'-sialyllactose alone or with 6'-sialyllatose, more ligands or carbohydrates receptors are still needed to be analyzed to reveal the gliding and related infection mechanisms. Current work now focuses on the immobilization of lactose sulfate, another receptor for attachment, on the using model. In order to statistically study the impact of lactose sulfate on attachment and gliding of *M. pneumoniae*, an accurate quantification method is necessary to estimate the actual amount of conjugated ligands on the surface especially when it comes to a mixture of itself and other receptors, such as 3'-sialyllactose.

In addition, our future work on this glycopolymer coating will shift to the conjugation of oligosaccharides with charges used as boundary biolubricant. Boundary lubrication, where the sliding surfaces are coated with lubricating layers, has been important since ancient time, and it remains under extensive investigation nowadays. Many biomaterials or macromolecules have been utilized to mimic the performance of cartilage, among which polyelectrolyte, polymer brushes, hyaluronic acid, and phospholipids are shown acceptable lubricity in a narrow range of applied loads and shear rates. With the developed glycosurface methodology, hydrazine linker or direct aminolysis can ligate a wide range of charged oligosaccharides. Also, the well-studied poly(PFPA) platform allows the incorporation of many variables, such as brushes structure and thickness, ligation density, and crosslinking density, etc., all of which need to be studied in terms of the boundary lubrication property.

Regarding the new sulfuric acid cation exchange resins, the future work will concentrate on the application of metal removal and catalysis. Compared to commercially available sulfonic acid exchange resins, the performance of sulfuric acid resins, even more acidic microbeads, needs to be tested on the metal ions capacity, adsorption kinetics, removal efficiency, and heterogeneous catalyst in different acid-catalyzed reactions. All of these studies will help to better understand the property and utility of this newly developed strong acid cation exchange resins. On the other hand, SuFEx click and the fluorosulfonated styrene microbeads provide a unique and powerful avenue to explore multifunctional (chelating) ion exchange resins. Multiple functional groups can be modified onto the microbeads through SuFEx reactions, and the synergistic function of the ligated groups is interesting to further explore in the context of bifunctional catalyst — effectively catalyzing multiple different reactions, or chelating heavy metal complexants — selectively removing heavy metal ions.

Final Remarks

Postpolymerization modification on polymer-based platform has shown great versatility and promise in manipulating polymer functionalities and tailoring materials properties for desired applications. Incorporating click-type reactions, the toolbox is further expanded, providing a handful of powerful strategies to couple a wide array of functional groups with high yields under mild conditions. This dissertation demonstrates a few examples of the combination of PPM and click chemistry in different fields and evaluates the properties and performances of the resulting materials used in real applications. With interdisciplinary collaboration, the polymer interface modification will show greater advantages and possibilities in many practical areas, such as sensors, functional membranes, cell proliferation, medical devices, chromatography, and microfluidics. Plenty of ongoing researches on the design of highly sophisticated surfaces using postpolymerization modification will promote the development of new applications where precisely controlled and defined multifunctional surfaces are required.

APPENDIX A

SURFACE CHARACTERIZATIONS OF CHEMICALLY FUNCTIONALIZED SUBSTRATES

Table A.1. Thickness and contact angle of polymer films in each modification steps

	Thickness (nm)	Contact angle (deg)
APTMS	1.2±0.09	48±1.5
Poly(PFPA)	14.9±0.56	100±0.5
0.1% hydrazine	8.9±0.29	wet
3'-sialyllactose	9.8±0.23	wet
6'-sialyllactose	9.8±0.29	wet
0.5% hydrazine	8.9±0.19	wet
3'-sialyllactose	10.1±0.39	wet
6'-sialyllactose	10.1±0.27	wet
1% hydrazine	9.0±0.30	wet
3'-sialyllactose	10.9±0.23	wet
6'-sialyllactose	10.3±0.25	wet
2.5% hydrazine	8.2±0.12	wet
3'-sialyllactose	10.0±0.12	wet
6'-sialyllactose	10.1±0.38	wet
100% hydrazine	7.6±0.30	wet
3'-sialyllactose	9.7±0.23	wet
6'-sialyllactose	10.0±0.52	wet

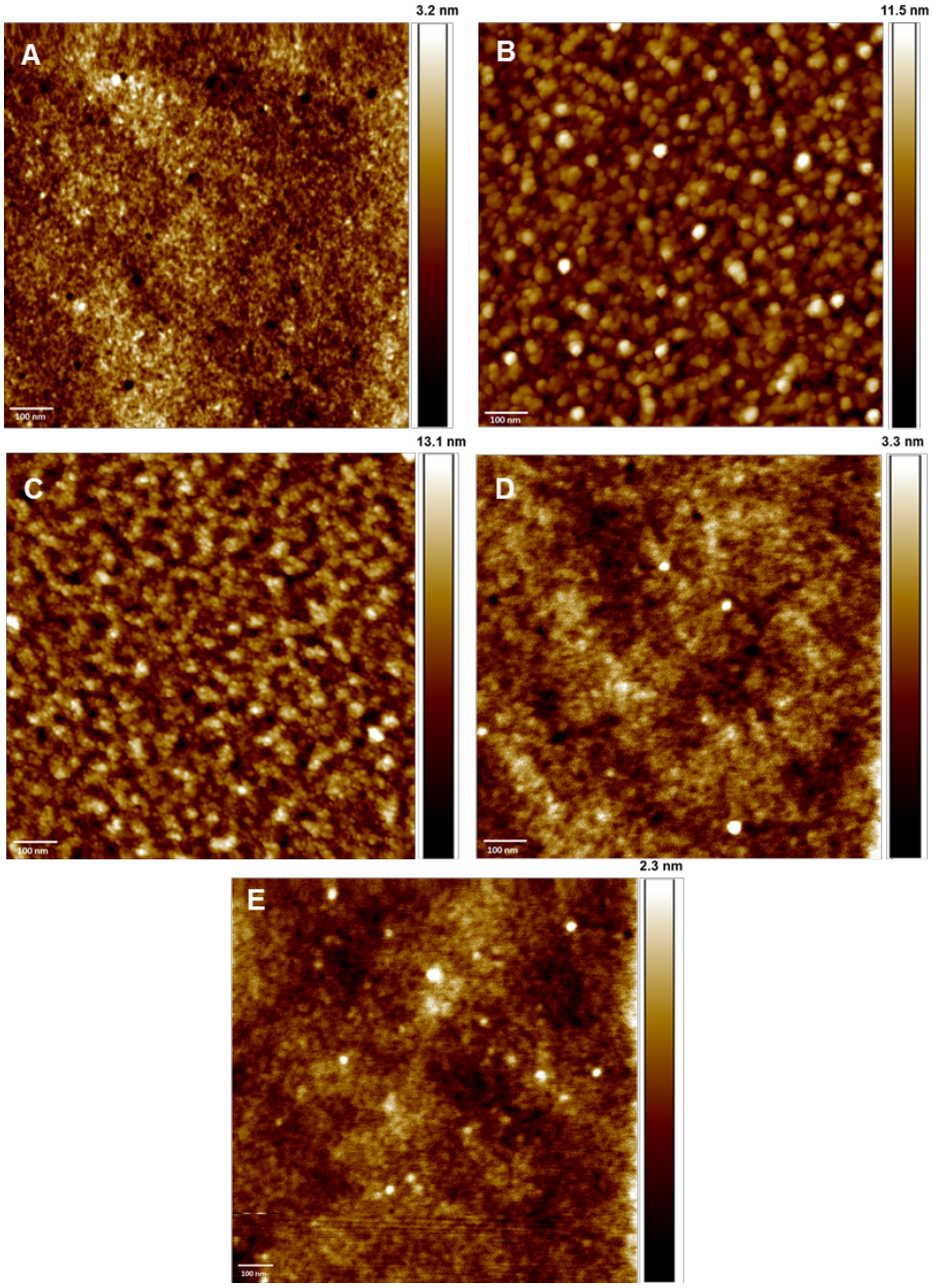

Figure A.1. AFM topography images of poly(PFPA) grafted-to brushes (A), 100% hydrazine conjugated (B) and corresponding 3'-sialyllatcose conjugated (C) slides, and 0.5% hydrazine conjugated (D) and corresponding 3'-sialyllactose conjugated (E) slides. The root mean squared (RMS) roughness is (A) 0.453 nm, (B) 1.55 nm, (C) 1.87 nm, (D) 0.339 nm, and (E) 0.308 nm.

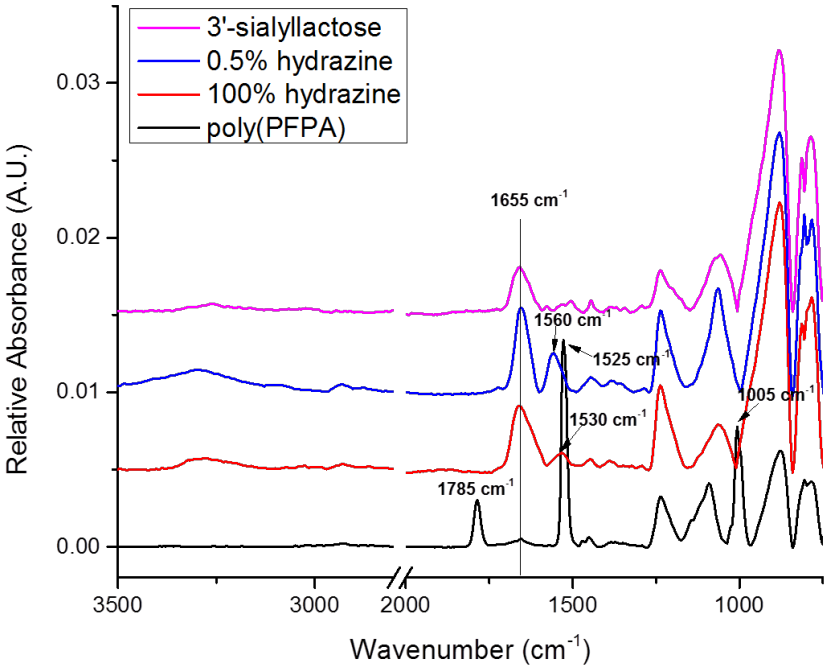

Figure A.2. FTIR spectra of poly(PFPA) and functionalized brushes, including 100% hydrazine and 0.5% hydrazine/ethanolamine modified surface as representative spectra of the five selected hydrazine/ethanolamine ratios conjugated substrates, and 3'-sialyllactose coated surface.

APPENDIX B

ANOTHER STRATEGY STUDIED FOR THE PREPARATION OF PHOSPHONIC/SULFURIC ACID ION EXCHANGE RESINS

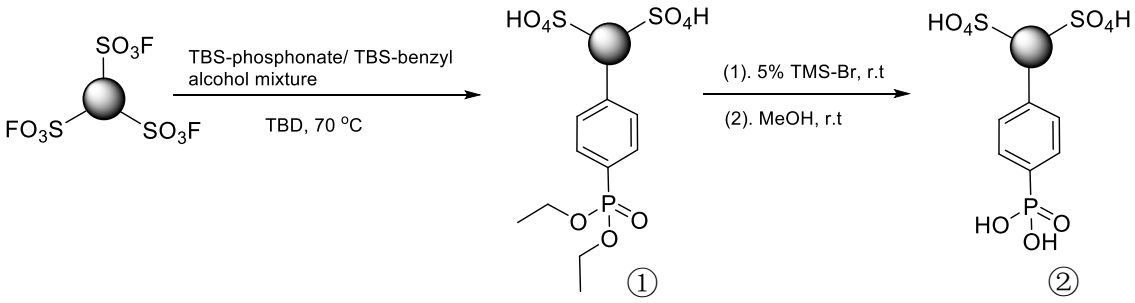

Scheme B.1. Phosphonic/sulfuric acid resins fabrication method using SuFEx chemistry, installing sulfuric acid and phophonate ester in one pot, followed by the cleavage of ester

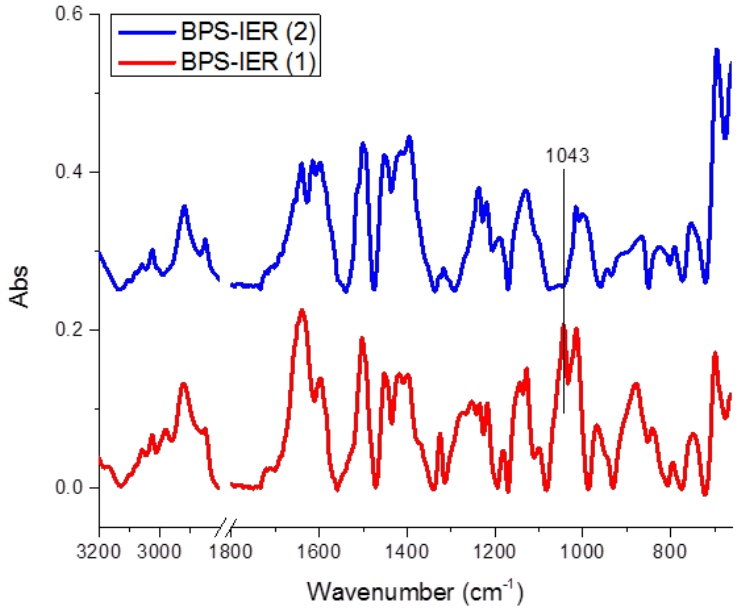

Figure B.1. IR spectra of BPS-IERs using strategy above

APPENDIX C

NMR SPECTRA OF COUMPOUNS

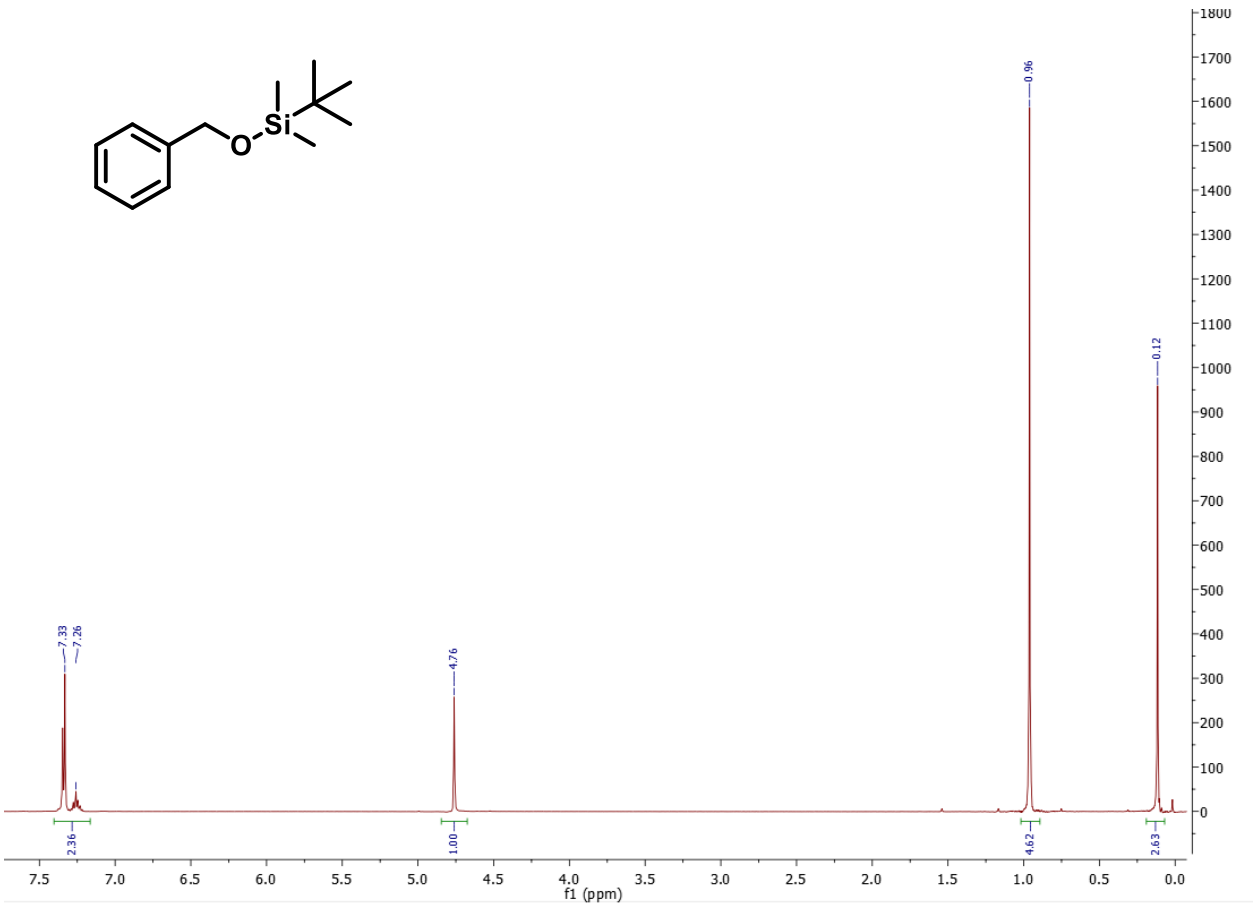

Figure C.1. ^{1}H NMR of *tert*-butyldimethylsilyl-protected benzyl alcohol

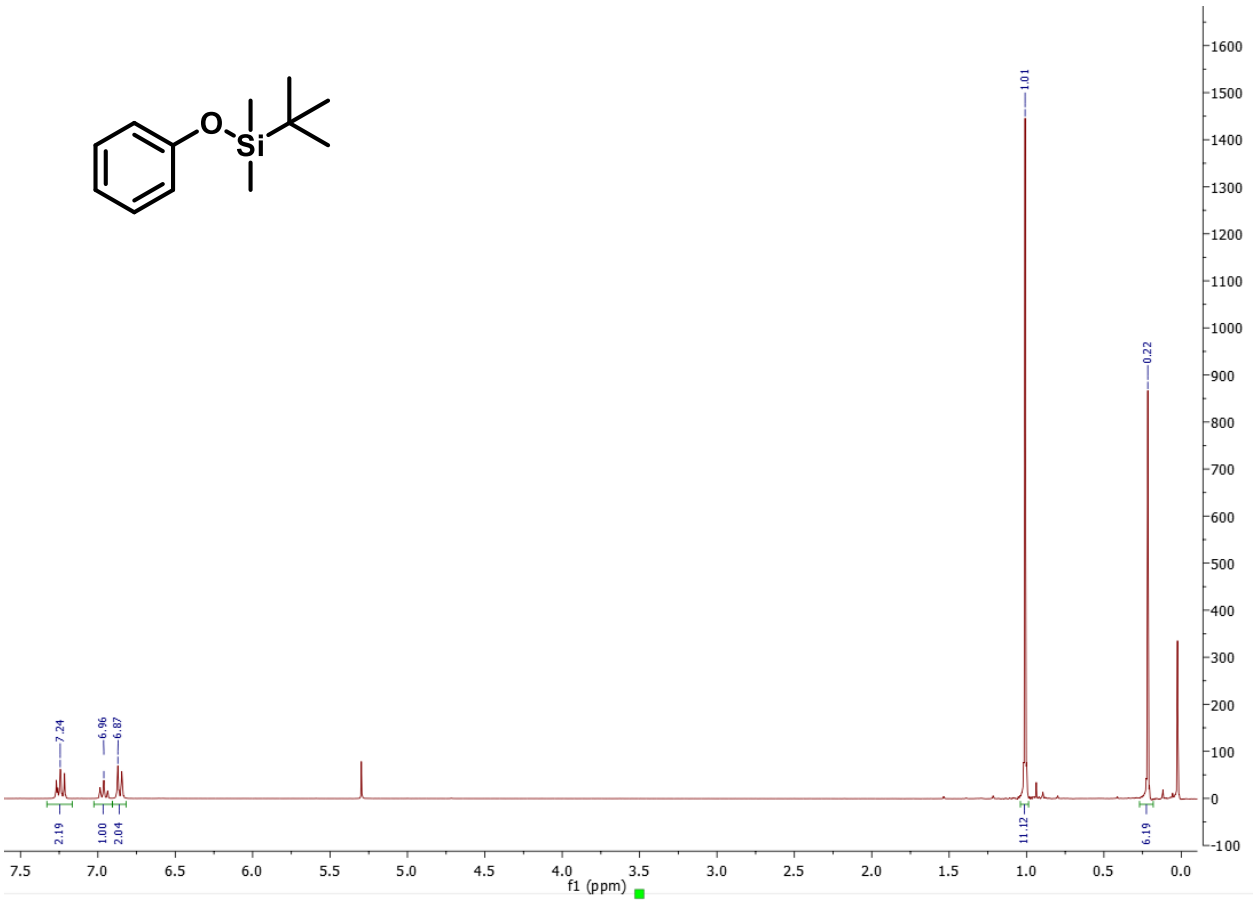

Figure C.2. ^{1}H NMR of *tert*-butyldimethylsilyl-protected phenol

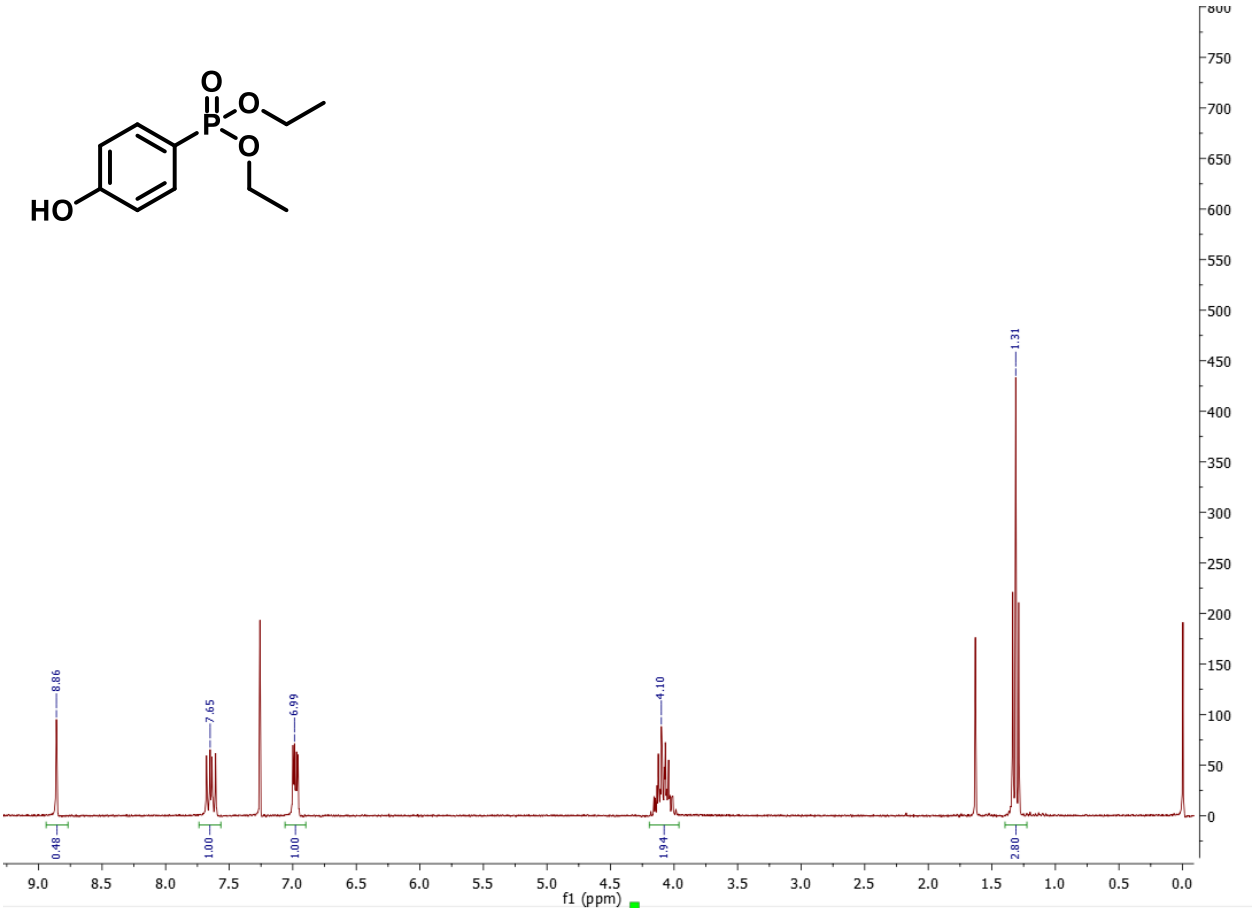

Figure C.3. ^{1}H NMR of diethyl 4-hydroxyphenylphosphonate

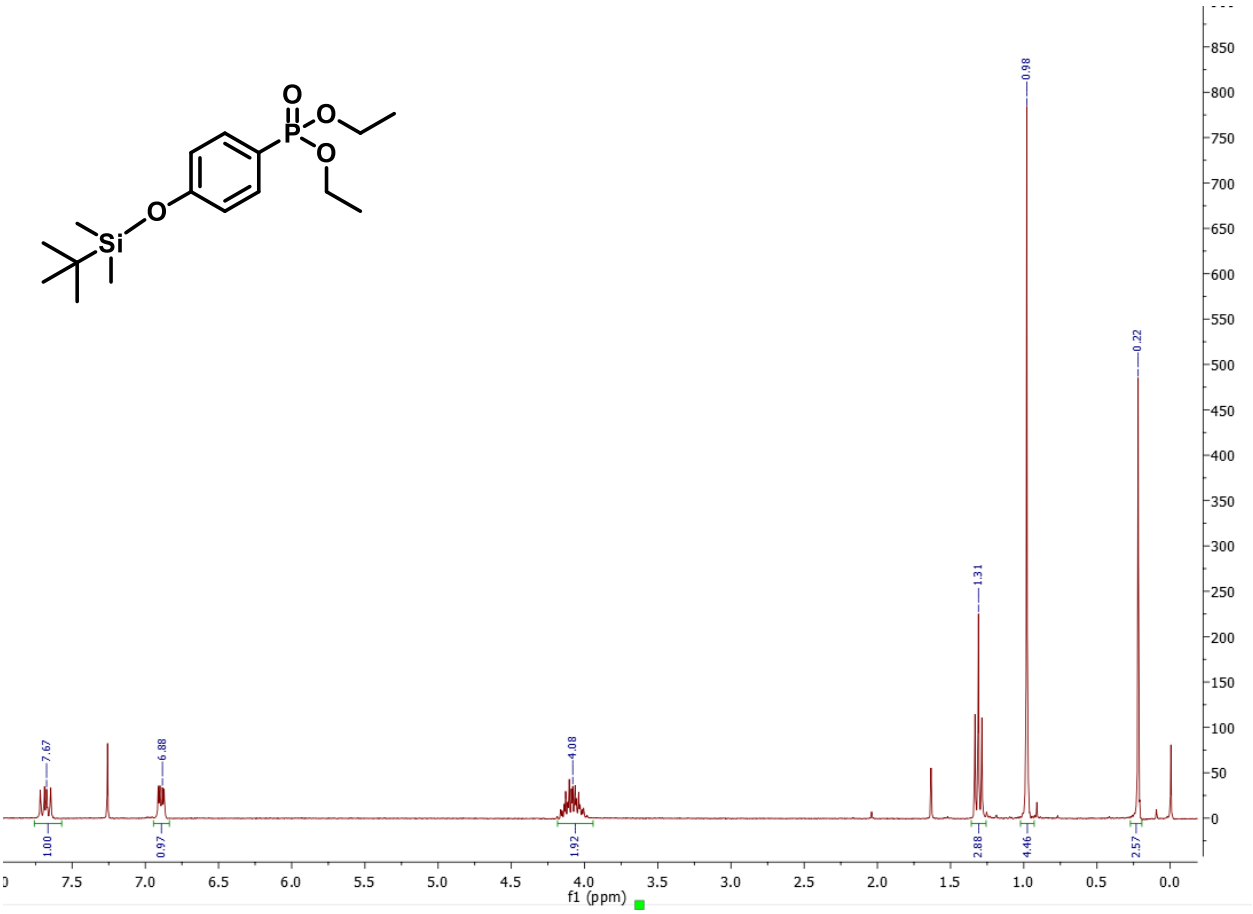

Figure C.4. ^{1}H NMR of *tert*-butyldimethylsilyl-protected diethyl 4-hydroxyphenylphosphonate